Table A6-3. Calculated Geochemical Parameters of Groundwater Samples Used in this Report

Well	Figure A6-5 Sample	Ionic Strength	Charge Balance Error (%)[1]	DIC as (mg/L HCO_3^-)	log P_{CO2} (atm)	Mineral Saturation Indices[2,3]							
						Calcite	Smectite	Ca-Clino.	SiO_2 (a)	Fluorite	Albite	K-Feldspar	Dolomite
Oasis Valley/NW Amargosa													
ER-EC-08	1	7.18×10^{-3}	–3.5	176.8	–2.68	–0.06	4.00	16.11	–0.49	–0.53	–1.51	–0.65	–0.73
ER-OV-01	2	7.43×10^{-3}	1.3	197.2	–3.02	–0.10	6.16	29.11	–0.24	–1.43	–0.80	0.22	–1.64
ER-OV-06a	3	7.46×10^{-3}	0.8	201.0	–2.99	–0.53	5.32	23.90	–0.39	–1.59	–1.04	–0.03	–1.14
ER-OV-05	4	7.27×10^{-3}	0.2	241.5	–2.46	–0.01	6.81	31.43	–0.13	–1.01	–1.25	0.11	–0.41
ER-OV-02	5	8.24×10^{-3}	–0.2	226.6	–2.90	0.12	6.80	30.85	–0.26	–0.91	–1.03	–0.16	–0.87
Springdale Upper Well (10S/47E-32adc)	6	8.51×10^{-3}	–0.3	303.0	–2.26	0.00	6.31	27.98	–0.21	–0.86	–1.40	–0.22	–0.41
Goss Springs North (11S/47E-10bad)	7	6.88×10^{-3}	–1.6	179.7	–3.01	0.08	6.88	31.04	–0.29	–0.77	-1.22	–0.12	–0.72
Er-OV-03a	8	7.02×10^{-3}	1.1	184.6	–2.90	–0.08	6.90	30.91	–0.27	–0.87	–1.25	–0.17	–1.06
ER-OV-03a3	9	7.19×10^{-3}	0.5	182.0	–3.08	0.14	6.47	29.69	–0.31	–1.03	–1.05	0.01	–0.50
ER-OV-03a2	10	2.06×10^{-2}	–3.0	241.6	–3.92	0.54	5.39	26.20	–0.81	—	–0.76	1.05	0.64
Goss Spring (11S/47E-10bcc)	11	7.21×10^{-3}	1.4	187.6	–2.47	–0.32	6.04	24.88	–0.34	–0.67	–1.73	–0.71	–1.46
ER-OV-04a	12	5.71×10^{-3}	0.2	162.7	–3.21	0.06	6.46	30.96	–0.23	–0.97	–0.86	0.40	–1.48
Beatty Well no. 1 (Wat&Sanit Distr)	13	—	—	—	—	—	—	—	—	—	—	—	—
Bond Gold Mining #1	14	5.90×10^{-3}	–2.4	158.7	–3.12	0.39	5.10	20.82	–0.62	–1.91	–1.89	–0.50	0.55
US Ecology MW-313	15	1.42×10^{-2}	–6.0	355.2	–2.00	0.18	6.08	26.48	–0.23	0.16	–1.59	–0.30	0.18
US Ecology MW-600	16	1.18×10^{-2}	–4.0	300.4	–2.45	0.12	6.04	27.07	–0.28	–0.20	–1.21	–0.15	0.34
Nucl. Eng. Co. Well	17	1.43×10^{-2}	–0.1	342.4	–2.11	0.28	6.15	27.23	–0.22	—	–1.40	–0.28	0.32
US Ecology MR-3	18	—	—	—	—	—	—	—	—	—	—	—	—
Timber Mountain													
UE-18r	19	4.84×10^{-3}	0.0	211.2	–2.85	0.42	5.01	21.03	–0.44	–0.73	–1.50	–0.66	–0.17
ER-18-2	20	1.54×10^{-2}	5.3	755.1	–1.55	0.02	1.65	2.43	–0.67	–0.29	–1.64	–1.68	–0.91
ER-EC-05	21	4.84×10^{-3}	6.5	144.8	–2.82	0.09	4.78	18.13	–0.50	–0.20	–1.84	–1.19	–0.95

Table A6-3. Calculated Geochemical Parameters of Groundwater Samples Used in this Report (Continued)

Well	Figure A6-5 Sample	Ionic Strength	Charge Balance Error (%)[1]	DIC as (mg/L HCO_3^-)	log P_{CO2} (atm)	Mineral Saturation Indices[2,3]							
						Calcite	Smectite	Ca-Clino.	SiO_2 (a)	Fluorite	Albite	K-Feldspar	Dolomite
Timber Mountain (Continued)													
Coffer's Ranch Windmill Well	22	4.63×10^{-3}	–1.4	182.4	–3.08	0.26	6.11	25.06	–0.43	–0.45	–1.55	–1.04	–1.10
ER-OV-03c	23	5.03×10^{-3}	0.1	160.8	–3.02	0.10	5.90	24.21	–0.42	–0.28	–1.54	–0.95	–1.07
ER-EC-07	24	3.69×10^{-3}	–2.9	150.6	–2.70	0.06	4.86	18.66	–0.47	–1.13	–2.17	–0.96	–0.58
Fortymile Wash—North													
Water Well 8	25	2.26×10^{-3}	2.6	86.1	–2.40	–1.29	5.51	19.66	–0.36	–2.12	–2.70	–1.32	–3.06
Test Well 1 (USGS HTH #1)	26	2.29×10^{-3}	7.7	99.6	–3.70	–0.60	4.15	13.12	–0.82	—	–1.97	–1.66	—
UE-18t	27	8.09×10^{-3}	0.5	320.8	–3.12	0.93	3.21	7.90	–1.25	—	–2.52	–1.41	0.89
ER-30-1 (upper)	28	3.17×10^{-3}	4.4	108.9	–4.43	0.43	5.26	23.32	–0.72	–1.78	–1.04	–0.21	–0.34
ER-30-1 (lower)	29	3.04×10^{-3}	7.1	113.2	–4.18	0.09	4.86	19.81	–0.76	–2.17	–1.27	–0.73	–0.79
a#2 (dp)	30	2.96×10^{-3}	–2.3	121.0	–2.16	–1.16	5.14	16.23	–0.42	–1.74	–2.76	–2.03	–3.66
a#2 (sh)	31	2.92×10^{-3}	–0.3	130.2	–1.98	–1.39	5.39	16.75	–0.40	–1.80	–2.95	–2.12	–3.98
UE-29a#1 HTH	32	3.09×10^{-3}	5.2	114.1	–2.57	–0.61	6.04	24.28	–0.29	–1.98	–2.21	–0.80	–1.71
WT#15	33	3.95×10^{-3}	2.3	175.2	–2.23	–0.50	4.55	16.64	–0.42	—	–2.20	–1.08	–1.42
WT#14	34	3.11×10^{-3}	0.2	130.5	–2.19	–0.95	4.97	18.11	–0.35	—	–2.45	–1.12	–2.59
J-13	35	3.23×10^{-3}	0.3	139.0	–2.06	–0.94	4.82	16.97	–0.36	–0.97	–2.58	–1.23	–2.22
J-12	36	3.29×10^{-3}	–1.3	138.1	–2.01	–1.04	5.22	18.33	–0.35	–0.98	–2.75	–1.31	–2.54
JF#3	37	3.78×10^{-3}	1.3	123.8	–2.61	–0.36	5.60	23.21	–0.33	–1.12	–2.13	–0.44	–1.11
Solitario Canyon Wash													
H-6(bh)	38	4.41×10^{-3}	–0.8	181.1	–2.76	–0.30	3.93	14.51	–0.50	–0.97	–1.57	–1.20	–1.75
H-6(Tct)	39	4.52×10^{-3}	–6.6	212.4	–2.87	–0.47	3.43	12.50	–0.55	–1.65	–1.41	–1.09	—
H-6(Tcb)	40	4.97×10^{-3}	-9.5	229.7	–2.87	0.03	4.10	16.23	–0.49	–0.93	–1.35	–0.95	–1.15
WT-7	41	4.76×10^{-3}	–2.5	241.0	–3.27	0.13	3.31	10.76	–0.88	—	–1.73	–1.16	–0.39
WT-10	42	4.64×10^{-3}	1.4	180.3	–3.06	–0.21	3.84	14.76	–0.53	–1.40	–1.28	–1.08	–1.36

Table A6-3. Calculated Geochemical Parameters of Groundwater Samples Used in this Report (Continued)

Well	Figure A6-5 Sample	Ionic Strength	Charge Balance Error (%)[1]	DIC as (mg/L HCO_3^-)	log P_{CO2} (atm)	Mineral Saturation Indices[2,3]							
						Calcite	Smectite	Ca-Clino.	SiO_2 (a)	Fluorite	Albite	K-Feldspar	Dolomite
Yucca Mountain—Crest													
G-2	43	2.89×10^{-3}	0.6	127.6	–2.35	–0.79	4.35	15.53	–0.44	–1.95	–2.35	–1.05	–2.33
USW WT-24	44	2.73×10^{-3}	2.4	120.9	–2.82	–1.93	5.49	21.06	–0.35	–3.34	–1.78	–1.01	—
UZ-14(sh)	45	3.41×10^{-3}	8.1	129.2	–3.29	–1.41	5.31	21.74	–0.45	–1.69	–1.35	–0.61	–2.95
UZ-14(dp)	46	3.53×10^{-3}	6.3	133.8	–3.26	–1.55	5.14	21.26	–0.43	–1.84	–1.29	–0.50	–3.04
H-1(Tcp)	47	2.78×10^{-3}	0.6	118.5	–2.58	–0.86	4.40	15.47	–0.46	–2.01	–2.17	–1.25	–2.95
H-1(Tcb)	48	2.93×10^{-3}	–0.7	125.7	–2.55	–0.68	3.96	12.49	–0.55	–2.05	–2.32	–1.60	–2.71
H-5	49	2.92×10^{-3}	2.1	127.8	–2.73	–0.95	4.08	14.59	–0.48	–2.26	–1.90	–1.14	—
USW SD-6	50	4.35×10^{-3}	–0.7	182.1	–3.08	–1.05	4.16	16.13	–0.51	–1.96	–1.30	–0.86	—
H-3	51	6.12×10^{-3}	–3.7	240.9	–3.85	–0.09	5.23	23.60	–0.55	–1.55	–0.57	–0.28	—
Yucca Mountain—Central													
G-4	52	3.56×10^{-3}	3.7	143.0	–2.49	–0.31	4.07	13.89	–0.50	–0.96	–2.18	–1.39	–1.98
b#1(Tcb)	53	3.59×10^{-3}	2.0	152.4	–1.89	–0.76	3.85	11.12	–0.46	–1.22	–2.76	–1.78	–2.47
b#1(bh)	54	3.94×10^{-3}	–3.4	170.1	–2.03	–0.51	4.13	13.61	–0.44	–1.22	–2.50	–1.43	–1.99
H-4	55	4.58×10^{-3}	3.9	185.2	–2.10	–0.42	4.11	13.31	–0.48	–0.33	–2.34	–1.57	–2.16
UZ#16	56	5.79×10^{-3}	10.8	185.9	–3.75	0.85	—	—	–0.62	—	–1.05	—	2.27
Yucca Mountain—Southeast													
ONC#1	57	3.40×10^{-3}	9.1	107.8	–3.64	0.49	4.24	16.99	–0.72	—	–1.72	–0.60	0.33
c#1	58	3.63×10^{-3}	–3.4	156.6	–2.31	–0.37	3.61	12.00	–0.45	–1.25	–2.12	–1.41	–1.82
c#3	59	3.48×10^{-3}	0.2	140.5	–2.46	–0.32	3.65	12.34	–0.47	–1.28	–2.07	–1.37	–1.60
c#3(95-97)	60	3.43×10^{-3}	3.6	144.5	–2.45	–0.30	3.78	13.30	–0.43	—	–1.98	–1.29	–1.69
c#2	61	3.53×10^{-3}	–0.2	142.5	–2.45	–0.28	3.72	12.85	–0.46	–1.20	–2.06	–1.31	–1.56
p#1(v)	62	8.25×10^{-3}	–1.2	438.7	–1.14	–0.32	2.90	6.20	–0.53	–0.44	–2.83	–1.93	–0.72
p#1(c)	63	1.85×10^{-2}	–2.5	976.6	–0.58	0.22	1.35	–1.76	–0.68	–0.02	–3.04	–2.14	0.53
WT-17	64	3.15×10^{-3}	–1.0	150.1	–1.96	–1.18	4.50	13.04	–0.51	–1.23	–2.93	–1.91	–2.96
WT#3	65	3.37×10^{-3}	–1.2	144.3	–2.41	–0.52	4.83	18.44	–0.37	–1.05	–2.13	–0.97	–1.66
WT#12	66	4.30×10^{-3}	0.1	174.0	–2.33	–0.31	4.43	15.67	–0.46	–0.71	–2.16	–1.32	–1.90

Table A6-3. Calculated Geochemical Parameters of Groundwater Samples Used in this Report (Continued)

Well	Figure A6-5 Sample	Ionic Strength	Charge Balance Error (%)[1]	DIC as (mg/L HCO_3^-)	log P_{CO2} (atm)	Mineral Saturation Indices[2,3]							
						Calcite	Smectite	Ca-Clino.	SiO_2 (a)	Fluorite	Albite	K-Feldspar	Dolomite
Jackass Flats													
J-11	67	1.69×10^{-2}	1.4	80.6	–3.23	0.24	6.09	28.57	–0.31	–1.00	–1.13	0.25	0.10
Crater Flat													
GEXA Well 4	68	4.56×10^{-3}	–2.3	151.8	–2.69	–0.21	4.72	18.48	–0.45	–0.80	–1.82	–0.89	–1.46
VH-1	69	4.77×10^{-3}	0.9	171.3	–2.32	–0.47	4.18	14.35	–0.46	–1.03	–2.05	–1.45	–1.33
Crater Flat—Southwest													
VH-2	70	1.29×10^{-2}	–1.3	446.9	–1.48	0.14	3.60	8.75	–0.71	–1.08	–3.15	–1.85	0.28
NC-EWDP-7S	71	1.44×10^{-2}	–0.6	461.8	–1.73	0.19	4.96	15.69	–0.68	–1.06	–2.95	–1.59	0.37
NC-EWDP-7SC	72	1.50×10^{-2}	–0.4	480.4	–1.60	0.18	4.47	12.52	–0.69	–1.17	–3.01	–2.00	0.36
NC-EWDP-1DX	73	1.19×10^{-2}	–3.5	414.1	–1.66	–0.03	5.42	20.19	–0.40	–1.52	–2.51	–1.04	0.03
NC-EWDP-1DX Zone 2	74	2.09×10^{-2}	–9.3	1,385.6	–0.70	–0.26	4.86	15.91	–0.38	0.62	–2.30	–1.72	–0.70
NC-EWDP-01S Zone 1	75	1.15×10^{-2}	–3.7	386.1	–1.86	0.20	5.39	21.01	–0.38	–1.65	–2.30	–0.84	0.49
NC-EWDP-01S Zone 2	76	1.14×10^{-2}	–3.8	389.0	–1.75	0.09	5.17	19.40	–0.40	–1.68	–2.44	–0.99	0.30
NC-EWDP-01S	77	1.16×10^{-2}	–1.9	390.9	–1.75	0.12	5.32	20.60	–0.35	–1.66	–2.31	–0.90	0.34
NC-EWDP-12PA	78	1.10×10^{-2}	–1.6	540.6	–1.18	–0.58	5.37	20.88	–0.25	–0.25	–2.28	–0.71	–1.35
NC-EWDP-12PB	79	1.08×10^{-2}	–1.7	491.4	–1.29	–0.48	5.28	20.77	–0.27	–0.23	–2.21	–0.64	–1.15
NC-EWDP-12PC	80	1.09×10^{-2}	0.0	340.5	–1.99	0.25	5.31	21.52	–0.35	–1.26	–2.08	–0.64	0.60

Table A6-3. Calculated Geochemical Parameters of Groundwater Samples Used in this Report (Continued)

Well	Figure A6-5 Sample	Ionic Strength	Charge Balance Error (%)[1]	DIC as (mg/L HCO_3^-)	log P_{CO2} (atm)	Mineral Saturation Indices[2,3]							
						Calcite	Smectite	Ca-Clino.	SiO_2 (a)	Fluorite	Albite	K-Feldspar	Dolomite
Yucca Mountain—South													
NC-EWDP-09SX	81	6.32×10^{-3}	–1.1	213.3	–2.67	0.21	5.33	22.48	–0.39	–0.89	–1.62	–0.57	0.37
NC-EWDP-9SX Zone 1	82	5.95×10^{-3}	–1.6	194.5	–3.02	0.37	5.41	23.28	–0.48	–0.92	–1.53	–0.35	0.62
NC-EWDP-9SX Zone 2	83	6.01×10^{-3}	–2.3	206.4	–2.59	0.03	5.20	20.88	–0.44	–0.96	–1.86	–0.76	0.04
NC-EWDP-9SX Zone 3	84	5.94×10^{-3}	–3.2	206.8	–2.78	0.22	5.20	21.43	–0.47	–0.93	–1.72	–0.64	0.44
NC-EWDP-9SX Zone 4	85	5.95×10^{-3}	–3.8	209.9	–2.68	0.15	5.23	21.43	–0.43	–0.96	–1.75	–0.71	0.28
NC-EWDP-03D	86	5.63×10^{-3}	–1.8	230.1	–2.99	–0.90	4.52	19.24	–0.43	–2.31	–1.06	–0.40	–2.05
NC-EWDP-3S Zone 2	87	6.27×10^{-3}	–0.7	234.5	–3.30	–0.45	4.97	22.47	–0.40	–2.09	–0.66	–0.26	–1.36
NC-EWDP-3S Zone 3	88	6.90×10^{-3}	–3.9	279.9	–3.44	–0.22	4.67	21.29	–0.51	–1.85	–0.67	–0.07	–0.89
CIND-R-LITE	89	5.26×10^{-3}	–2.0	195.9	–2.35	0.04	2.69	8.92	–0.53	–1.18	–1.88	–1.08	0.29
NC-EWDP-15P	90	5.02×10^{-3}	–1.0	192.2	–2.50	–0.30	4.95	19.33	–0.42	–1.17	–1.83	–0.94	–0.81
NC-EWDP-02D	91	3.74×10^{-3}	–2.9	158.2	–2.33	–0.45	5.52	20.90	–0.38	–1.07	–2.39	–1.06	–1.76
NC-EWDP-19D	92	5.31×10^{-3}	–0.4	233.7	–3.31	–0.10	5.36	25.23	–0.36	–1.96	–0.69	0.11	–1.03
NC-EWDP-19P	93	3.40×10^{-3}	–1.9	115.4	–3.62	0.53	5.52	25.93	–0.38	–1.22	–1.13	0.09	0.26
NC-EWDP-19D (alluvial)	94	4.88×10^{-3}	–2.6	228.2	–3.22	–0.08	5.17	23.71	–0.39	–1.84	–0.88	–0.07	–0.79
NC-EWDP-19D (zone #1)	95	4.63×10^{-3}	0.4	204.5	–3.26	0.10	5.08	23.52	–0.39	–1.72	–0.90	–0.03	–0.45
NC-EWDP-19D (zone #2)	96	3.77×10^{-3}	1.9	149.8	–3.11	0.13	5.54	24.92	–0.33	–1.33	–1.29	–0.20	–0.37
NC-EWDP-19D (zone #3)	97	4.78×10^{-3}	0.5	212.1	–3.15	–0.44	5.08	22.61	–0.40	–2.16	–0.99	–0.21	–1.58
NC-EWDP-19D (zone #4)	98	5.20×10^{-3}	–0.8	234.4	–3.51	–0.22	5.14	24.52	–0.40	–2.11	–0.56	0.21	—

Table A6-3. Calculated Geochemical Parameters of Groundwater Samples Used in this Report (Continued)

Well	Figure A6-5 Sample	Ionic Strength	Charge Balance Error (%)[1]	DIC as (mg/L HCO_3^-)	log P_{CO2} (atm)	Mineral Saturation Indices[2,3]							
						Calcite	Smectite	Ca-Clino.	SiO_2 (a)	Fluorite	Albite	K-Feldspar	Dolomite
Amargosa Valley													
NC-EWDP-4PB	99	3.98×10^{-3}	–0.9	113.6	–4.53	0.78	5.18	23.61	–0.73	–1.56	–0.90	–0.10	—
NC-EWDP-4PA	100	3.91×10^{-3}	–0.4	107.8	–3.18	–0.11	5.25	20.58	–0.56	–1.51	–1.95	–0.88	–1.51
Desert Farms Garlic Plot	101	6.54×10^{-3}	0.0	127.7	–2.71	–0.09	5.22	20.39	–0.48	–1.58	–2.06	–0.88	–0.99
15S/49E-13dda	102	—	—	—	—	—	—	—	—	—	—	—	—
15S/50E-18ccc	103	6.35×10^{-3}	–1.0	153.5	–3.23	0.32	5.32	22.38	–0.55	–0.97	–1.50	–0.53	–0.54
NDOT	104	6.76×10^{-3}	–0.4	161.0	–2.80	–0.04	5.22	21.28	–0.45	–1.11	–1.64	–0.75	–1.03
15S/50E-18cdc	105	6.16×10^{-3}	–3.5	158.4	–2.81	–0.20	5.15	19.90	–0.54	–1.20	–1.88	–0.92	–1.44
Airport Well	106	3.93×10^{-3}	0.0	121.5	–3.61	0.12	5.08	21.47	–0.54	–1.56	–1.28	–0.63	–1.14
15S/50E-19b1	107	7.69×10^{-3}	1.5	167.5	–2.90	0.10	5.72	24.44	–0.43	–1.26	–1.52	–0.42	–0.18
Amargosa River													
16S/48E-8ba	108	1.42×10^{-2}	1.4	299.8	–2.46	0.56	5.42	22.83	–0.49	—	–1.61	–0.42	0.49
16S/48E-7bba	109	1.23×10^{-2}	0.8	269.6	–2.02	–0.03	6.09	25.98	–0.23	—	–1.69	–0.48	–0.47
16S/48E-7cbc	110	1.21×10^{-2}	0.8	246.8	–2.35	0.18	6.16	27.12	–0.25	—	–1.49	–0.28	0.24
16S/48E-18bcc	111	1.30×10^{-2}	1.7	272.1	–2.60	0.60	6.48	30.96	–0.17	—	–0.95	0.28	0.84
16S/48E-17ccc	112	1.47×10^{-2}	3.4	246.3	–2.35	0.31	6.34	29.10	–0.18	—	–1.21	–0.02	0.19
16S/48E-18dad	113	1.25×10^{-2}	3.1	243.3	–2.35	0.24	6.32	28.73	–0.18	—	–1.27	–0.08	0.02
16S/48E-8cda	114	1.25×10^{-2}	1.2	276.1	–2.21	0.12	6.32	27.88	–0.22	—	–1.44	–0.28	–0.28
16S/48E-17abb	115	1.33×10^{-2}	0.8	324.8	–1.95	0.08	6.31	27.59	–0.18	—	–1.57	–0.33	–0.39
Barrachman Dom/Irr.	116	1.26×10^{-2}	–4.2	304.4	–2.10	0.04	6.83	29.73	–0.20	–0.63	–1.65	–0.35	–0.29
McCracken Domestic	117	1.71×10^{-2}	3.2	257.3	–2.17	0.16	6.64	29.58	–0.18	–0.57	–1.40	–0.23	–0.22

Table A6-3. Calculated Geochemical Parameters of Groundwater Samples Used in this Report (Continued)

Well	Figure A6-5 Sample	Ionic Strength	Charge Balance Error (%)[1]	DIC as (mg/L HCO_3^-)	log P_{CO2} (atm)	Mineral Saturation Indices[2,3]							
						Calcite	Smectite	Ca-Clino.	SiO_2 (a)	Fluorite	Albite	K-Feldspar	Dolomite
Fortymile Wash—West													
16S/48E-15ba	118	1.30×10^{-2}	–0.2	265.4	–2.61	0.62	5.42	22.86	–0.50	—	–1.62	–0.45	0.71
16S/48E-10cba	119	4.25×10^{-3}	–0.9	163.3	–3.10	0.03	6.21	28.67	–0.27	—	–1.22	0.08	0.04
16S/48E-15aaa	120	3.95×10^{-3}	1.7	152.8	–2.92	–0.15	6.10	27.61	–0.25	—	–1.39	–0.04	–0.43
Selbach Domestic	121	7.48×10^{-3}	–0.9	178.9	–2.77	0.10	6.33	28.77	–0.23	–1.19	–1.29	–0.08	0.08
16S/48E-15dda	122	5.41×10^{-3}	6.8	176.5	–2.77	0.10	6.26	28.59	–0.22	—	–1.35	0.01	0.00
16S/49E-23add	123	4.02×10^{-3}	7.5	125.0	–3.11	0.07	6.39	30.06	–0.19	—	–1.20	0.21	–0.48
16S/48E-23bdb	124	3.97×10^{-3}	3.0	172.3	–2.11	–0.97	6.12	24.99	–0.19	—	–2.04	–0.68	–2.56
16S/48E-23da	125	—	—	—	—	—	—	—	—	—	—	—	—
Funeral Mountain Ranch Irrig.	126	5.29×10^{-3}	–2.0	198.4	–2.93	0.08	6.94	33.28	–0.11	–0.97	–0.93	0.39	–0.22
Fortymile Wash—South													
16S/49E-05acc	127	4.07×10^{-3}	5.0	134.3	–2.98	0.26	6.09	27.16	–0.28	–1.31	–1.68	–0.18	–0.24
16S/49E-8abb	128	4.42×10^{-3}	2.2	161.4	–2.33	–0.29	5.96	23.69	–0.32	—	–2.36	–0.82	–1.30
16S/49E-8acc	129	3.91×10^{-3}	1.4	139.7	–2.76	–0.01	5.83	25.07	–0.31	—	–1.91	–0.33	–0.64
16S/49E-18dc	130	4.05×10^{-3}	0.5	149.7	–2.93	0.15	6.03	27.13	–0.30	—	–1.65	0.02	–0.22
16s/48E-24aaa	131	4.06×10^{-3}	3.5	146.1	–2.93	0.12	6.15	28.67	–0.20	—	–1.29	0.13	–0.80
16S/49E-19daa	132	3.92×10^{-3}	0.1	131.9	–3.08	0.29	6.22	29.24	–0.21	—	–1.41	0.27	–0.35
DeLee Large Irrigation	133	3.85×10^{-3}	2.5	136.6	–2.94	–0.06	7.79	36.15	–0.10	–1.16	–1.54	0.29	–1.25
16S/48E-25aa	134	3.73×10^{-3}	0.6	132.1	–2.98	0.10	6.10	28.06	–0.23	—	–1.47	0.09	–0.87
16S/48E-36aaa	135	3.56×10^{-3}	0.1	128.3	–3.30	0.31	6.50	31.26	–0.19	—	–1.13	0.41	0.03
Bray Domestic	136	3.75×10^{-3}	0.9	131.8	–2.91	–0.01	6.87	31.56	–0.17	–1.37	–1.61	0.18	–0.82
Amargosa Estates #2	137	3.68×10^{-3}	1.4	133.3	–2.99	0.09	6.56	30.50	–0.17	–1.04	–1.43	0.17	–0.45
17S/48E-1ab	138	3.65×10^{-3}	1.2	134.1	–2.98	0.08	6.42	29.84	–0.18	—	–1.42	0.17	–0.58
17S/49E-7bb	139	4.37×10^{-3}	2.8	149.5	–3.14	0.42	6.52	31.32	–0.18	—	–1.14	0.39	0.04
17S/49E-8ddb	140	3.68×10^{-3}	4.6	118.6	–3.34	0.35	6.69	32.46	–0.17	—	–1.15	0.52	0.16
17S/49E-35ddd	141	4.43×10^{-3}	–0.9	158.3	–2.82	–0.09	6.68	31.02	–0.15	—	–1.38	0.19	–0.36

Table A6-3. Calculated Geochemical Parameters of Groundwater Samples Used in this Report (Continued)

Well	Figure A6-5 Sample	Ionic Strength	Charge Balance Error (%)[1]	DIC as (mg/L HCO_3^-)	log P_{CO2} (atm)	Mineral Saturation Indices[2,3]							
						Calcite	Smectite	Ca-Clino.	SiO_2 (a)	Fluorite	Albite	K-Feldspar	Dolomite
Fortymile Wash—East													
15S/49E-22a1	142	4.27×10^{-3}	0.0	145.5	–2.83	0.17	5.44	23.00	–0.38	–1.12	–1.87	–0.46	–0.31
15S/49E-22dcc	143	4.41×10^{-3}	1.2	207.6	–1.50	–1.05	4.64	13.63	–0.41	–1.40	–3.20	–1.88	–2.84
15S/49E-27acc	144	4.26×10^{-3}	–1.3	153.3	–2.50	0.14	1.93	1.05	–0.94	–1.73	–2.94	–2.04	–0.37
O'Neill Domestic	145	4.56×10^{-3}	2.2	143.4	–2.79	–0.05	6.84	30.57	–0.21	–1.50	–1.72	–0.07	–0.85
16S/49E-9cda	146	5.43×10^{-3}	2.6	149.9	–2.46	–0.22	6.15	26.24	–0.24	—	–1.96	–0.38	–1.06
16S/49E-9dcc	147	5.16×10^{-3}	0.5	139.2	–3.08	0.22	6.57	31.04	–0.20	—	–1.25	0.32	–0.16
16S/49E-16ccc	148	4.62×10^{-3}	0.6	133.8	–2.79	0.06	6.32	28.15	–0.19	—	–1.64	–0.26	–0.73
Ponderosa Dairy #1	149	6.29×10^{-3}	–1.2	153.1	–2.33	–0.29	5.72	24.50	–0.23	–1.24	–1.91	–0.34	–1.02
17S/49E-9aa	150	5.10×10^{-3}	0.0	131.5	–2.90	0.06	6.25	28.64	–0.23	—	–1.54	0.11	–0.38
17S/49E-15bbd	151	3.85×10^{-3}	–0.7	119.6	–3.05	0.04	6.65	30.72	–0.19	—	–1.58	0.21	–0.34
M. Gilgan Well	152	3.82×10^{-3}	1.8	127.0	–3.11	0.15	6.49	30.56	–0.19	–1.08	–1.33	0.28	–0.27
17S/49E-15bc	153	—	—	—	—	—	—	—	—	—	—	—	—
Gravity Fault													
NC-EWDP-5S	154	—	—	—	—	—	—	—	—	—	—	—	—
NC-EWDP-5SB	155	6.60×10^{-3}	–0.2	221.3	–2.29	–0.42	4.59	14.45	–0.73	–1.50	–2.63	–1.46	–1.42
16S/50E-7bcd	156	1.13×10^{-2}	1.4	303.4	–2.12	0.27	4.19	14.45	–0.65	—	–2.37	–1.03	0.51
Nelson Domestic	157	1.12×10^{-2}	–3.8	325.0	–2.00	0.14	4.12	13.15	–0.70	–0.20	–2.58	–1.27	0.23
16S/49E-12ddd	158	1.14×10^{-2}	1.6	301.5	–2.16	0.18	4.39	13.17	–0.76	—	–2.62	–1.72	0.27
Lowe Domestic	159	1.07×10^{-2}	–1.5	284.4	–2.32	0.16	6.38	26.74	–0.38	–0.90	–1.88	–0.47	–0.03
16S/49E-15aaa	160	8.50×10^{-3}	–1.3	201.8	–2.43	0.08	5.75	23.76	–0.39	—	–1.97	–0.53	–0.25
Anvil Ranch Irrigation	161	8.09×10^{-3}	1.5	139.8	–2.81	0.15	6.88	31.83	–0.18	–1.06	–1.47	0.21	–0.33
16S/49E-36aaa	162	1.25×10^{-2}	3.8	321.1	–2.33	0.45	5.39	22.40	–0.49	—	–1.89	–0.37	0.88
16S/49E-35baa	163	1.21×10^{-2}	0.1	325.8	–1.95	0.04	5.36	20.36	–0.48	—	–2.30	–0.88	–0.05
Payton Domestic	164	1.19×10^{-2}	–0.8	304.0	–2.19	0.16	5.88	23.63	–0.47	0.01	–2.16	–0.59	0.17
16S/49E-36aba	165	1.14×10^{-2}	2.3	302.3	–2.26	0.27	5.51	22.89	–0.44	—	–1.92	–0.39	0.54
16S/49E-35aaa	166	1.11×10^{-2}	4.8	280.3	–2.29	0.24	5.29	21.29	–0.50	—	–2.01	–0.54	0.38
Oettinger Well	167	1.14×10^{-2}	–2.0	307.9	–2.06	0.12	5.28	20.55	–0.48	–0.20	–2.22	–0.72	0.09

Table A6-3. Calculated Geochemical Parameters of Groundwater Samples Used in this Report (Continued)

Well	Figure A6-5 Sample	Ionic Strength	Charge Balance Error (%)[1]	DIC as (mg/L HCO_3^-)	log P_{CO2} (atm)	Mineral Saturation Indices[2,3]							
						Calcite	Smectite	Ca-Clino.	SiO_2 (a)	Fluorite	Albite	K-Feldspar	Dolomite
Gravity Fault (Continued)													
Amargosa Motel (b)	168	1.12×10^{-2}	–1.1	298.8	–2.17	0.20	5.63	22.94	–0.42	–0.27	–2.05	–0.54	0.28
17S/49E-11ba	169	1.00×10^{-2}	1.2	209.6	–2.82	0.44	6.34	29.04	–0.33	—	–1.38	0.16	0.74
Spring Meadows Well #8	170	—	—	—	—	—	—	—	—	—	—	—	—
17S/50E-19aab	171	1.46×10^{-2}	1.2	405.5	–3.08	0.35	6.95	33.70	–0.38	—	–0.67	0.82	0.99
USFWS - Five Springs Well	172	8.94×10^{-3}	4.9	261.4	–2.07	0.18	3.38	8.48	–0.80	–0.91	–2.93	–1.63	0.42
Spring Meadows Well #10	173	—	—	—	—	—	—	—	—	—	—	—	—
18S/49E-1aba	174	8.51×10^{-3}	–0.8	253.0	–3.27	0.75	7.53	38.08	–0.16	—	–0.62	1.11	1.44
18S/50E-6dac	175	8.45×10^{-3}	3.1	227.2	–2.87	0.41	6.52	31.77	–0.17	—	–0.91	0.56	0.87
18S/50E-7aa	176	1.06×10^{-2}	1.7	258.0	–3.08	0.50	7.53	35.92	–0.30	—	–1.00	0.63	0.75
Amargosa River/Fortymile Wash													
16S/48E-36dcc	177	1.04×10^{-2}	0.4	336.8	–1.73	–0.09	5.88	24.31	–0.23	—	–2.02	–0.58	–0.57
Crane Domestic	178	1.42×10^{-2}	–0.5	504.9	–1.56	0.12	5.24	19.91	–0.42	–0.14	–2.25	–0.89	0.04
27N/4E-27bbb	179	1.30×10^{-2}	2.4	448.3	–2.21	0.61	6.70	31.22	–0.19	—	–1.27	0.26	1.05
IMV on Windjammer	180	9.65×10^{-3}	–0.8	321.2	–2.05	0.10	6.25	26.99	–0.23	–0.32	–1.75	–0.35	–0.12
17S/49E-29acc	181	1.37×10^{-2}	5.0	288.6	–2.21	0.15	6.75	30.78	–0.18	—	–1.39	0.10	0.05
17S/49E-28bcd	182	9.34×10^{-3}	1.8	307.7	–2.15	0.19	6.15	27.12	–0.22	—	–1.62	–0.20	0.10
18S/49E-2cbc	183	9.42×10^{-3}	0.1	360.7	–2.28	0.28	6.11	26.86	–0.29	—	–1.49	–0.23	0.51
Mom's Place	184	6.77×10^{-3}	–0.5	241.7	–2.45	0.10	6.57	29.79	–0.18	–0.55	–1.47	–0.01	–0.08
18S/49E-11bbb	185	8.40×10^{-3}	4.5	234.5	–2.26	–0.01	6.28	28.08	–0.18	—	–1.53	–0.12	–0.28
Skeleton Hills													
TW-5	186	1.10×10^{-2}	–1.5	400.0	–2.30	0.54	3.77	12.02	–0.83	–0.41	–2.37	–1.12	1.19
Unnamed Well 15S/50E-22-7	187	4.19×10^{-3}	8.6	171.5	–1.62	–1.20	5.23	16.45	–0.38	–1.43	–3.18	–1.81	–3.18

Table A6-3. Calculated Geochemical Parameters of Groundwater Samples Used in this Report (Continued)

Well	Figure A6-5 Sample	Ionic Strength	Charge Balance Error (%)[1]	DIC as (mg/L HCO_3^-)	log P_{CO2} (atm)	Mineral Saturation Indices[2,3]							
						Calcite	Smectite	Ca-Clino.	SiO_2 (a)	Fluorite	Albite	K-Feldspar	Dolomite
Amargosa Flat													
Amargosa Tracer Hole #2	188	8.57×10^{-3}	–0.4	279.8	–2.54	0.64	3.94	13.13	–0.78	–0.77	–2.45	–1.11	1.32
Cherry Patch Well, 17S/52E-08cdb	189	2.37×10^{-2}	2.5	307.4	–1.88	–0.02	4.48	14.33	–0.67	–0.77	–2.39	–1.52	0.01
USDOE-MSH-C shallow Well	190	7.40×10^{-3}	–0.7	263.9	–2.63	0.07	5.82	23.92	–0.50	–1.14	–1.93	–0.47	0.46
Mine Mountain													
UE-17a	191	9.51×10^{-3}	14.9	208.5	–2.31	0.03	3.34	5.62	–1.01	–1.42	–3.27	–2.38	0.30
UE-1a	192	9.02×10^{-3}	–3.7	432.9	–1.81	0.21	4.21	11.64	–0.79	—	–3.24	–1.66	0.48
UE-1b	193	5.32×10^{-3}	18.9	197.6	–2.13	–0.15	5.94	25.26	–0.18	—	–2.20	–0.35	–0.37
UE-16f	194	2.66×10^{-2}	–15.7	902.7	–2.98	0.31	1.82	–0.30	–1.51	–1.59	–2.25	–1.88	1.08
UE-14b	195	4.87×10^{-3}	2.2	113.0	–3.36	0.01	5.59	23.60	–0.44	—	–1.36	–0.73	–1.35
Pluto 1	196	5.92×10^{-3}	5.9	150.4	–2.84	0.32	5.90	25.75	–0.34	—	–1.89	–0.22	0.38
Pluto 5	197	7.65×10^{-3}	7.4	220.2	–2.59	0.49	5.95	25.27	–0.31	—	–2.07	–0.51	0.93
USGS Test Well F (HTH)	198	7.90×10^{-3}	9.4	252.6	–1.31	–0.11	0.35	–6.49	–0.79	–0.57	–3.24	–2.17	–0.19

Table A6-3. Calculated Geochemical Parameters of Groundwater Samples Used in this Report (Continued)

Well	Figure A6-5 Sample	Ionic Strength	Charge Balance Error (%)[1]	DIC as (mg/L HCO_3^-)	log P_{CO2} (atm)	Mineral Saturation Indices[2,3]							
						Calcite	Smectite	Ca-Clino.	SiO_2 (a)	Fluorite	Albite	K-Feldspar	Dolomite
Funeral Mountains													
Woodcamp Spring	199	4.17×10^{-3}	3.7	139.1	–2.15	–0.84	6.45	25.84	–0.26	–2.73	–2.59	–0.61	–2.26
Bond Gold Mining #13	200	2.44×10^{-2}	-5.3	296.7	–1.86	0.30	3.09	5.38	–0.91	–1.53	–3.29	–2.13	0.74
Nevares Spring	201	1.27×10^{-2}	–2.1	375.7	–1.78	0.20	2.87	6.81	–0.77	–0.49	–2.59	–1.53	0.53
Travertine Spring	202	1.19×10^{-2}	–2.3	366.1	–1.82	0.04	3.55	10.70	–0.67	–0.41	–2.45	–1.30	0.25

Source: DTN: LA0310EK831232.001 [DIRS 165995].

[1] PHREEQC calculates percent error in the selected output file as 100 x (*cations* - |*anions*|)/(*cations* + |*anions*|), where *cations* is the electrical charge of the cations in equivalents per liter and *anions* is the electrical charge of the anions in equivalents per liter (Parkhurst and Appelo 1999 [DIRS 159511], p. 140).

[2] The saturation index of a mineral phase is calculated as the base-ten logarithm of the ratio of the ion activity product (IAP) to the solubility constant (K_{sp}) of the mineral at the prevailing temperature: log (IAP/K_{sp}). Values of log (IAP/K_{sp}) less than zero indicate the groundwater is undersaturated with that mineral. Conversely, values of log (IAP/K_{sp}) greater than zero indicate the groundwater is oversaturated with that mineral. Values of log (IAP/K_{sp}) equal to zero indicate the groundwater is at equilibrium with the mineral (Langmuir 1997 [DIRS 100051], p. 8).

[3] The log P_{CO2} and saturation indices for calcite, SiO_2(a), fluorite, albite and K-feldspar were calculated using the database *phreeqc.dat* (Parkhurst and Appelo 1999 [DIRS 159511], Table 55). The saturation indices for smectite and Ca-clinoptilolite were calculated based on the Gibbs free-energy data listed in Table A6-4 of this report.

Clino. = Clinoptilolite.

Table A6-4. Yucca Mountain Mineral Phase Compositions and Thermodynamic Data Used in PHREEQC Analyses

Phase	Formula	ΔG^{O}_{f} (kJ/mol-°K)	ΔH^{O}_{f} (kJ/mol)	Reference
Smectite	$K_{0.1}Na_{0.02}Ca_{0.14}Al_{4.4}Si_{7.6}O_{20}(OH)_4 \cdot 4H_2O$	–11,619.6	–12,595.6	Chipera et al. (1995 [DIRS 100025], Table 1)
Ca-Clinoptilolite	$K_{2.5}Na_{1.1}Ca_{1.2}Al_{6.0}Si_{30.0}O_{72.0} \cdot 26.8\ H_2O$	-39,067.7	-42,491.3	Chipera and Bish (1997 [DIRS 105079], Tables 1 to 2)
Na-Clinoptilolite	$K_{2.8}Na_{1.5}Ca_{0.9}Al_{6.1}Si_{29.9}O_{72.0} \cdot 26.8\ H_2O$	-39,093.8	-42,512.1	Chipera and Bish (1997 [DIRS 105079], Tables 1 to 2)

The geochemical parameters calculated in this section provide an indication of which minerals are potentially dissolving or precipitating in Yucca Mountain groundwater and, thus, provide important constraints on groundwater mixing and reaction models. Table A6-3 indicates that groundwater in the Yucca Mountain area is generally slightly undersaturated with amorphous silica [SiO_2(a)], fluorite, and albite and greatly supersaturated with Ca-clinoptilolite and smectite typical of Yucca Mountain. The spatial distribution of saturation indices of minerals whose saturation state in groundwater are more variable are discussed in more detail in the following subsections.

In addition to the saturation indices shown in Table A6-3, saturation indices were also calculated for other common minerals (DTN: LA0310EK831232.001 [DIRS 165995]). The calculated Na-clinoptilolite saturation indices generally are similar to those shown in Table A6-3 for Ca-clinoptilolite. All groundwaters in the Yucca Mountain area are significantly undersaturated with gypsum and halite and slightly oversaturated with quartz (chalcedony). Yucca Mountain area groundwaters are generally undersaturated with respect to sepiolite ($Mg_2Si_3O_{7.5}(OH) \cdot 3H_2O$), except in areas of the Amargosa Desert such as the Gravity fault area where Si-rich groundwater from the volcanic alluvium mixes with Mg-rich discharge from the carbonate aquifer. Kaolinite saturation indices are zero in all cases because of the assumption (Table A5-1, Assumption 2) that all groundwaters are in equilibrium with kaolinite.

A6.3.5.1 Ionic Strength

Ionic strength (I) is a measure of the interionic effects resulting from the electrical attraction and repulsion between various ions in solution. It is defined by $I = 1/2 \sum_i C_i Z_i^2$ (Langmuir 1997 [DIRS 100051], p. 123), where C_i is the concentration (mol/kg solution) and Z_i is the charge of ion i. Ionic strength is expressed in this report as moles per kilogram of groundwater.

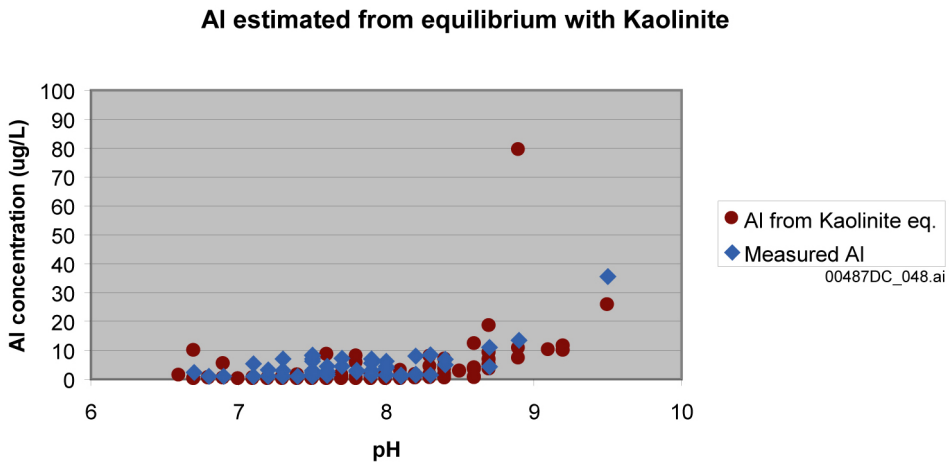

DTNs: GS980908312322.008 [DIRS 145412; GS990808312322.002 [DIRS 162917]; GS010308312322.002 [DIRS 162910]; GS011108312322.006 [DIRS 162911].

NOTE: The single, large calculated Al value is from a sample with very small SiO2 value (UE-16f, sample 194).

Figure A6-33. Comparison between Measured Dissolved Aluminum Concentrations and Dissolved Aluminum Concentrations Calculated by PHREEQC Assuming Equilibrium with Kaolinite

Excluding groundwater from the carbonate aquifer at borehole p#1, groundwater at Yucca Mountain has an ionic strength that ranges from about 2.2×10^{-3} to 4.8×10^{-3} mole/kg (Figure A6-34). A single groundwater from the Yucca Crest area from borehole H-3 (Site 51) has a somewhat higher value (6.12×10^{-3} mole/kg). The ionic strength of groundwater at the NC-EWDP wells in southern Yucca Mountain and south of Crater Flat increases toward the west, reflecting the differences in the ionic strength of the groundwater to the north and west of these wells. North of Yucca Mountain, groundwater shows a westward increase in ionic strength from the northern Fortymile Wash area through Timber Mountain and toward Oasis Valley. The highest ionic strength groundwaters are associated with the southwestern Crater Flat, the Amargosa River, the Gravity fault area, and central Jackass Flats.

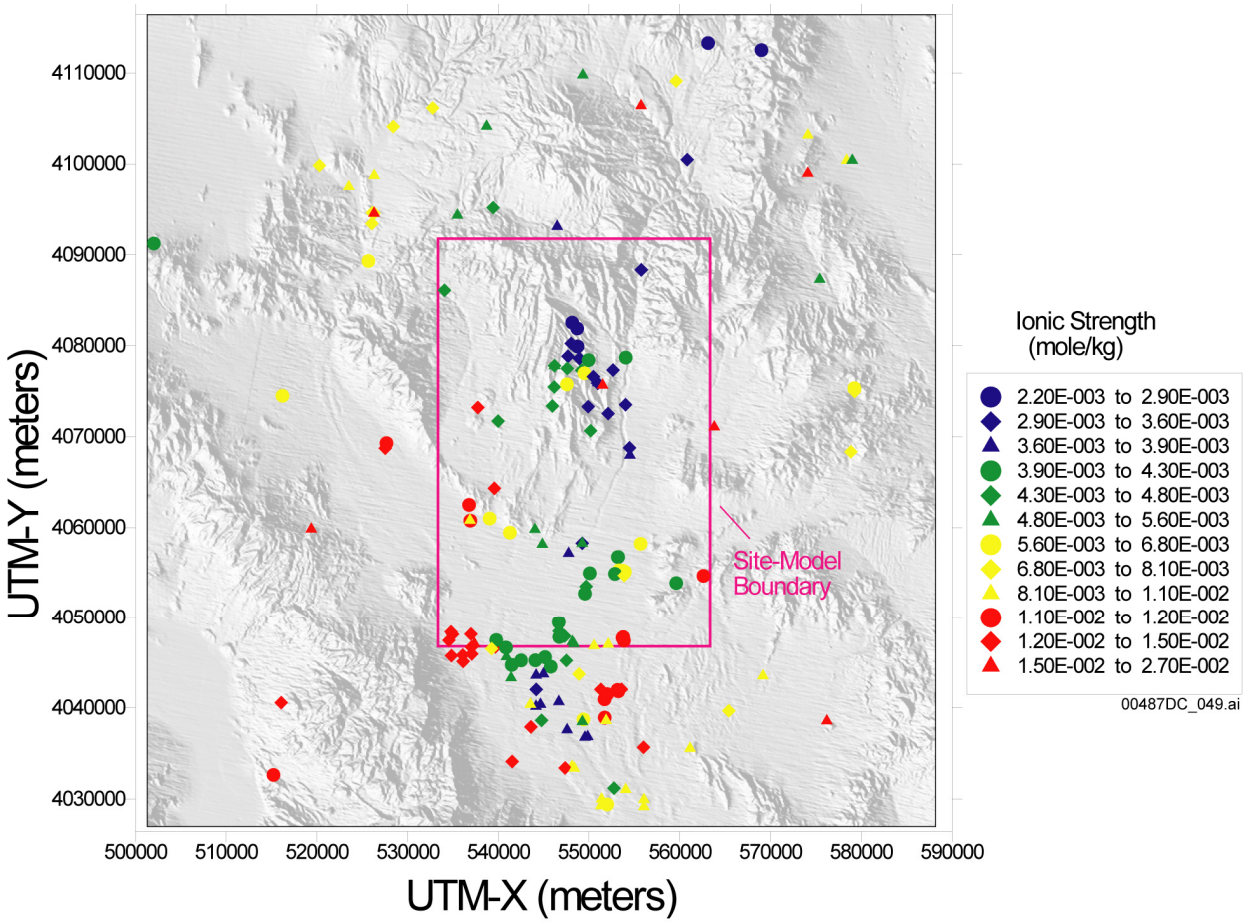

Sources: Table A6-1; DTN: LA0310EK831232.001 [DIRS 165995].

NOTE: This figure has color-coded data points and should not be read in a black and white version.

UTM-X = UTM-Easting; UTM-Y = UTM-Northing; and UTM=Universal Transverse Mercator.

Figure A6-34. Areal Distribution of Ionic Strength in Groundwater

A6.3.5.2 Dissolved Inorganic Carbon

Dissolved inorganic carbon (DIC) represents the total amount of carbon present in all dissolved carbon species, including H_2CO_3, HCO_3^-, and CO_3^{2-}. It is expressed in Table A6-6 and Figure A6-35 as the mg/L HCO_3^- having the same number of moles of carbon per liter. Although alkalinity changes can result from groundwater interactions with noncarbonate rocks, the DIC of groundwater can change only if the groundwater: (1) mixes with groundwater having different DIC concentrations, (2) dissolves carbon-bearing minerals such as calcite or dolomite, (3) precipitates calcite, or (4) interacts with CO_2(g) in the overlying unsaturated zone. The last process tends to be of limited importance due to the very low diffusion of CO_2(g) in water. Hence, in the absence of mixing, downgradient increases in DIC are a good indicator of contact between groundwater and either calcite or dolomite.

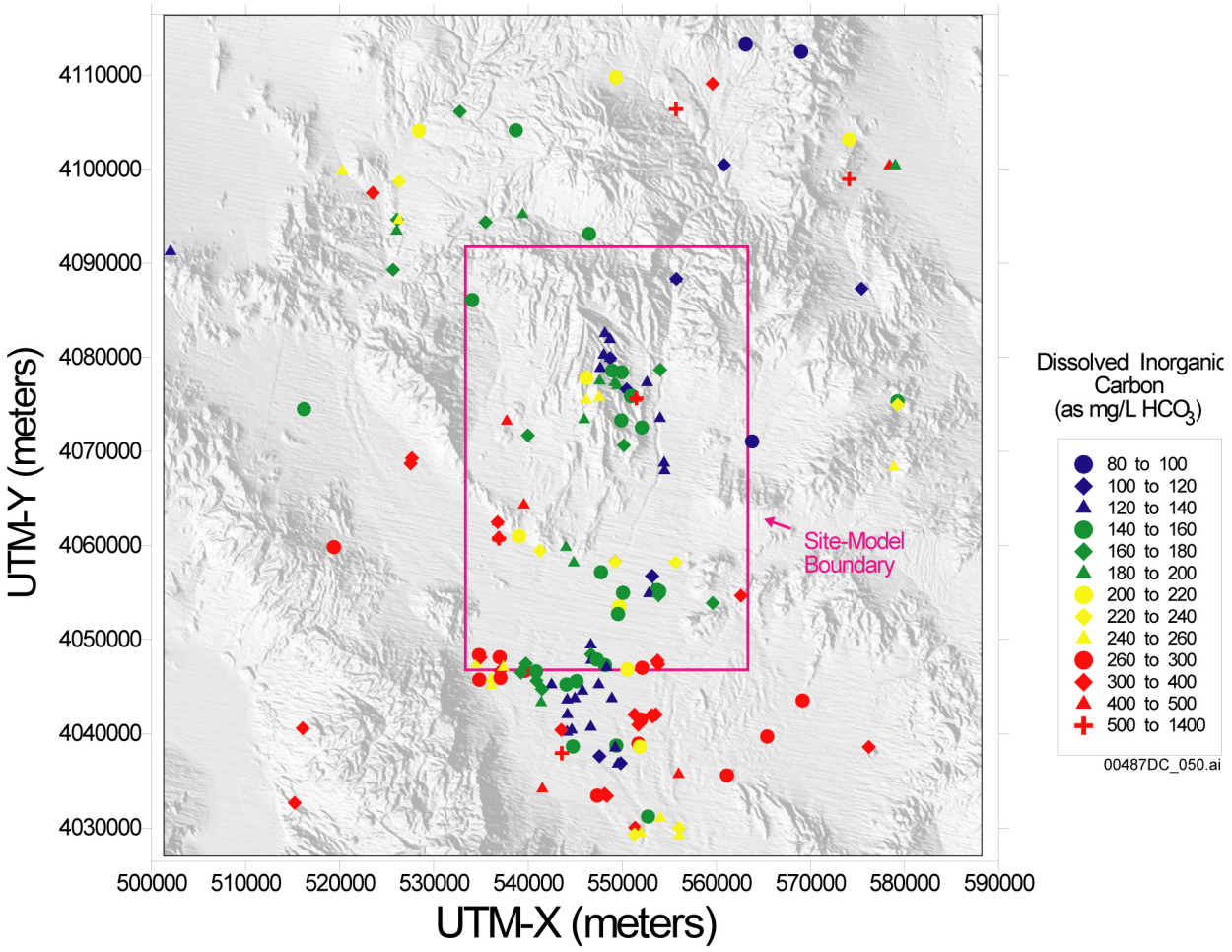

Sources: Table A6-1; DTN: LA0310EK831232.001 [DIRS 165995].

NOTE: This figure has color-coded data points and should not be read in a black and white version.

UTM-X = UTM-Easting; UTM-Y = UTM-Northing; and UTM=Universal Transverse Mercator.

Figure A6-35. Areal Distribution of Dissolved Inorganic Carbon in Groundwater

Groundwater in the northern part of Yucca Mountain has relatively low concentrations of DIC (Figure A6-35). Somewhat higher DIC concentrations are found near Solitario Canyon in some of the SCW and YM-CR wells. Groundwater DIC concentrations increase toward the south at Yucca Mountain. The groundwater in Beatty Wash directly north of Yucca Mountain at well ER-EC-07 (Site 24) has similarly low DIC concentrations as northern Yucca Mountain, as does groundwater at most of the FMW-N wells northeast and east of Yucca Mountain. Southward along Fortymile Wash, the DIC concentrations of groundwater in the FMW-S wells increases and then decreases slightly but are generally low compared to the higher values found in groundwater in the surrounding AR, AR/FMW, and GF area wells. Groundwater in several of the wells in the Amargosa Valley area (LW group) has DIC concentrations that are nearly as low as that found at well J-11 (Site 67) in Jackass Flats. Groundwater in western and southwestern Crater Flat has much higher DIC concentrations than groundwater in the eastern part of the Crater Flat area, reflecting the presence of carbonate rocks at Bare Mountain.

A6.3.5.3 Dissolved Carbon-Dioxide Partial Pressure

The logarithm of dissolved carbon-dioxide partial pressure [log P_{CO_2} (atm)] is generally higher than expected due to equilibrium with the atmosphere (log P_{CO_2} = –3.5 atm) because of the much higher carbon-dioxide partial pressures found in the soil zone through which the water recharging the groundwater has passed. Soil-zone log P_{CO_2} values can be –2.0 atm or greater depending on climate and vegetation cover. Unsaturated-zone log P_{CO_2} at Yucca Mountain under the present climate is about –3.0 atm (Yang et al. 1996 [DIRS 100194]; Thorstenson et al. 1998 [DIRS 126827]). However, CO_2(g) production rates in the soil zones depend on climate, which has changed over time and presently changes with elevation and latitude (Quade and Cerling 1990 [DIRS 100073]), so unsaturated zone log P_{CO_2} values could have been higher under past wetter climates. Most Yucca Mountain area groundwaters have log P_{CO_2} values that are higher than are found in the unsaturated zone at Yucca Mountain.

In the absence of climate change, the tendency in groundwater is for log P_{CO_2} values to decrease downgradient from the recharge area as hydrogen ions and dissolved CO_2 react with the rock to form secondary minerals and HCO_3^- (Drever 1988 [DIRS 118564]). However, as stated above, climate change and other conditions particular to the recharge area can complicate this simple model.

At Yucca Mountain, groundwater in the Solitario Canyon and Yucca Crest area generally has lower log P_{CO_2} values than groundwater further to the east at Yucca Mountain (Figure A6-36). Along Fortymile Wash, groundwater log P_{CO_2} values show an overall southward decrease between the FMW-N and FMW-S area wells. Groundwater log P_{CO_2} values for well J-11 (Site 67) in Jackass Flats and at some LW area wells are also relatively low, whereas log P_{CO_2} values are relatively high at wells in southwest Crater Flat and AR and AR/FMW area wells.

A6.3.5.4 Calcite Saturation Index

In general, calcite saturation indices ($SI_{calcite}$) are expected to increase along a flow path as H^+ ions and dissolved CO_2 are converted to HCO_3^- and CO_3^{2-} during silicate weathering reactions or Ca^{2+} and HCO_3^- are added to the groundwater from calcite dissolution. Downgradient decreases in $SI_{calcite}$ could result from loss of Ca^{2+} through mineral precipitation or ion exchange.

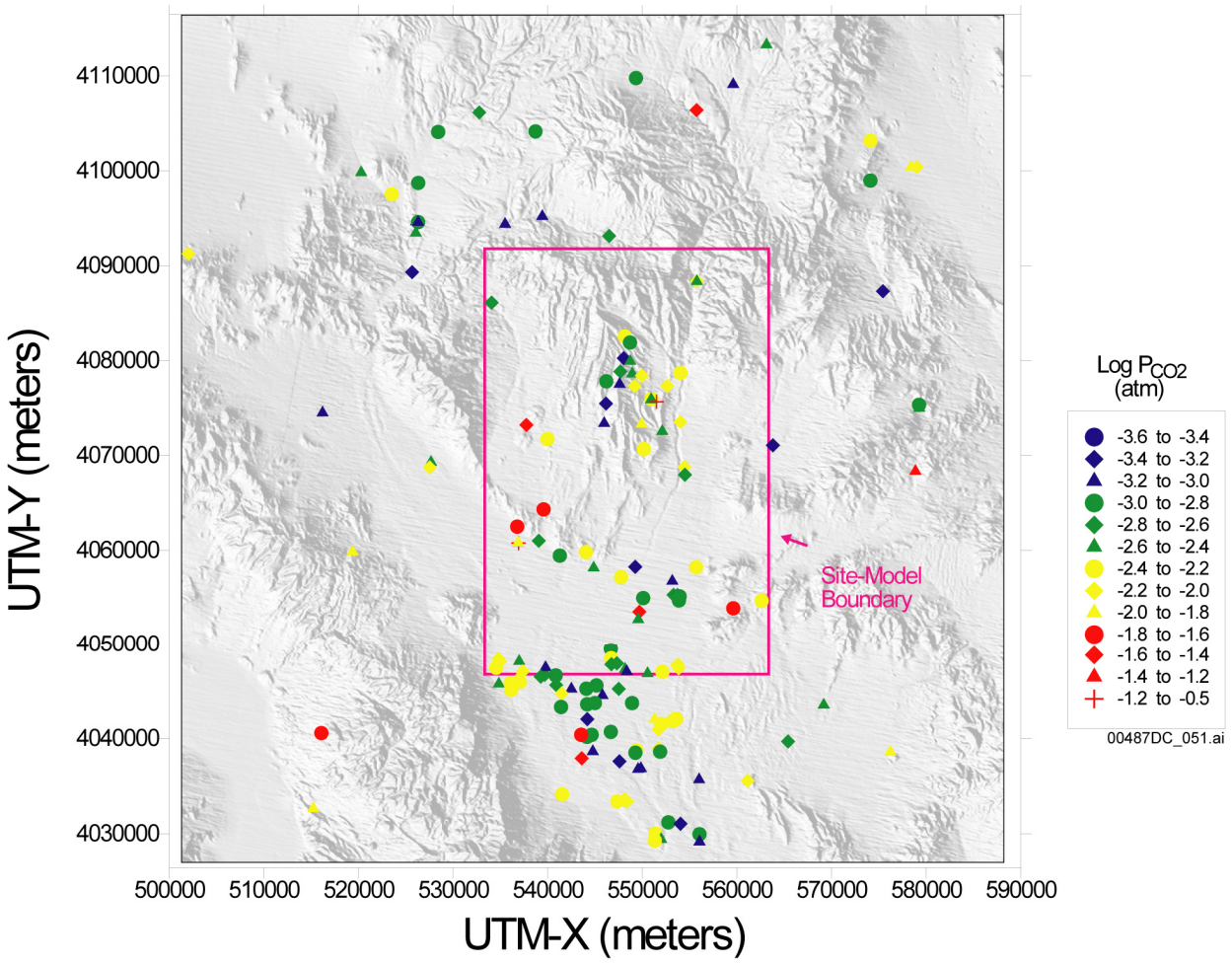

Sources: Table A6-1; DTN: LA0310EK831232.001 [DIRS 165995].

NOTE: This figure has color-coded data points and should not be read in a black and white version.

UTM-X = UTM-Easting; UTM-Y = UTM-Northing; and UTM=Universal Transverse Mercator.

Figure A6-36. Areal Distribution of Dissolved Carbon-Dioxide Partial Pressure in Groundwater

Groundwater north and northwest of Yucca Mountain in the Timber Mountain and Oasis Valley/Northwest Amargosa areas is generally saturated or supersaturated with calcite (Figure A6-37). Groundwater throughout most of Yucca Mountain is undersaturated with calcite, with the most undersaturated groundwater present in northern Yucca Mountain. Along Fortymile Wash, groundwater shows a southward increase in $SI_{Calcite}$. Almost all groundwater in the Amargosa Desert south of U.S. Highway 95 is saturated or supersaturated with calcite. Groundwater in most of the Crater Flat area is saturated or supersaturated with calcite.

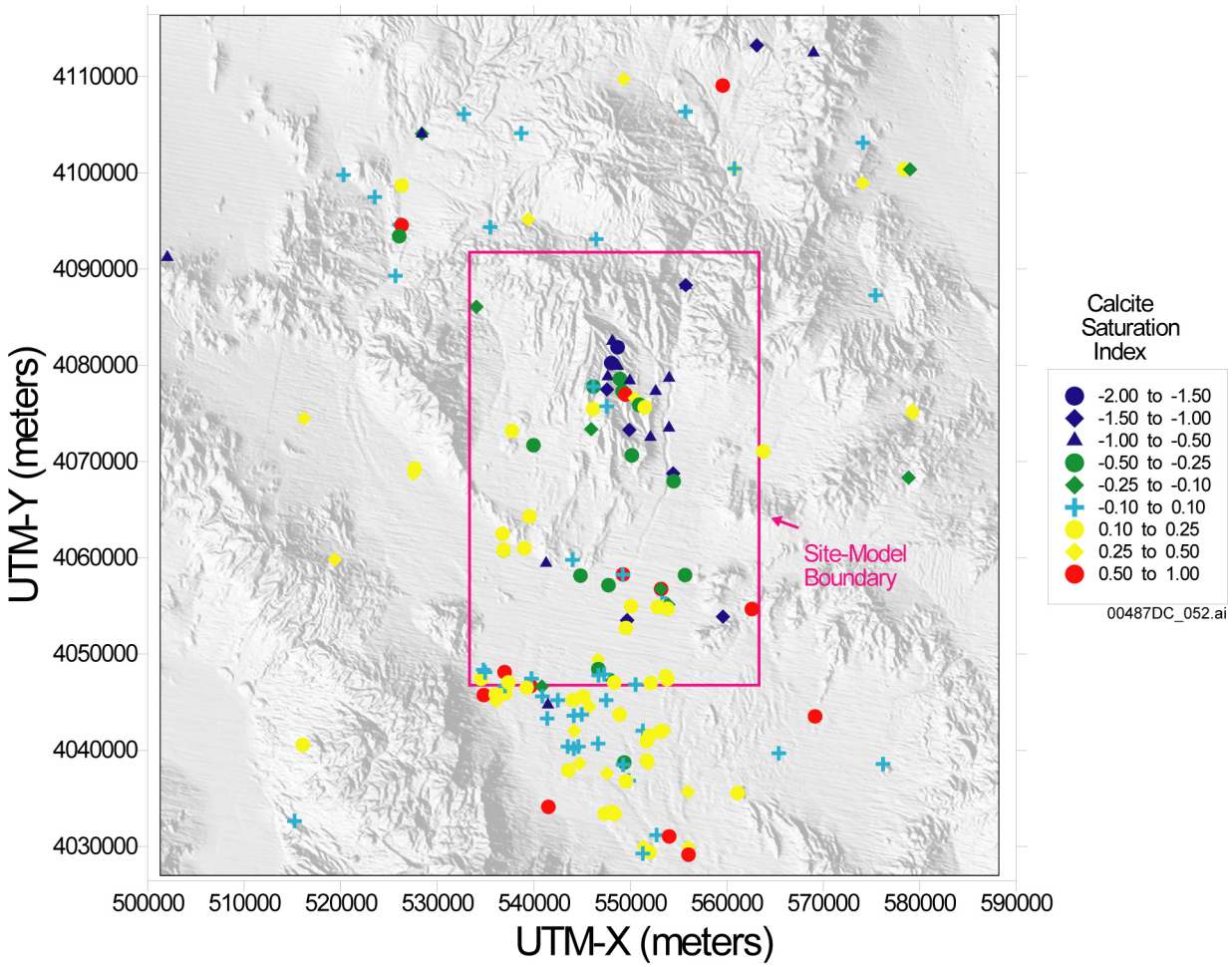

Sources: Table A6-1; DTN: LA0310EK831232.001 [DIRS 165995].

NOTE: This figure has color-coded data points and should not be read in a black and white version.

UTM-X = UTM-Easting; UTM-Y = UTM-Northing; and UTM=Universal Transverse Mercator.

Figure A6-37. Areal Distribution of Calcite Saturation Index in Groundwater

A6.3.5.5 Smectite Saturation Index

Except for a few samples in the Mine Mountain area, groundwater throughout the Yucca Mountain region is supersaturated with smectite (Figure A6-38). The degree of supersaturation increases southward from Yucca Mountain toward the Amargosa Desert. If groundwater from Yucca Mountain and Fortymile Wash flows southward toward the Amargosa Desert, the southward increase in smectite saturation indices suggests that silicate-weathering reactions are providing ions to the groundwater faster than they can be removed by smectite precipitation.

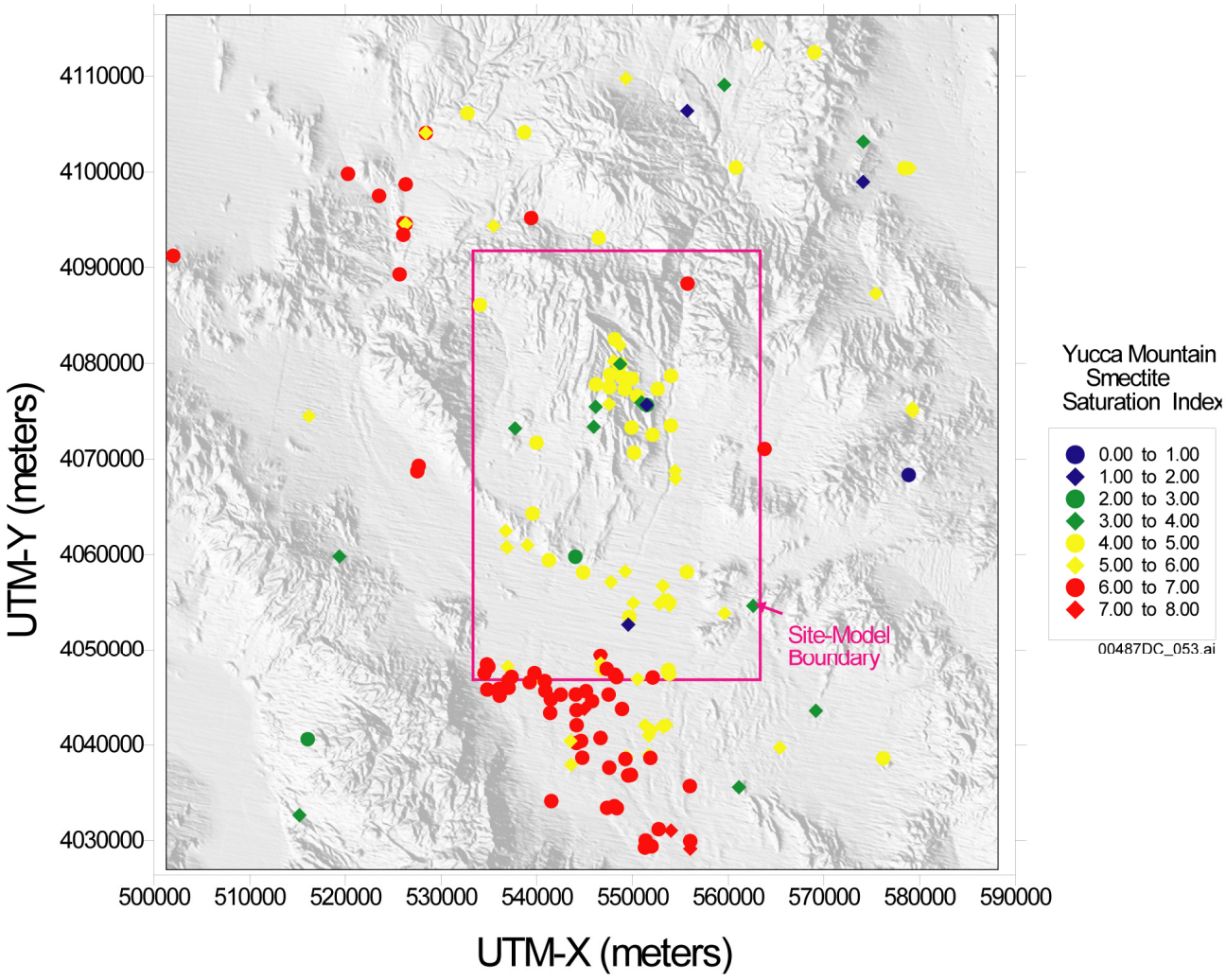

Sources: Table A6-1; DTN: LA0310EK831232.001 [DIRS 165995].

NOTE: This figure has color-coded data points and should not be read in a black and white version.

UTM-X = UTM-Easting; UTM-Y = UTM-Northing; and UTM=Universal Transverse Mercator.

Figure A6-38. Areal Distribution of Smectite Saturation Index in Groundwater

A6.3.5.6 Calcium Clinoptilolite Saturation Index

Throughout most of the Yucca Mountain region, groundwater is also supersaturated with Ca-clinoptilolite (Figure A6-39). As is the case for smectite, the degree of supersaturation increases southward from the Yucca Mountain area toward the Amargosa Desert.

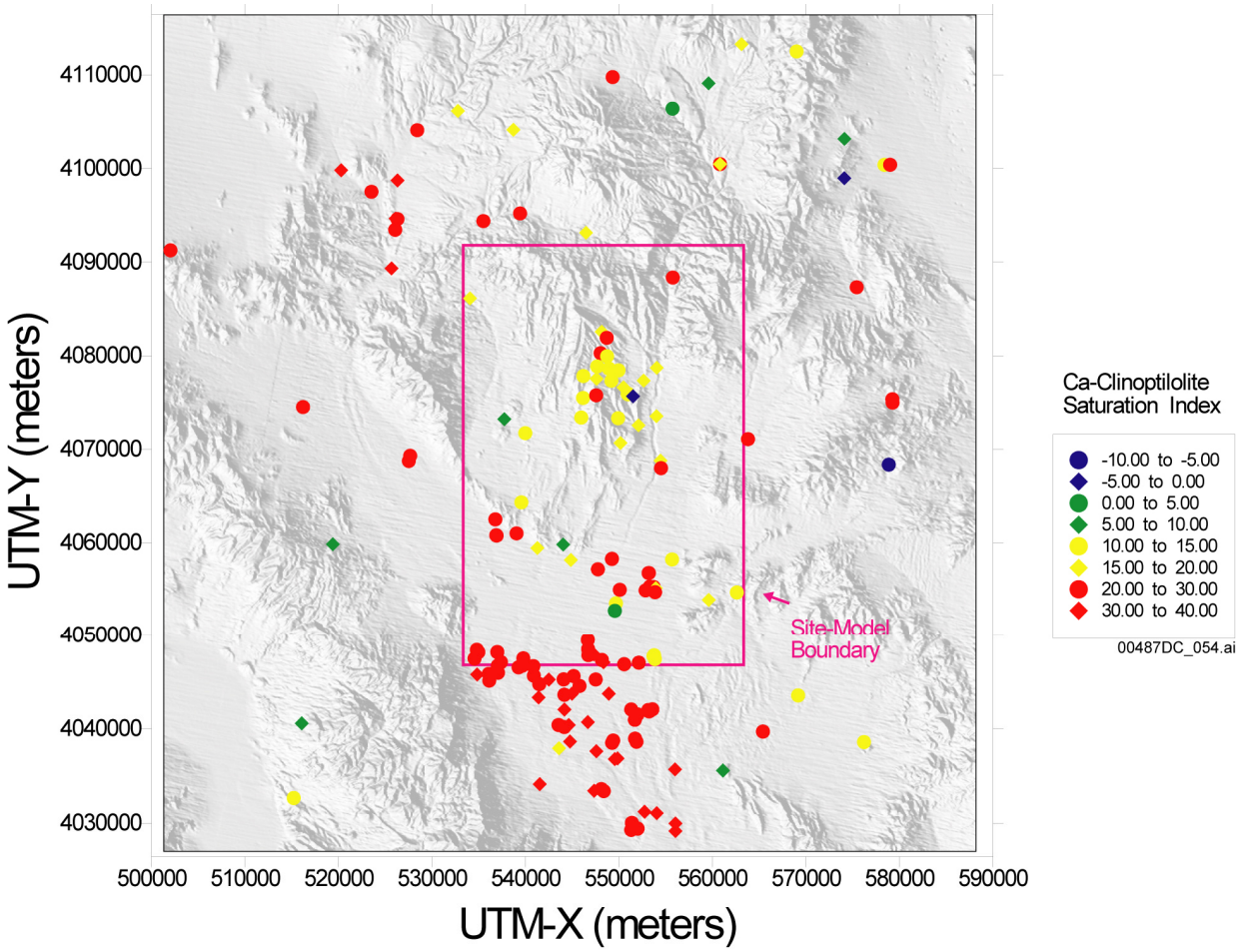

Sources: Table A6-1; DTN: LA0310EK831232.001 [DIRS 165995].

NOTE: This figure has color-coded data points and should not be read in a black and white version.

UTM-X = UTM-Easting; UTM-Y = UTM-Northing; and UTM=Universal Transverse Mercator.

Figure A6-39. Areal Distribution of Calcium Clinoptilolite Saturation Index in Groundwater

A6.3.5.7 Potassium Feldspar Saturation Index

Except for some wells in the Oasis Valley area, the groundwater at most wells along or north of U.S. Highway 95 are undersaturated with K-feldspar (Figure A6-40). Conversely, south of the site model area, most groundwater along or adjacent to Fortymile Wash is saturated or slightly supersaturated with K-feldspar, reflecting the much higher K and dissolved SiO_2 concentrations of groundwater in these areas.

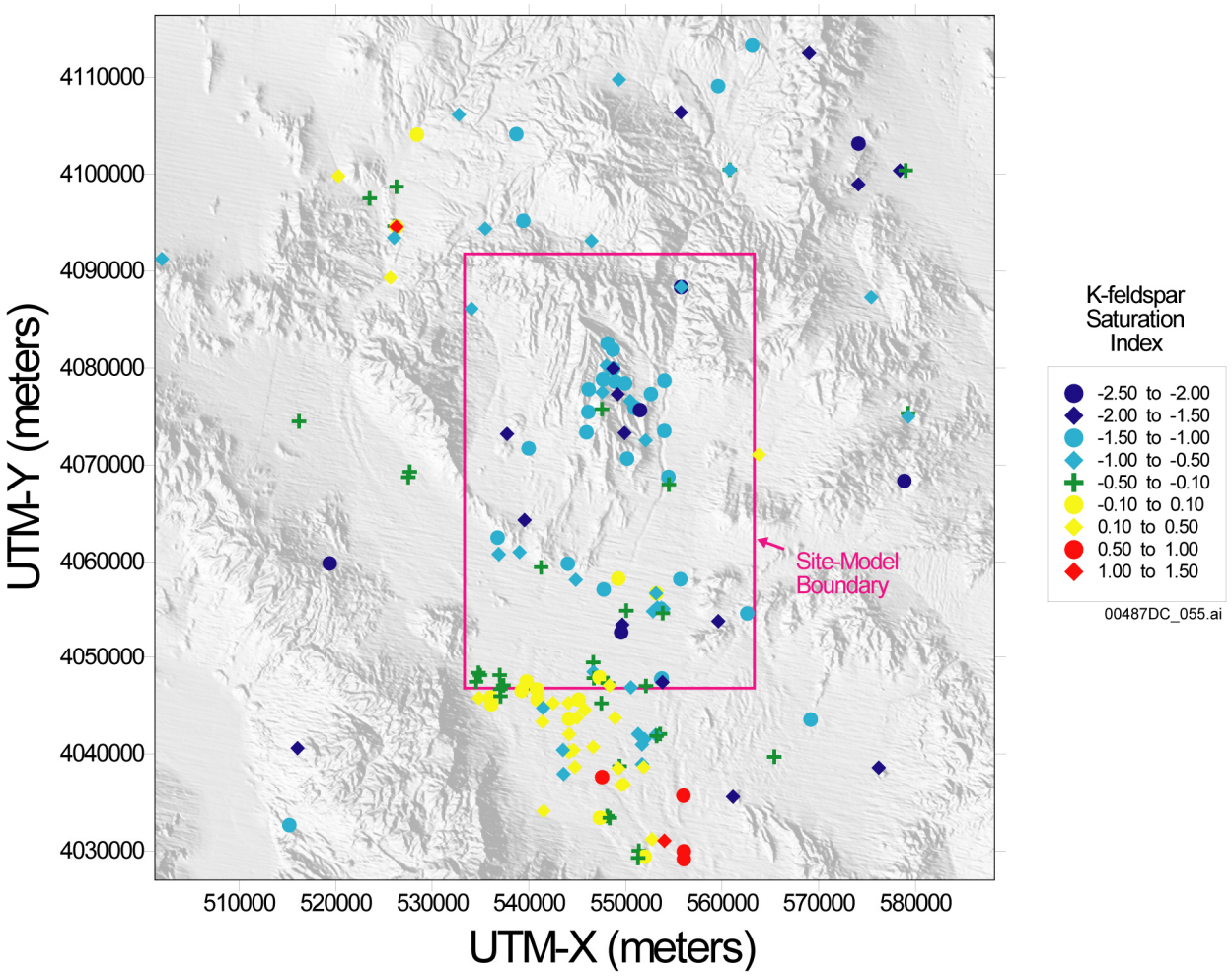

Sources: Table A6-1; DTN: LA0310EK831232.001 [DIRS 165995].

NOTE: This figure has color-coded data points and should not be read in a black and white version.

UTM-X = UTM-Easting; UTM-Y = UTM-Northing; and UTM=Universal Transverse Mercator.

Figure A6-40. Areal Distribution of K-Feldspar Saturation Index in Groundwater

A6.3.5.8 Summary of Areal Distribution of Calculated Geochemical Parameters

If groundwater is moving southward from Yucca Mountain and Fortymile Wash into the northern Amargosa Desert, the areal distributions of calculated geochemical parameters presented in Table A6-3 and shown in Figures A6-34 to A6-40, combined with the areal distribution plots shown in Section A6.3.4, provide some insight into the potential reactions affecting groundwater compositions. Groundwater in these areas has low and relatively constant Cl^- concentrations (6 to 8 mg/L) compared to surrounding areas, and so downgradient changes in composition and in saturation indices can be attributed to water/rock interaction rather then evaporation.

Silicate weathering reactions are indicated by the overall increase in dissolved SiO_2 near the southern boundary of the SZ site model (Figure A6–3.6) and increases in pH (Figure A6–3.1), HCO_3^- (Figure A6–3.4), and $SI_{calcite}$ (Figure A6-37). Weathering of primary silicate minerals like plagioclase or K-feldspar typically involves the consumption of H^+ ions and dissolved CO_2 and the production of cations, HCO_3^-, dissolved SiO_2, and secondary minerals like kaolinite or smectite, consistent with these trends (Drever 1988 [DIRS 118564], p. 151; Langmuir 1997 [DIRS 100051], p. 325). The overall southward increase in $SI_{K\text{-}feldspar}$ (Figure A6-40) and accompanying increase in $SI_{Smectite}$ (Figure A6-38) and $SI_{Ca\text{-}clinoptilolite}$ (Figure A6-39) indicate that, if secondary minerals are precipitated, the primary silicate dissolution reactions may be faster than the precipitation rates for the secondary minerals. The extreme supersaturation of smectite and Ca-clinoptilolite may be indicating that these precipitation reactions are kinetically inhibited.

The saturation indices of alumino-silicate minerals are based on the apparent control of Al^{3+} concentrations by kaolinite (Figure A6-33). Kaolinite has been documented only in trace amounts in the Yucca Mountain area, unlike zeolites, which are prevalent throughout the saturated zone near Yucca Mountain (Vaniman et al. 1996 [DIRS 105946]). Although this assumption is somewhat empirical (see Table A5-1, Assumption 2), it is reasonable because reaction pathways represented on phase-stability diagrams typically represent kaolinite as an intermediate weathering product that is eventually replaced by more stable secondary phases (Drever 1988 [DIRS 118564], Figure 8-8, pp. 156 to 158; Langmuir 1997 [DIRS 100051], Figure 9.14).

A6.3.6 Sources and Evolution of Groundwater beneath Yucca Mountain

The following sections provide an analysis of the origin and evolution of groundwater at Yucca Mountain. Data on perched water from the unsaturated zone at Yucca Mountain are presented in Section A6.3.6.1. Perched water compositions are taken to approximate the composition of local recharge from Yucca Mountain itself. Perched water compositions and other groundwaters upgradient from Yucca Mountain are compared to groundwater presently beneath Yucca Mountain evaluate the possible sources of Yucca Mountain groundwaters.

A6.3.6.1 Description of Perched-Water Data

Perched water was encountered in at least five boreholes at Yucca Mountain: USW UZ-14, USW NRG-7a, USW SD-9, USW SD-7, and USW WT-24. The perched-water samples were obtained by bailing or by pumping, depending on factors related to the drilling of the borehole. In general, it is believed that pumping produces a water sample that is more likely to represent in situ chemical and isotopic conditions for the following reasons. Drilling may affect the chemical and isotopic composition of water in the borehole by introducing foreign drilling fluids (generally air) into the water and by grinding the rock, thereby exposing fresh, unaltered rock surfaces that may react with the water. To minimize these drilling effects, a borehole is typically purged of water present in the borehole, and many additional borehole water volumes are pumped from the formation before sampling. This process increases confidence that the water sample represents actual hydrochemical conditions in the formation. In cases for which a water sample is bailed without first pumping the borehole, the water sample may not be representative of in situ hydrochemical conditions.

Of the perched-water samples considered in this analysis, samples from boreholes SD-9 and NRG-7a (Table A6-5) were obtained exclusively by bailing (Yang and Peterman 1999 [DIRS 149596], Table 19) during a hiatus in drilling following the encounter with the perched water. No pumping was done prior to sample collection at these boreholes.

Perched-water samples from UZ-14 (Table A6-5) obtained prior to August 17, 1993, were obtained without first pumping the borehole. Pumped samples were obtained between August 17 and August 27, and an additional bailed sample was taken after pumping on August 31, 1993. A time series of delta strontium-87 ($\delta^{87}Sr$) versus water production showed that $\delta^{87}Sr$ values continued to change until about 12,000 liters had been pumped from the borehole, or sometime after August 25, 1993 (Yang and Peterman 1999 [DIRS 149596], Table 19, Figure 113). Therefore, the $\delta^{87}Sr$ data, and likely other data, obtained from samples collected from UZ-14 after this date probably best represent in situ conditions. These samples include UZ-14 PT-4 and UZ-14 D (Table A6-5).

Perched water from borehole SD-7 sampled on March 8, 1995, was obtained by bailing prior to pumping. Perched-water samples obtained from borehole SD-7 between March 16 and March 21, 1995, were obtained by pumping (Yang et al. 1996 [DIRS 100194], p. 37).

Perched water was sampled by pumping from borehole WT-24. However, according to Patterson et al. (1998 [DIRS 107402], p. 277), the isotopic data obtained prior to the end of the 24-hour pumping test conducted on October 21 to 22, 1997, were collected during what the authors considered a clean-out period. Only data collected from borehole WT-24 following this clean-out period are presented in this report.

In summary, the perched-water data are thought to represent in situ conditions to varying degrees, depending on whether the samples were bailed or pumped and the extent to which the borehole was cleaned out prior to sampling. The data collected from borehole SD-7 on or after March 16, 1995, from borehole UZ-14 after August 25, 1993, and from borehole WT-24 on or after October 22, 1997, are thought to best represent the actual chemical and isotopic conditions of the perched water at Yucca Mountain. These samples are weighted more heavily than the remaining samples in developing the conclusions of this report.

Table A6-5. Chemical and Isotopic Composition of Perched Water at Yucca Mountain

Water Sample	Depth (m)	Sampling Method	Date	pH	Chemical Concentrations (mg/L)								^{13}C(‰)	^{14}C(pmc)	^{3}H[a] (TU)	δD (‰)	$\delta^{18}O$ (‰)	$^{234}U/^{238}U$ Activity Ratio	$^{36}Cl/Cl$ (x 10^{-15})
					Ca^{2+}	Mg^{2+}	Na^{+}	K^{+}	Cl^{-}	SO_4^{2-}	HCO_3^{-}	SiO_2							
SD-7	479.76	Bailed	03-08-95	—	14.2	0.13	45.5	5.3	4.4	9.1	112	62.3	–10.4	34.4	6.2	–99.8	–13.4	—	511
	488.29	Pumped	03-16-95	8.1	13.3	0.13	45.5	5.3	4.1	9.1	128	57.4	–9.4	28.6	—	–99.7	–13.3	—	—
	488.29	Pumped	03-17-95	8.2	12.8	0.08	45.8	5.5	4.1	8.6	130	50.9	–9.5	28.4	—	–99.6	–13.4	3.504	657
	488.29	Pumped	03-20-95	8.0	12.9	0.07	45.5	5.4	4.1	8.5	127	55	–9.5	27.9	—	–99.6	–13.4	3.58	—
	488.29	Pumped	03-21-95	8.2	13.5	0.08	44.6	5.5	4.1	10.3	128	55.9	–9.5	28.4	< 0.3	–99.6	–13.3	3.69	609, 635
SD-9	—	Bailed	03-07-94	—	—	—	—	—	—	—	—	—	–14.4	41.8	0	–97.8	–13.3	—	—
	—	Bailed	07-07-94	—	—	—	—	—	—	—	—	—	—	—	—	—	—	2.42[b]	—
	453.85	Bailed	07-17-94	8.6	2.9	0.2	98	9.8	5.6	27.6	197[c]	64.2	–14.4	41.8	0	–97.8	–13.3	—	449
	—	Bailed	09-12-94	—	—	—	—	—	—	—	—	—	—	—	—	—	—	2.42[b]	497
UZ-14 A	384.60	Bailed	08-02-93	7.6	23	1.8	39	5.6	7.9	14.3	150	34.2	–10.2	41.7	0.3	–98.6	–13.8	—	559
UZ-14 A2	384.60	Bailed	08-02-93	7.8	24	1.8	38	3.9	9.1	13.8	148.8	36.4	–10.1	40.6	3.1	–97.5	–13.5	—	538
UZ-14 B	387.68	Bailed	08-03-93	8.1	31	2.7	40	4.4	8.3	16.3	147.6	51.4	–9.5	36.6	0	–97.1	–13.4	—	566
UZ-14 C	390.75	Bailed	08-05-93	8.3	45	4.1	88	5.8	15.5	223	106.1	7.7	–9.2	66.8	0.4	–87.4	–12.1	—	389
UZ-14 PT-1	390.75	Pumped	08-17-93	—	37	3.1	40	6.3	7.2	57.3	144	21.4	–9.8	32.3	1.8	–97.8	–13.3	—	644
UZ-14 PT-2	390.75	Pumped	08-19-93	—	30	2.4	35	3.3	7.0	22.9	144	25.7	—	28.9	3.1	–97.9	–13.4	—	656
UZ-14 PT-4	390.75	Pumped	08-27-93	—	27	2.1	34	1.8	6.7	14.1	141.5	32.1	–9.6	27.2	0	–97.3	–13.4	7.56	675
UZ-14 D	390.75	Bailed	08-31-93	7.8	31	2.5	35	4.1	7.0	24.2	146.4	40.7	–11.3	29.2	0	–97.6	–13.1	—	690

Table A6-5. Chemical and Isotopic Composition of Perched Water at Yucca Mountain (Continued)

Water Sample	Depth (m)	Sampling Method	Date	pH	Chemical Concentrations (mg/L)								^{13}C(‰)	^{14}C (pmc)	^{3}H[a] (TU)	δD (‰)	$\delta^{18}O$ (‰)	$^{234}U/^{238}U$ Activity Ratio	$^{36}Cl/Cl$ ($\times 10^{-15}$)
					Ca^{2+}	Mg^{2+}	Na^{+}	K^{+}	Cl^{-}	SO_4^{2-}	HCO_3^{-}	SiO_2							
WT-24[d]	—	Pumped	10-22-97	8.1	23	1.4	37	2.4	9.0	16	135	46	–11.8	29.6	<0.3	–99.4	–13.5	8.34	596
		Pumped	12-10-97	8.6	18.0	1.3	37.5	2.9	8.9	16.0	121.0	36.5	–10.8	—	—	–100.6	–13.5	8.12	—
NRG-7a	—	Bailed	03-04-94	—	—	—	—	—	—	—	—	—	—	—	—	—	—	5.17[b]	518
	460.25	Bailed	03-07-94	8.7	3	0	42	6.8	7	4	114	9	–16.6	66.9	10	–93.9	–12.8	—	491
	—	Bailed	03-08-94	—	—	—	—	—	—	—	—	—	—	—	—	—	—	—	474

Sources: DTNs: GS980108312322.005 [DIRS 149617] (ions, pH, $\delta^{13}C$, δD, $\delta^{18}O$, ^{3}H)[d], GS950808312322.001[DIRS 148114] (^{3}H), GS010808312322.004 [DIRS 156007] ($^{234}U/^{238}U$ activity ratios), GS951208312272.002 [DIRS 151649] (^{3}H), LAJF831222AQ98.011[DIRS 145402] ($^{36}Cl/Cl$), MO0007GNDWTRIS.013 [DIRS 151504] ($\delta^{13}C$, δD, $\delta^{18}O$, ^{14}C), MO0007MAJIONPH.016 [DIRS 151533] (ions and pH), GS980908312322.008 [DIRS 145412] (^{14}C)[d].

NOTES: "—" not available.

[a] Tritium analyses have an accuracy of plus or minus 12 TU.
[b] These results are not representative of in situ conditions due to sample contamination.
[c] This sample also contains 10 mg/L CO_3^{2-}.
[d] Average values of samples collected on the indicated date.

A6.3.6.2 Evidence from $^{234}U/^{238}U$ Activity Ratios for Local Recharge

Precipitation typically contains low concentrations of solutes, including uranium. As the precipitation infiltrates through the soil, uranium is dissolved from the readily soluble soil components. Measured $^{234}U/^{238}U$ activity ratios in secondary minerals formed in soil zones on Yucca Mountain range from 1.4 to 1.8 reflecting both enrichment and dissolution processes (DTNs: GS010608315215.002 [DIRS 156187], GS970808315215.012 [DIRS 145921], and GS980908312322.009 [DIRS 118977]). Pore waters extracted from a small number of core samples from the unsaturated zone at Yucca Mountain have $^{234}U/^{238}U$ activity ratios that range from 1.5 to 3.8. Pore waters extracted from the top of the Paintbrush tuff nonwelded hydrogeologic unit (PTn) have $^{234}U/^{238}U$ activity ratios of 1.5 to 2.5, whereas pore waters from the stratigraphically lower upper lithophysal unit of the welded Topopah Spring tuff (Tpt) have $^{234}U/^{238}U$ activity ratios of 2.5 to 3.8 (DTN: MO0012URANISOT.000 [DIRS 153384], pp. 1 to 4). These data, as well as data from fracture-lining minerals (Paces et al. 1998 [DIRS 107408], Figure 3), suggest a general increase in $^{234}U/^{238}U$ activity ratios in pore waters from the soil zone down through the upper unsaturated zone.

Activity ratios of $^{234}U/^{238}U$ in perched-water samples range from 3.5 at borehole SD-7 to 8.4 at borehole WT-24 (DTNs: GS010608315215.002 [DIRS 156187] and GS010808312322.004 [DIRS 156007]). The values at the high end of this range are unusual and suggest the existence of certain flow conditions. In particular, the high ratios require that the ^{234}U enrichment processes discussed in Section A6.3.1.2.4 dominate over dissolution of uranium-bearing minerals. This situation suggests small water-to-rock ratios. For the unsaturated zone at Yucca Mountain, the high $^{234}U/^{238}U$ ratios are consistent with small water fluxes passing through a fracture network. In fractures with small, and probably intermittent water fluxes, ^{234}U will accumulate over time whereas the relative amount of ^{238}U that may be incorporated into the water via dissolution will likely be small. In this way, a small flux of water flowing through a fracture may preferentially incorporate ^{234}U relative to ^{238}U, resulting in water with an elevated $^{234}U/^{238}U$ ratio, as suggested by Paces et al. (2001 [DIRS 156507] and 2002 [DIRS 158817]). The progressive accumulation of such small water fluxes could result in perched water with the observed high $^{234}U/^{238}U$ ratios. The changes to the $^{234}U/^{238}U$ activity ratios that would occur over time within the perched water depend on the ^{238}U content of the host rock, the weathering characteristics of the rock, the water volume to rock surface area, redox conditions, and other factors (Clark and Fritz 1997 [DIRS 105738], pp. 238 to 240). The $^{234}U/^{238}U$ activity ratio of the perched water may either increase or decrease with time, depending on the relative importance of these factors.

The elevated $^{234}U/^{238}U$ activity ratios found in Yucca Mountain perched water and shallow groundwater are attributable to unsaturated zone flow through the thick sequence of fractured, welded tuffs that constitute the Topopah Spring tuff. Figure A6-41 summarizes the change in $^{234}U/^{238}U$ ratios with depth in the vicinity of Yucca Mountain. In surface water and pore water from the nonwelded PTn, $^{234}U/^{238}U$ activity ratios are small, reflecting the relatively important contribution of ^{238}U from dissolution. Deeper in the subsurface, calcite and opal from the ESF have higher, though variable $^{234}U/^{238}U$ activity ratios. The variability of these ratios is attributed to precipitation of these materials from waters that have experienced variable transport times and paths through the unsaturated zone (Paces et al. 2001 [DIRS 156507], p. 63). Permeable vitric tuffs are absent beneath the Topopah Spring tuff in the northern part of Yucca Mountain

(Rousseau et al. 1999 [DIRS 102097], Figure 16) where perched water has high $^{234}U/^{238}U$. In this part of the mountain, recharge to the saturated zone is estimated to occur mainly along faults and other preferential pathways due to the low permeability of the underlying zeolitic tuffs (BSC 2004 [DIRS 169861], Appendix A and Figure 6.6-3). Toward the southern part of the central block, however, thick permeable vitric intervals are present beneath the Topopah Spring Tuff, and recharge to the saturated zone is expected to take place primarily through these permeable vitric tuffs. Matrix flow through the vitric tuffs may lower the $^{234}U/^{238}U$ activity ratios through bulk−rock dissolution. Support for this hypothesis is provided by comparing the $^{234}U/^{238}U$ activity ratios and U concentrations in perched water below vitric tuffs at borehole SD-7 in southern Yucca Mountain to the $^{234}U/^{238}U$ activity ratios and uranium in perched water at boreholes UZ-14 and WT-24 in northern Yucca Mountain, where vitric tuffs are thin or absent. The relatively low $^{234}U/^{238}U$ activity ratio (3.5) and higher uranium concentrations for perched water at borehole SD-7 compared to perched water in boreholes WT-24 and UZ-14 (Paces et al. 2002 [DIRS 158817], Table 2) are consistent with this conceptual model.

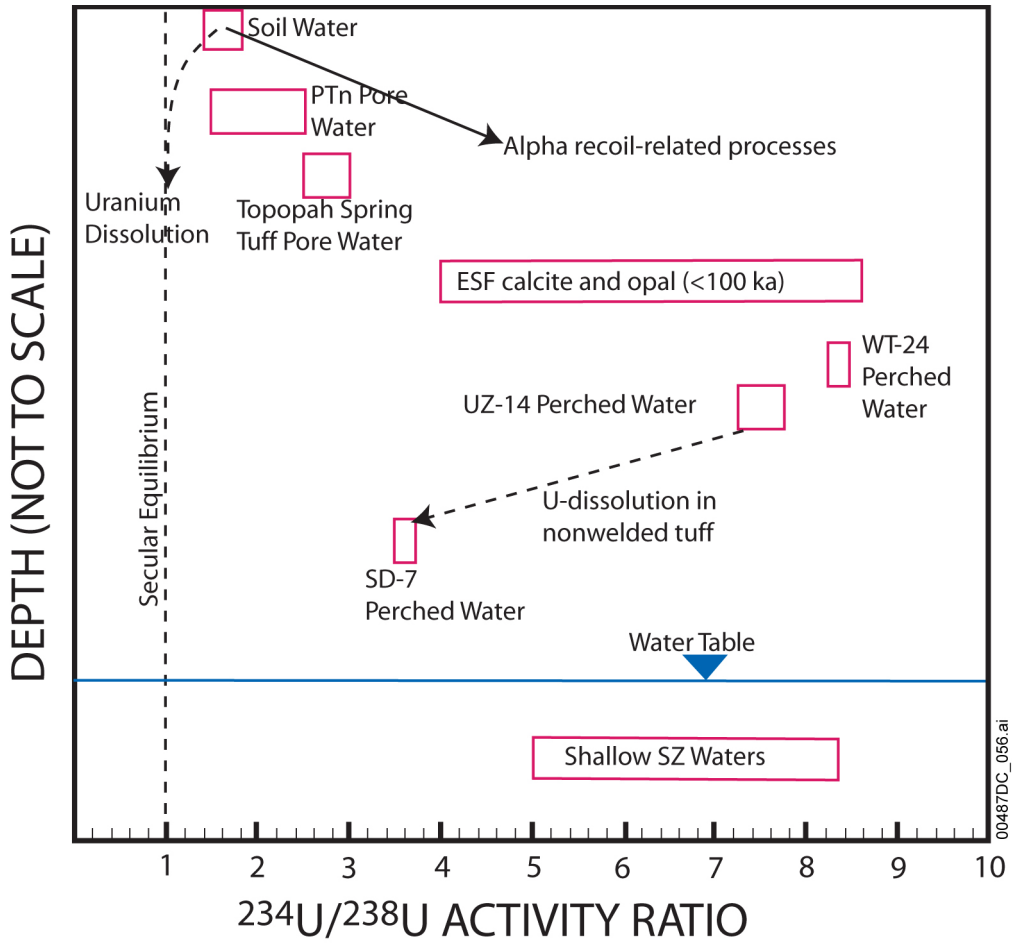

Source: Modified from Paces et al. 2001 [DIRS 156507], Figure 37.

Figure A6-41. Uranium Isotopic Compositions and Schematic Evolutionary Trends at Yucca Mountain

In summary, the high $^{234}U/^{238}U$ activity ratios found in some Yucca Mountain perched water are interpreted to be due to percolation of groundwater through a very thick unsaturated interval of fractured, welded tuff. In the northern part of Yucca Mountain where deep, permeable vitric tuffs are absent and recharge occurs by preferential flow along faults, the relatively high $^{234}U/^{238}U$ activities are unmodified by further bulk-rock dissolution. In the southern part of Yucca Mountain where deep unsaturated flow takes place through the matrix of vitric, nonwelded tuffs, bulk-rock dissolution may reduce the high $^{234}U/^{238}U$ activity ratios acquired by fracture flow through the welded tuffs. One inference of this conceptual model is that the high $^{234}U/^{238}U$ activity ratios found in groundwater near Dune Wash at boreholes WT-3, WT-12, and WT-17 may reflect recharge through areas where deep vitric tuffs are absent, such as north of the Drill Hole Wash area (the reader should note that in this appendix the location WT-3 refers to UE-25 WT #3 and WT-12 refers to UE-25 WT #12). However, the necessary data from the deep unsaturated zone are too few to fully substantiate this hypothesis at this time.

A6.3.6.3 Evidence for Local Recharge from Other Chemical Constituents

This section compares other chemical and isotopic characteristics of perched water and groundwater to further evaluate the concept that Yucca Mountain recharge, as represented by perched water, is the principal source of groundwater beneath Yucca Mountain. Comparisons of perched water analyses from Table A6-5 with SZ groundwater from Yucca Mountain (YM-CR, YM-C, YM-SE, and YM-S groups) and groundwater upgradient from Yucca Mountain in the TM, FMW-N, SCW, and CF groups are shown in Figures A6-42 to A6-46.

The scatter plot of SO_4^{2-} versus Cl^- (Figure A6-42) shows that perched waters pumped from boreholes UZ-14, WT-24, and SD-7 have SO_4^{2-} and Cl^- concentrations that are similar to those of groundwaters at many YM-CR area wells. These concentrations plot near a line, termed the Southern Nevada Precipitation line that was derived by considering how the SO_4^{2-} and Cl^- concentrations measured in precipitation from the Kawich Range, just north of the Nevada Test Site, would change with progressive evaporation. With progressive evaporation, the dissolved SO_4^{2-} and Cl^- concentrations in the remaining water would increase and plot along a line with a slope (2.7) equal to the ratio of their concentrations in precipitation (96 and 35 mg/L, respectively) (Meijer 2002 [DIRS 158813], Table 1). Groundwaters that plot on or near the Southern Nevada Precipitation line are likely to have had most of their SO_4^{2-} and Cl^- derived from atmospheric deposition of salts composed of these ions.

In contrast, other Yucca Mountain groundwaters, particularly groundwaters at some YM-S sites, show elevated SO_4^{2-} concentrations relative to perched water and appear to trend from the perched-water data toward the p#1 mixing line. This line (slope = 5.7) is defined by the origin and groundwater SO_4^{2-} and Cl^- concentrations from the carbonate aquifer at borehole p#1 (160 and 28 mg/L, respectively). Groundwaters that included a component of groundwater from the carbonate aquifer would be expected to trend toward this line, depending on the concentrations of SO_4^{2-} and Cl^- dissolved in the groundwater before mixing occurred. Elevated groundwater SO_4^{2-} concentrations relative to the Southern Nevada Precipitation line could also indicate the addition of SO_4^{2-} through the dissolution of S-bearing minerals like gypsum, pyrite, or alunite.

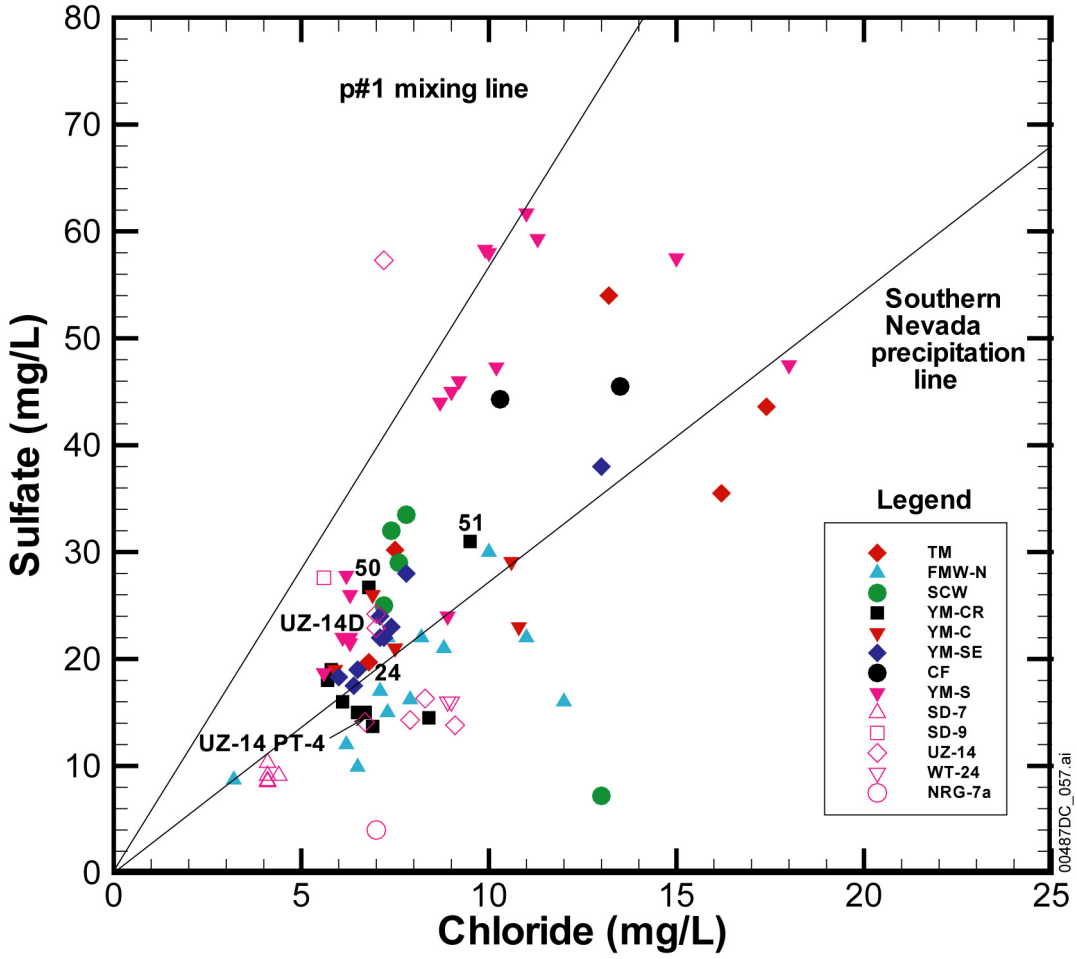

Sources: Tables A6-1 and A6-5.

NOTES: Sample p#1 plots well above limits of the figure. This figure has color-coded data points and should not be read in a black and white version. Perched water data are represented by open symbols. The more representative samples of perched water from borehole UZ-14 are labeled in the figure.

Figure A6-42. Scatter Plot Comparing Sulfate and Chloride Compositions of Perched Waters and Saturated Zone Groundwaters

The scatter plot of $\delta^{13}C$ versus 1/DIC (Figure A6-43) shows that perched water at Yucca Mountain is generally more dilute in DIC and has lighter $\delta^{13}C$ than most Yucca Mountain groundwater, although some groundwater from the YM-CR group in northern Yucca Mountain has comparable DIC and $\delta^{13}C$ values. No systematic differences between the northern (boreholes UZ-14 and WT-24) and central Yucca Mountain perched water (borehole SD-7) compositions are evident in $\delta^{13}C$ and DIC compositions, suggesting the relative uniformity of recharge compositions throughout Yucca Mountain. The Yucca Mountain groundwater shows an overall southward trend toward heavier $\delta^{13}C$ and higher DIC concentrations (lower 1/DIC).

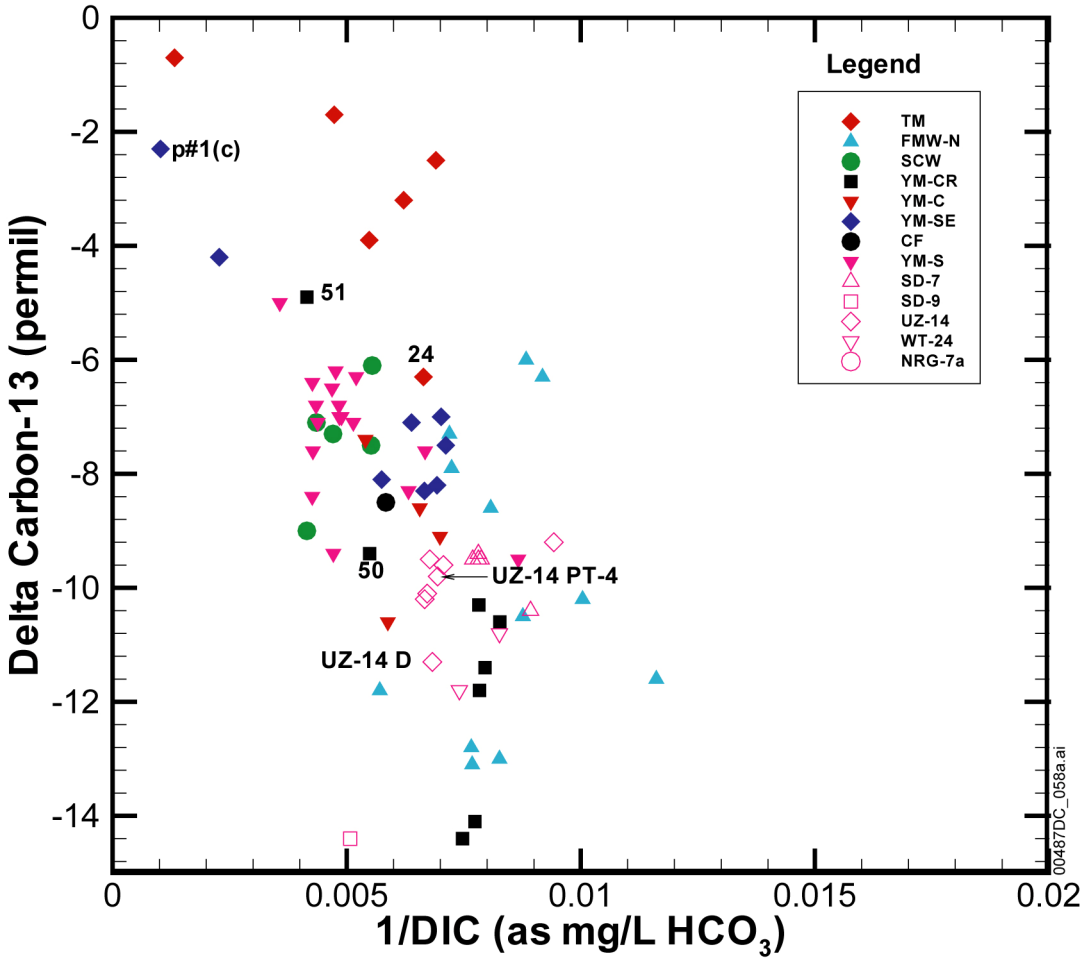

Sources: Tables A6-2, A6-3, and A6-5.

NOTES: This figure has color-coded data points and should not be read in a black and white version. Perched water data are represented by open symbols. The more representative samples of perched water from borehole UZ-14 are labeled in the figure.

Figure A6-43. Scatter Plot Comparing Delta Carbon-13 and Dissolved Inorganic Carbon Compositions of Perched Waters and Saturated Zone Groundwaters

Perched groundwater at Yucca Mountain has $\delta^{18}O$ and δD compositions that are slightly heavier in δD but generally similar to many YM-CR groundwaters (Figure A6-44). Elsewhere at Yucca Mountain, groundwaters tend to be lighter in δD than the perched water. There is an overall southward trend toward lighter δD among the YM-CR, YM-C, YM-SE and YM-S groups.

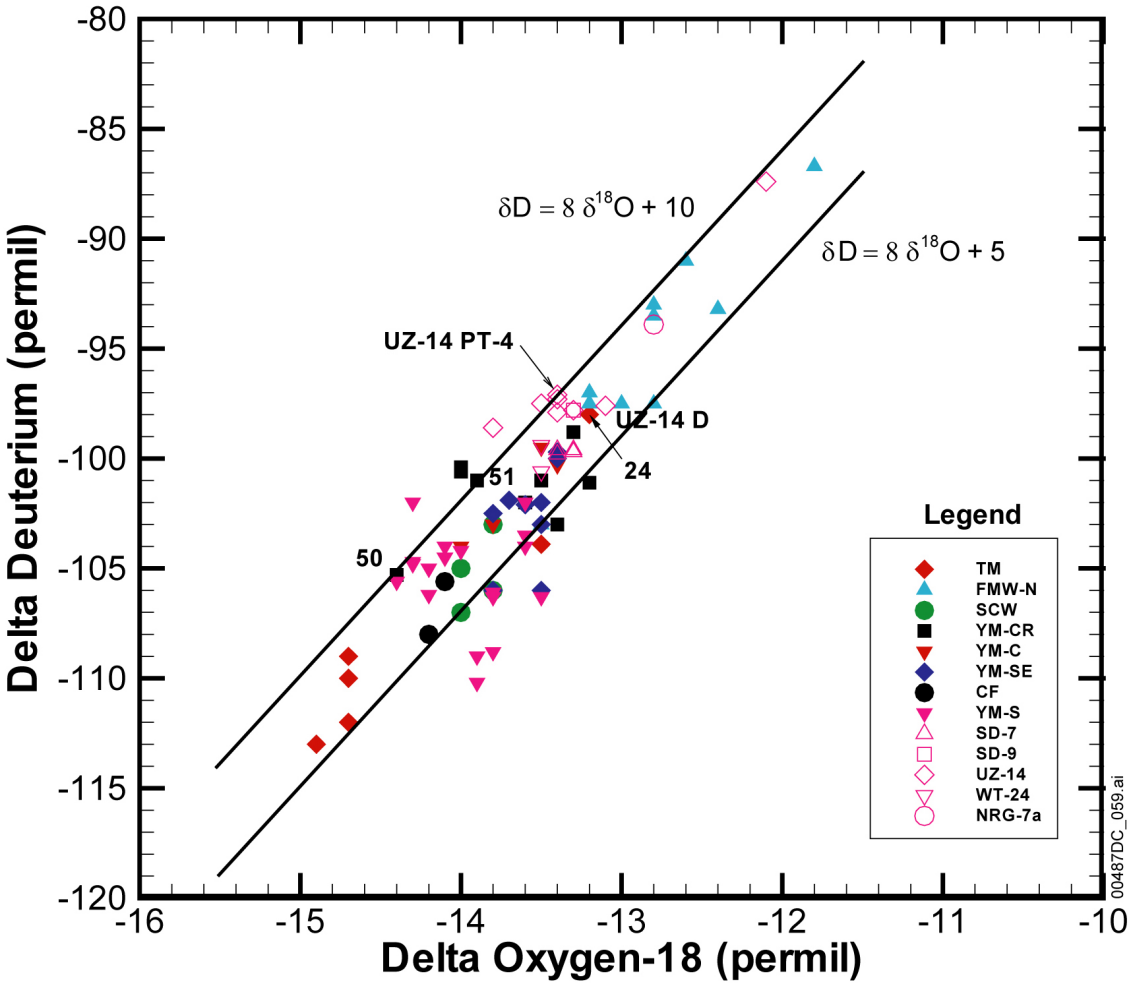

Sources: Tables A6-2 and A6-5.

NOTE: This figure has color-coded data points and should not be read in a black and white version. The solid lines are the global meteoric water line (δD = 8 δ^{18}O + 10) (Clark and Fritz 1997 [DIRS 105738], p. 36) and a possible paleometeoric water line for southern Nevada (δD = 8 δ^{18}O + 5) (White and Chuma 1987 [DIRS 108871], pp. 573 to 574). Perched water data are represented by open symbols. The more representative samples of perched water from borehole UZ-14 are labeled in the figure.

Figure A6-44. Scatter Plot Comparing Delta Deuterium and Delta Oxygen-18 Data for Perched Water and Groundwater near Yucca Mountain

Perched waters at Yucca Mountain have ^{14}C activities that are higher than most Yucca Mountain area groundwaters (Figure A6-45). As discussed in connection with Figure A6-43, the δ^{13}C values of perched water are comparable to or lighter than all but a few of the Yucca Mountain area groundwaters. These groundwaters show a southward trend toward heavier δ^{13}C and lower ^{14}C activities.

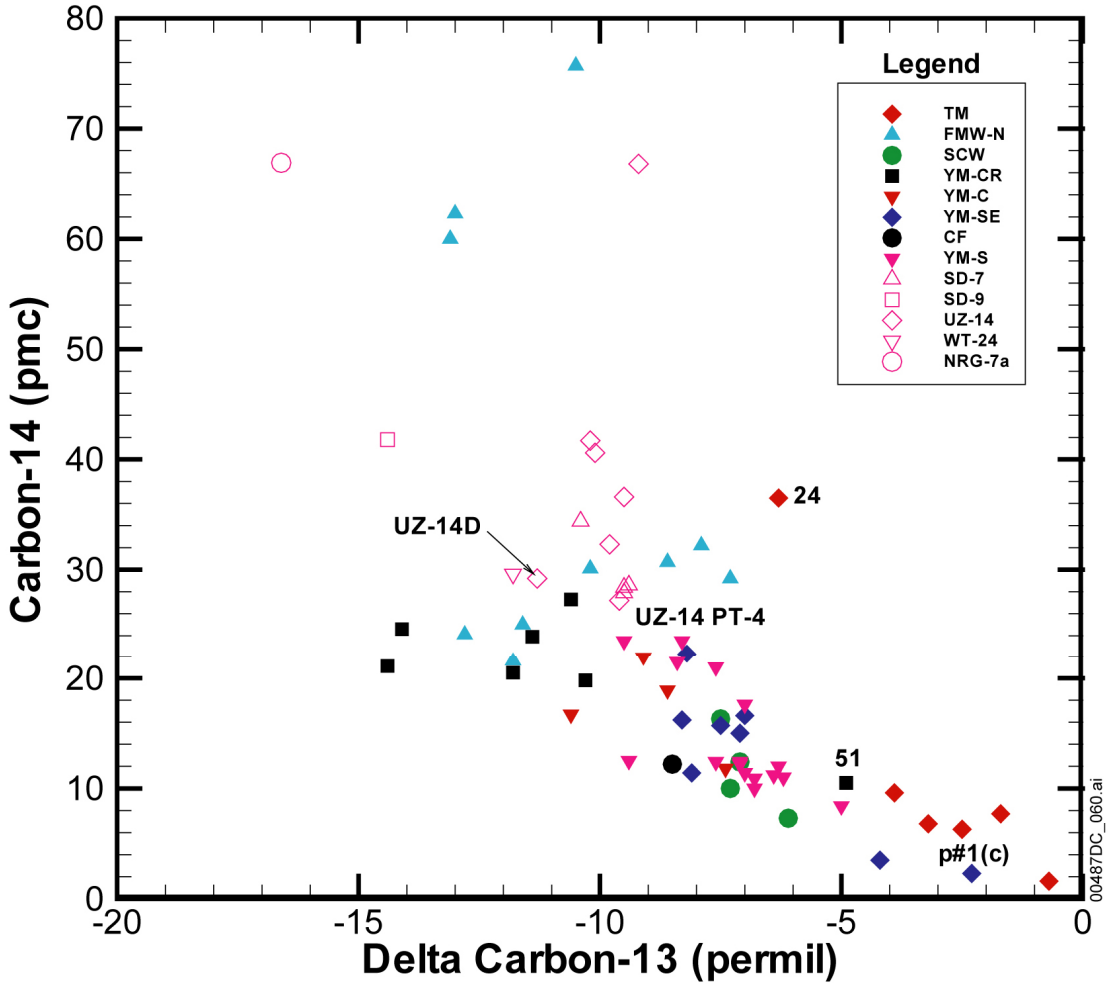

Sources: Tables A6-2 and A6-5.

NOTE: This figure has color-coded data points and should not be read in a black and white version. Perched water data are represented by open symbols. The more representative samples of perched water from borehole UZ-14 are labeled in the figure.

Figure A6-45. ^{14}C Activity versus Delta ^{13}C of Perched Water and Groundwater near Yucca Mountain

Perched waters at Yucca Mountain have higher Ca^{2+} and lower Na^{+} concentrations than most Yucca Mountain groundwaters (Figure A6-46). The YM-C and YM-SE area groundwaters are most similar to the perched water with regard to Ca^{2+} and Na^{+} concentrations, whereas most YM-CR and YM-S groundwater have substantially less Ca^{2+} and more Na^{+} than the perched water. Some YM-S groundwaters and one YM-C groundwater (from well H-4) also appear to be affected by mixing with carbonate aquifer groundwater like that found at borehole p#1, indicated by increased Ca^{2+} and Na^{+} concentrations in these groundwaters along a mixing trend defined by the groundwaters from well p#1.

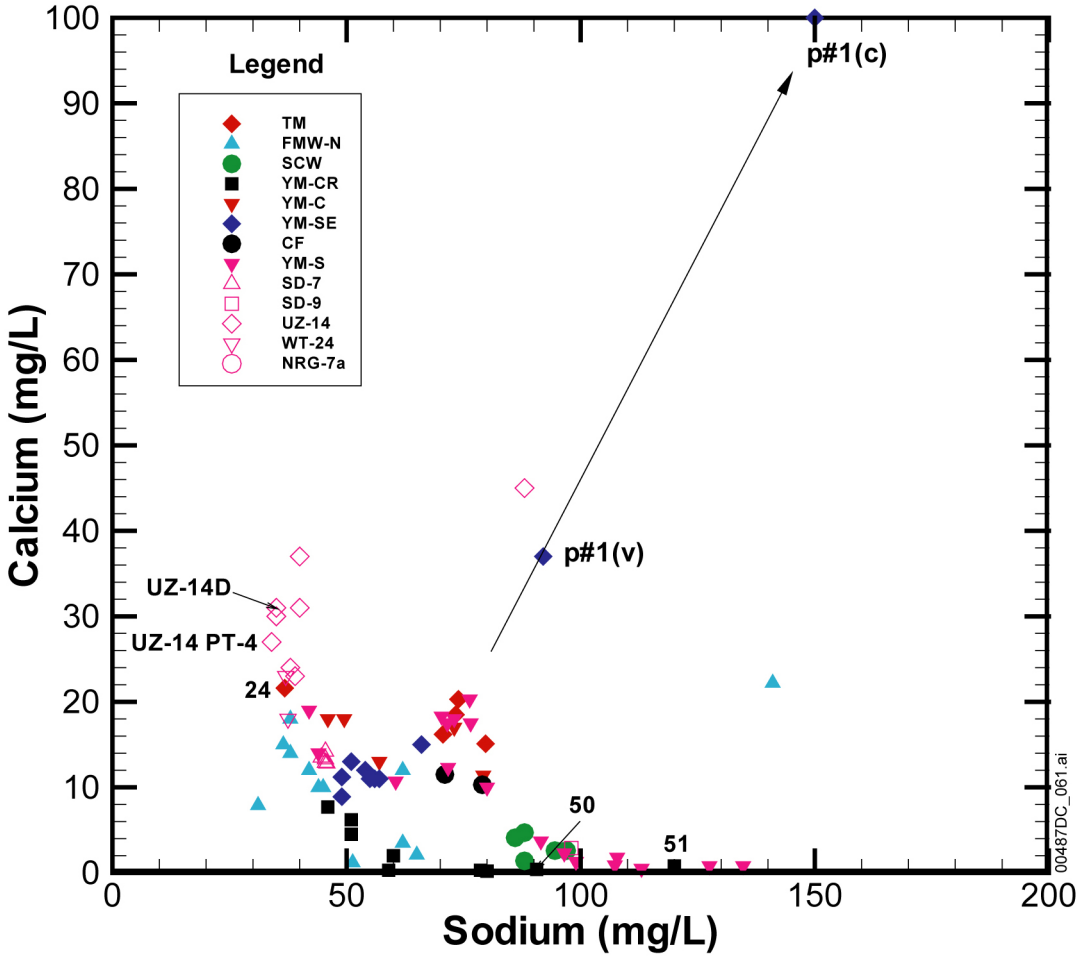

Sources: Tables A6-1 and A6-5.

NOTE: This figure has color-coded data points and should not be read in a black and white version. Perched water data are represented by open symbols. The more representative samples of perched water from borehole UZ-14 are labeled in the figure.

Figure A6-46. Scatter Plot Comparing Calcium and Sodium Compositions of Perched Waters and Saturated Zone Groundwaters

In summary, groundwater chemical and isotopic compositions at Yucca Mountain are compatible with the hypothesis that much or most of the groundwater is derived from local recharge. The perched-water and groundwater Cl^- and SO_4^{2-} concentrations are similar, although southward increases in groundwater SO_4^{2-} concentrations require some additional sources of SO_4^{2-} through water-rock interaction or mixing with groundwater having higher SO_4^{2-} concentrations. Similarly, the $\delta^{13}C$ and DIC concentrations of perched water are similar to those of groundwater in northern Yucca Mountain, but water-rock interactions involving isotopically heavy calcite or mixing with small amounts of a groundwater having high DIC concentrations and heavy $\delta^{13}C$ is required to explain the southward increases in $\delta^{13}C$ and DIC. Perched water $\delta^{18}O$ and δD compositions are similar to those found in groundwater in northern Yucca Mountain but are slightly heavier than those found toward the southern end of the mountain. Because climate change has probably affected the $\delta^{18}O$ and δD composition of recharge over time (see

Section A6.3.1.2), the differences between the perched water $\delta^{18}O$ and δD compositions and groundwater $\delta^{18}O$ and δD compositions elsewhere at Yucca Mountain do not rule out local recharge as a source for these groundwaters. The higher ^{14}C activities of the perched water compared to Yucca Mountain groundwater are compatible with the hypotheses that Yucca Mountain groundwater is derived from local recharge. Groundwater is expected to be older than the recharge from which it is derived. Similarly, the fact that perched water has high Ca^{2+} and lower Na^{+} than the underlying groundwater is compatible with local recharge being the source of the groundwater. Pore-water analyses from the deep unsaturated zone indicate that Ca^{2+} is exchanged for Na^{+} on minerals in the deep unsaturated zone (Meijer 2002 [DIRS 158813], p. 799), consistent with the observed relation between Ca^{2+} and Na^{+} in the perched and SZ waters. Likewise, it appears that other divalent cations like Mg^{2+} and Sr^{2+}, as well as Ca^{2+}, are selectively removed by zeolites in exchange for Na^{+} (and perhaps for K^{+}) in the deep unsaturated zone (Vaniman et al. 2001 [DIRS 157427], Table 2).

A6.3.6.4 Evaluation of Saturated Zone Flow beneath Yucca Mountain

The steep gradient in the potentiometric surface to the north and along the west side of Yucca Mountain requires flow in southerly or easterly directions beneath Yucca Mountain. The N-S and NW-SE fault orientations in the area may also focus flow in these directions. Therefore, if SZ groundwater does contribute to flow beneath Yucca Mountain, then this groundwater would most likely originate from the north, northwest or west. These possibilities are evaluated below.

For the most part, the hydrochemistry of groundwater north of Yucca Mountain that was sampled as part of the NTS Underground Test Area Restoration Project (DTN: LA0311EK831232.001 [DIRS 166068]) differs from that of SZ groundwater beneath Yucca Mountain. As shown in Figures A6-32, A6-33, and A6-42, the Cl^{-} and SO_4^{2-} concentrations of most samples in the Timber Mountain group are substantially higher than those for Yucca Mountain groundwater. Similarly, $\delta^{13}C$ are generally too heavy and the ^{14}C too low for groundwater near Timber Mountain to be the primary source of Yucca Mountain groundwater (Figure A6-45). Only one well (ER-EC-07, Sample 24) in Beatty Wash has Cl^{-}, SO_4^{2-}, $\delta^{13}C$, and ^{14}C values that suggest it could be a major component of the groundwater beneath Yucca Mountain (Figures A6-42 and A6-45). Although limited data for $\delta^{87}Sr$ are available from Yucca Mountain, the $\delta^{87}Sr$ in groundwater from the northernmost well at Yucca Mountain (G-2) is too high for this groundwater to have originated from groundwater at well ER-EC-07 (Figure A6-49). The much higher Sr^{2+} concentrations in groundwater at well ER-EC-07 compared to all northern Yucca Mountain groundwater (Figure A6-48) indicates that acquisition of more radiogenic strontium through water-rock interaction during flow between wells ER-EC-07 and G-2 is not a likely explanation for the difference in $\delta^{87}Sr$ values at these wells.

It has been suggested that water may upwell from the carbonate aquifer into the tuff aquifer of Yucca Mountain (Stuckless et al. 1991 [DIRS 101159]). The Cl^{-} and SO_4^{2-} concentrations in groundwater from borehole p#1(c) are substantially elevated over those of the tuff aquifer, as discussed above. The Cl^{-} and SO_4^{2-} concentrations of groundwater at borehole p#1 are similar to those of groundwater from other areas where carbonate rocks are present (e.g., Crater Flat–SW), suggesting that groundwater from borehole p#1 may be representative of compositions in the carbonate aquifer beneath Yucca Mountain. Groundwater from sample p#1(c) also has much

higher $\delta^{13}C$, lower ^{14}C, and much higher concentrations of DIC, Ca^{2+}, and Na^{+} (Figures A6-43 A6-46) when compared to the tuff aquifer. As is evident from Figures A6-42 to A6-46, most of the groundwater samples from the volcanic aquifer do not resemble the groundwater sampled at p#1(c). These data clearly indicate that groundwater from the carbonate aquifer does not constitute a major part of the groundwater beneath Yucca Mountain. However, the higher Cl^{-} and SO_4^{2-} concentration as well as other constituents (Figure A6-46) of sample p#1(v) are readily explained by mixing between groundwater from the carbonate and volcanic aquifers within the borehole. It is estimated from flow logs that the p#1(v) sample received about 28.6% of its water from the carbonate aquifer as a result of upward flow in the borehole, despite an attempt to isolate the volcanic and carbonate aquifers from each other with a temporary plug (Craig and Robison 1984 [DIRS 101040], p. 49).

Carbon isotope data can be used to limit the amount of mixing of waters in the volcanic and Paleozoic aquifers, as follows. The $\delta^{13}C$ and DIC of the carbonate aquifer at p#1(c) are –2.3 per mil (Table A6-2) and 976.6 mg/L as HCO_3^{-} (Table A6-3), respectively. In contrast, for groundwater samples where uranium isotopes indicate only Yucca Mountain recharge exists (i.e., samples 43, 44, 60, 64, 65, and 66) the average DIC concentration is about 143.6 ± 18.6 mg/L as HCO_3^{-} and the average $\delta^{13}C$ is -9.1 ± 1.4 per mil (Note: uncertainty is given as 1 standard deviation and the $\delta^{13}C$ of sample 59 was used for sample 60). Mixing calculations were done using the composition for sample p#1(c) and the average composition of Yucca Mountain recharge from samples 43, 44, 60, 64, 65, and 66 as end members. The calculations employed the relations $DIC_{mix} = X_c \bullet DIC_c + (1\text{-}X_c) \bullet DIC_v$ and $\delta^{13}C_{mix} \bullet DIC_{mix} = X_c \bullet \delta^{13}C_c \bullet DIC_c + (1\text{-}X_c) \bullet \delta^{13}C_v \bullet DIC_v$, where X_c is the fraction of groundwater from the carbonate aquifer in the mixture and the subscripts *mix, c*, and *v* indicate that the variables pertain to the mixture, carbonate aquifer, and volcanic aquifer, respectively. These calculations indicate that the presence of 10% carbonate aquifer water would increase the DIC and $\delta^{13}C$ of Yucca Mountain recharge water to 227 and –6.2 per mil, respectively; similarly, the presence of 20% carbonate aquifer water in the mixture would increase DIC and $\delta^{13}C$ to 310 and –4.8 per mil, respectively. On the basis of these calculations, groundwater from borehole USW H-3 (Site 51) with a DIC concentration of 240.9 mg/L HCO_3 and a $\delta^{13}C$ of –4.9 per mil may have approximately 10% to 20% carbonate aquifer water. However, all other samples from the Yucca Mountain block have less than 5% carbonate aquifer water. These relatively small amounts of carbonate aquifer water in the volcanic aquifer probably form upper limits because isotopically heavy calcite is present in the volcanic aquifer that, if dissolved, would result in effects on DIC and $\delta^{13}C$ compositions similar to those produced by mixing.

Groundwater from the Solitario Canyon Wash (SCW) area wells is similar with respect to most chemical and isotopic constituents to groundwater in the southern Yucca Mountain (YM-S) well grouping and to groundwater from wells H-3 (Site 51) and SD-6 (Site 50) in the Yucca Crest (YM-CR) grouping (Figures A6-42 to A6-46). The chemical and isotopic similarities between the SCW and YM-S groupings indicates the generally southward flow of groundwater from the SCW area wells, whereas the chemical and isotopic similarities between groundwaters at wells H-3 and SD-6 and SCW area groundwater is compatible with at least a small amount of groundwater leakage eastward across the Solitario Canyon fault. However, because the vast majority of YM-C and YM-SE area groundwaters appear to be unrelated to groundwater from

the Solitario Canyon area, groundwater leakage from Solitario Canyon to these areas must be relatively small compared to other groundwater sources, such as local recharge.

In summary, considerable hydrochemical evidence exists to support the hypothesis that the bulk of the SZ water beneath Yucca Mountain was derived from local recharge. Similarly, evidence in support of groundwater flow to Yucca Mountain from upgradient areas is weak. Exceptions to this are leakage of groundwater from the Solitario Canyon area into groundwater at wells SD-6 and H-3, and potentially wells in southern Yucca Mountain, including those near Fortymile Wash. Local upwelling of relatively small amounts (generally less than 5%) of carbonate aquifer water into the volcanic aquifer is permitted by the groundwater data from most YM-CR, YM-C, and YM-SE area wells.

On the basis of the above discussions, groundwater beneath Yucca Mountain is best characterized by generally low concentrations of dissolved solids and by high $^{234}U/^{238}U$ activity ratios. Lower $^{234}U/^{238}U$ ratios do not, however, exclude the presence of Yucca Mountain recharge in the groundwater. Low $^{234}U/^{238}U$ activity ratios (less than 6) in downgradient groundwater can result from recharge in southern Yucca Mountain with a lower $^{234}U/^{238}U$ activity ratio, mixing of Yucca Mountain recharge with groundwater from other sources, and water-rock interactions that add dissolved uranium to the groundwater.

A6.3.6.5 Evaluation of Evidence for the Magnitude of Recharge at Yucca Mountain

The magnitude of recharge at Yucca Mountain is estimated in this section on the basis of the concentrations of constituents such as chloride that are considered conservative in groundwater systems of the type present at Yucca Mountain. In particular, the chloride mass balance (CMB) method will be used for this purpose. This method is based on the premise that the flux of Cl^- deposited at the surface equals the flux of Cl^- carried beneath the root zone by infiltrating water. With increasing depth in the root zone, Cl^- concentrations in soil waters increase and apparent infiltration rates decrease as water is extracted by the processes of evapotranspiration (Figure A6-47). However, once soil waters move below the zone of evapotranspiration, they become net infiltration, and their Cl^- concentrations are assumed to remain constant. It is these Cl^- concentrations that are used to calculate net infiltration rates and, ultimately, recharge rates.

The CMB method (e.g., Dettinger 1989 [DIRS 105384], p. 59) uses the following equation to calculate the infiltration rate (I, in mm) when runoff or run-on is negligible:

$$I = (P\ C_0)/C_p \qquad \text{(Eq. A6-7)}$$

where

P is average annual precipitation (mm)

C_0 is average Cl^- concentration in precipitation, including the contribution from dry fallout (mg/L)

C_p is the measured Cl^- concentration in groundwaters (mg/L).

The CMB method (Figure A6-47) assumes steady one-dimensional, downward piston flow, constant average annual precipitation rate, constant average annual Cl^- deposition rate (PC_0), no run-on or run-off, no Cl^- source other than precipitation (e.g., it is assumed that the concentrations of Cl^- brought in by surface runoff and Cl^- released from weathering of surface rocks are negligible), and no Cl^- sink (Table A5-1, Assumption 5). When these conditions are met, the estimates of infiltration rate are equal to the recharge rate at the water table; the terms infiltration rate and recharge rate are used interchangeably in the remainder of this section.

Estimates of recharge using the CMB technique for 15 groundwater basins in Nevada were found to be in fairly good agreement with estimates obtained by the Maxey-Eakin linear step function (Dettinger 1989 [DIRS 105384], p. 75). Using a 6-year study of two upland basins selected as analogue wetter climate sites for Yucca Mountain, Lichty and McKinley (1995 [DIRS 100589], p. 1) showed the CMB method to be more robust than a water-balance modeling approach using a deterministic watershed model for estimating basin-wide recharge for two comparatively wet sites in the Kawich Range north of Yucca Mountain. They attributed the robustness of the CMB method to the small number of measured parameters required as compared to the number of parameters needed for defining a deterministic watershed model.

Point estimates of net infiltration or recharge using the CMB method tend to be less robust than basin-wide estimates because of additional assumptions concerning vertical groundwater flow and surface water flow. Conditions under which these assumptions may not be valid at Yucca Mountain are discussed in another scientific analysis report (BSC 2001 [DIRS 160247], Section A6.9.2.2). Values of net infiltration estimated at Yucca Mountain using the CMB method range from less than 0.5 mm/yr in washes to a maximum of nearly 20 mm/yr beneath ridgetops and side slopes (based on data and calculations in DTNs: LA0002JF831222.001, [DIRS 147077]; LA0002JF831222.002 [DIRS 147079]; LA9909JF831222.010 [DIRS 122733]; LA9909JF831222.012 [DIRS 122736]; and BSC 2001 [DIRS 160247], Section A6.9.2.4), depending on the Cl^- deposition rate assumed in the calculation.

Table A6-6 lists recharge rates calculated from measured groundwater Cl^- concentrations using the CMB method. This method requires that the Cl^- deposition rate, which is the product of precipitation and effective Cl^- concentration in precipitation (including both wet and dry fallout), be known. The average annual precipitation rate for Yucca Mountain is 170 mm (Hevesi et al. 1992 [DIRS 116809], p. 677), and estimates of average Cl^- concentrations in precipitation at Yucca Mountain range from 0.3 to 0.6 mg/L (BSC 2001 [DIRS 160247], Section A6.9.2.3). To bound the recharge rate estimates, Rate 1 in Table A6-6 is calculated using the lower estimate for Cl^- concentration whereas Rate 2 is calculated using the higher estimate. The CMB recharge estimates average 7 ± 1 mm/yr for Rate 1 and 14 ± 2 mm/yr for Rate 2 (Table A6-6). The much narrower range of fluxes estimated for the saturated-zone samples compared to the unsaturated zone samples can probably be attributed to the greater volume averaging of the SZ samples, as well as to mixing in the aquifer and in the borehole when the SZ samples were pumped.

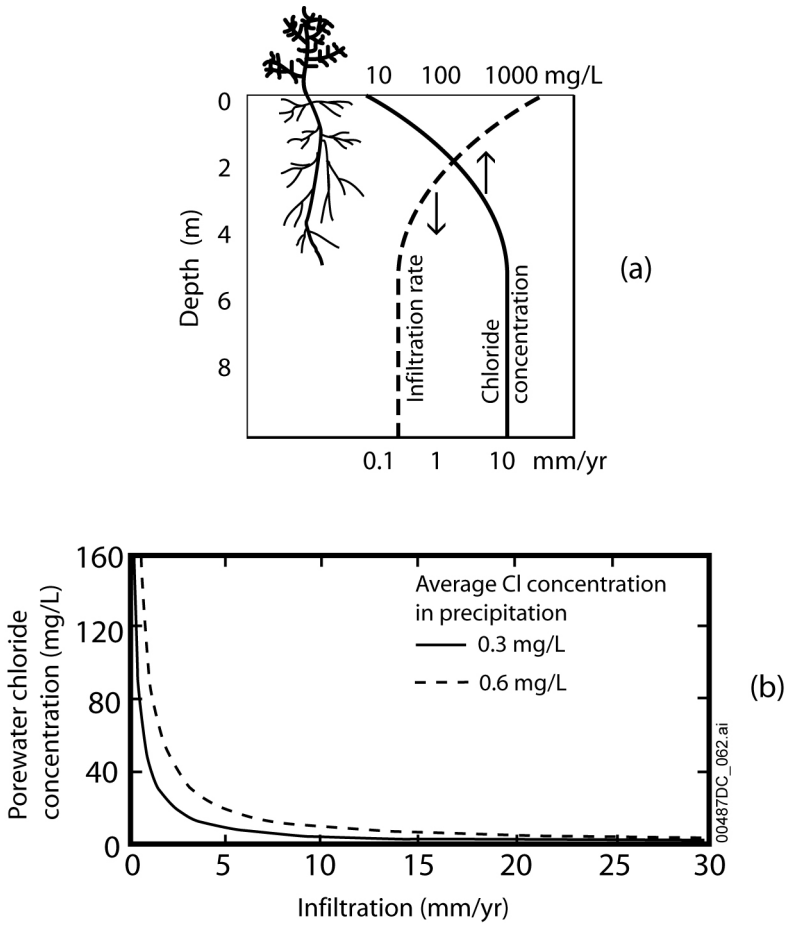

For illustration only.

NOTES: Part (a) illustrates the underlying basis of the CMB method. Part (b) shows porewater Cl^- concentrations as a function of infiltration, assuming a range of chloride deposition rates (106 to 183 mg porewater $Cl^-/(m^2$ year). Using an average annual precipitation rate of 170 mm (Hevesi et al. 1992 [DIRS 116809], p. 677), these deposition rates correspond to effective Cl^- concentrations of 0.62 mg/L to 1.07 mg/L in local precipitation.

Figure A6-47. Chloride Mass-Balance Method for Estimating Infiltration

As indicated in the following section, it appears from interpretations of both stable isotope (δD and $\delta^{18}O$) and ^{14}C data that most of the groundwater presently beneath Yucca Mountain infiltrated in the late Pleistocene, when precipitation and Cl^- deposition rates were potentially different from present conditions. It is estimated from wood rat midden data that mean annual precipitation during the Pleistocene was 1.9 times present precipitation at a 1,500-m elevation and 1.3 times present precipitation at a 750-m elevation (Forester et al. 1999 [DIRS 109425], p. 32). For the elevation range of 1,000 to 1,500-m that encompasses the surface elevations of most wells listed in Table A6-6 (DTN: GS010908312332.002 [DIRS 163555]), an average increase in Pleistocene precipitation of 1.7 times present precipitation can be estimated for Yucca Mountain. However, it is not clear if Cl^- concentrations in precipitation were the same during the Pleistocene or if Cl^- concentrations decreased so that Cl^- deposition rates (the product of P and C_0) were constant or even lower than today. If Cl^- concentrations in precipitation were similar in the late Pleistocene to those of the present day, Pleistocene infiltration rates may have

been approximately 70% higher, on average, than the rates listed in Table A6-6 using present-day precipitation rates and Cl^- concentrations. On the other hand, if Cl^- deposition rates in the Pleistocene were approximately the same as today, as inferred by (Plummer et al. 1997 [DIRS 107034], p. 540) from $^{36}Cl/Cl$ ratios in packrat middens, the infiltration rates listed in Table A6-8 using present-day Cl^- deposition rates are valid.

A6.3.6.6 Evaluation of Evidence for Timing of Recharge

Hydrochemical data that bear on the question of the age or timing of local recharge include hydrogen and oxygen isotope ratios and ^{14}C activities. Hydrogen and oxygen isotope ratios may contain age information because the numerical values of these ratios in groundwaters reflect the climate under which the waters were infiltrated. Therefore, if waters were recharged in a climatic regime different from the current regime, this fact should be reflected in the isotope ratios of the groundwaters.

The activity of ^{14}C in a particular groundwater sample potentially offers a more direct indication of the time at which that groundwater was recharged. In general, the older the sample, the lower the ^{14}C activity. However, the interpretation of the age of a groundwater sample from ^{14}C activity data is complicated by the fact that groundwaters can undergo soil-water-rock-gas interactions that can alter the proportions of carbon isotopes in a groundwater sample. This process, in turn, can lead to modification of the age calculated for the sample based on ^{14}C activity as discussed further below.

Table A6-6. Recharge Rates Based on the Chloride Mass Balance Method

Well Identifier	Chloride concentration (mg/L)	Apparent Recharge Rate[a] (mm/yr)	
		Rate 1	Rate 2
G-2	6.5	7.8	15.7
UZ-14 (sh)	6.9	7.4	14.8
H-1 (Tcp)	5.7	8.9	17.9
b#1(bh)	10.8	4.7	9.4
c#1	7.4	6.9	13.8
c#2	7.1	7.2	14.4
c#3	7.2	7.1	14.2
c#3('95-97)	6.5	7.8	15.7
ONC#1	7.1	7.2	14.4
p#1(v)[b]	13.0	3.9	7.8
G-4	5.9	8.6	17.3
H-3	9.5	5.4	10.7
H-4	6.9	7.4	14.8
H-5	6.1	8.4	16.7
UZ#16	10.6	4.8	9.6
WT#12	7.8	6.5	13.1

Table A6-6. Recharge Rates Based on the Chloride Mass Balance Method (Continued)

Well Identifier	Chloride concentration (mg/L)	Apparent Recharge Rate[a] (mm/yr)	
		Rate 1	Rate 2
WT-17	6.4	7.7	15.5
WT#3	6.0	8.2	16.5

Source: Table A6-1.

[a] Infiltration rates were calculated based on equation (7). Rate 1 is calculated using the lower estimate for Cl^- concentration in precipitation (0.3 g/L); Rate 2 is calculated using the higher estimate (0.6 mg/L). Recharge estimates obtained by the CMB method are based on Table A5-1, Assumption 5.

[b] Approximately 28.6% of the water in this sample is from upward flow in the borehole from the carbonate aquifer (Craig and Robison 1984 [DIRS 101040], p. 49).

A6.3.6.6.1 Evidence for the Timing of Recharge from Hydrogen and Oxygen Isotope Ratios

Many of the effects of seasonal and long-term temperature changes on hydrogen and oxygen values in groundwater described in Section A6.3.1.2.1 have been reported for the Yucca Mountain area. Benson and Klieforth (1989 [DIRS 104370], Figure 11) noted a correlation between $\delta^{18}O$ values and the ^{14}C age of groundwaters near Yucca Mountain. Waters are lighter in $\delta^{18}O$ with increasing age between 9,000 and 18,500 years ago, a trend they attributed to the colder temperatures existing at the time the older water was recharged. Variations in the $\delta^{18}O$ compositions of groundwater discharging in the Ash Meadows area at Devils Hole 55-km southeast of Yucca Mountain were preserved in calcites deposited between 570,000 and 60,000 years before the present (Winograd et al. 1992 [DIRS 100094], Figures 2 and 3). These variations were shown to correlate well with known glacial and interglacial episodes during the period of record, with $\delta^{18}O$ decreasing, on average, by 1.9 per mil during glacial periods.

The δD and $\delta^{18}O$ values of regional groundwater samples and perched-water samples at Yucca Mountain are plotted in Figure A6-48. The modern global meteoric water line ($\delta D = 8\ \delta^{18}O + 10.0$) shown on Figure A6-48 is approximately equal to the local Yucca Mountain meteoric water line ($\delta D = 8\ \delta^{18}O + 8.9$) as defined by Benson and Klieforth (1989 [DIRS 104370], Figure 14) from snow samples obtained from Yucca Mountain. Snow samples were used to define the local meteoric water line because these samples were less likely to be affected by evaporation than rain samples, especially samples of light summer rains that can have a substantial fraction of their volume evaporated before reaching the ground. A paleometeoric water line of $\delta D = 8\ \delta^{18}O + 5.0$ was suggested by White and Chuma (1987 [DIRS 108871], pp. 573 to 574) to fit data from the Amargosa Desert and Oasis Valley.

Although considerable variability in δD and $\delta^{18}O$ values is evident in Figure A6-48, much of this variability is attributable to the heavy δD and $\delta^{18}O$ values of the FMW-N samples and the light δD and $\delta^{18}O$ values of the TM samples. The Yucca Mountain groundwaters (YM groupings only) and most perched waters (excluding NRG-7a and one UZ-14 sample) vary in δD by about 13 per mil and in $\delta^{18}O$ by about 1 per mil. The high ^{14}C activities associated with the

FMW-N groundwater and the low ^{14}C activities associated with the TM groundwater suggest that some of the differences between the δD and $\delta^{18}O$ values in these groups is attributable to changes in the δD and $\delta^{18}O$ composition in response to climate change, with the heavy values representing the composition of groundwater recharged under the modern climate.

Because the groundwaters shown in Figure A6-48 probably originated from different recharge areas and recharge elevations, the effects of climate-induced changes and these other factors are mixed. The effects of time- and climate-induced changes on δD and $\delta^{18}O$ composition can be isolated from these other effects by examining the changes in the composition of pore and perched water with depth in the unsaturated zone at Yucca Mountain (Figure A6-48). In this case, because all of the perched and porewater data from borehole UZ-14 probably originated close to the borehole, the effects of spatial and elevation distributions of recharge are minimal. At borehole UZ-14, the porewater data from borehole UZ-14 show a general trend of lighter δD and $\delta^{18}O$ in the deeper (Tac and Tcp) pore waters and heavier δD and $\delta^{18}O$ in shallow pore waters (PTn). The shallow pore water that results from infiltration at Yucca Mountain is similar in δD and $\delta^{18}O$ composition to the modern groundwater from upper Fortymile Canyon, suggesting that the δD and $\delta^{18}O$ composition of modern precipitation is similar in both locations. Note that none of the porewater data in Figure A6-48 show systematic trends that indicate evaporative effects (Section A6.3.1.2.1, Figure A6-4). This observation suggests that the relatively high porewater salinities observed in the shallow part of this borehole (Yang et al. 1996 [DIRS 100194], Table 3), and perhaps other parts of Yucca Mountain, are due to plant transpiration rather than evaporation (Section A6.3.1.2.1). Other groundwaters from the Yucca Mountain area, like those in the FMW-S group, may indicate more significant evaporative effects (Figure A6-48).

Perched waters from UZ-14 have δD and $\delta^{18}O$ compositions that are intermediate between the shallow and deep pore waters. The deep pore water from the relatively impermeable Tac unit is lighter than the pore water from the underlying, but more permeable Tcp unit, suggesting that it has been more difficult to flush the older, lighter pore water in the Tac with younger water (Yang et al. 1998 [DIRS 101441]). The porewater data indicate that groundwater from the YM-C and YM-SE is similar in composition to the deep pore water from the Tac unit at borehole UZ-14, supportive of their possible origin from local recharge. The decrease in $\delta^{18}O$ composition of about 2 per mil between the shallow pore water and the deep porewater and Yucca Mountain groundwater compositions from the YM-CR, YM-C, and YM-SE groupings is comparable to the approximately 1.9 per mil differences in calcite $\delta^{18}O$ composition at Devils Hole (Winograd et al. 1992 [DIRS 100094], Figure 2) for glacial and subsequent interglacial periods, suggesting the deep pore water and Yucca Mountain groundwater were recharged under a paleoclimatic conditions that existed until the late Pleistocene.

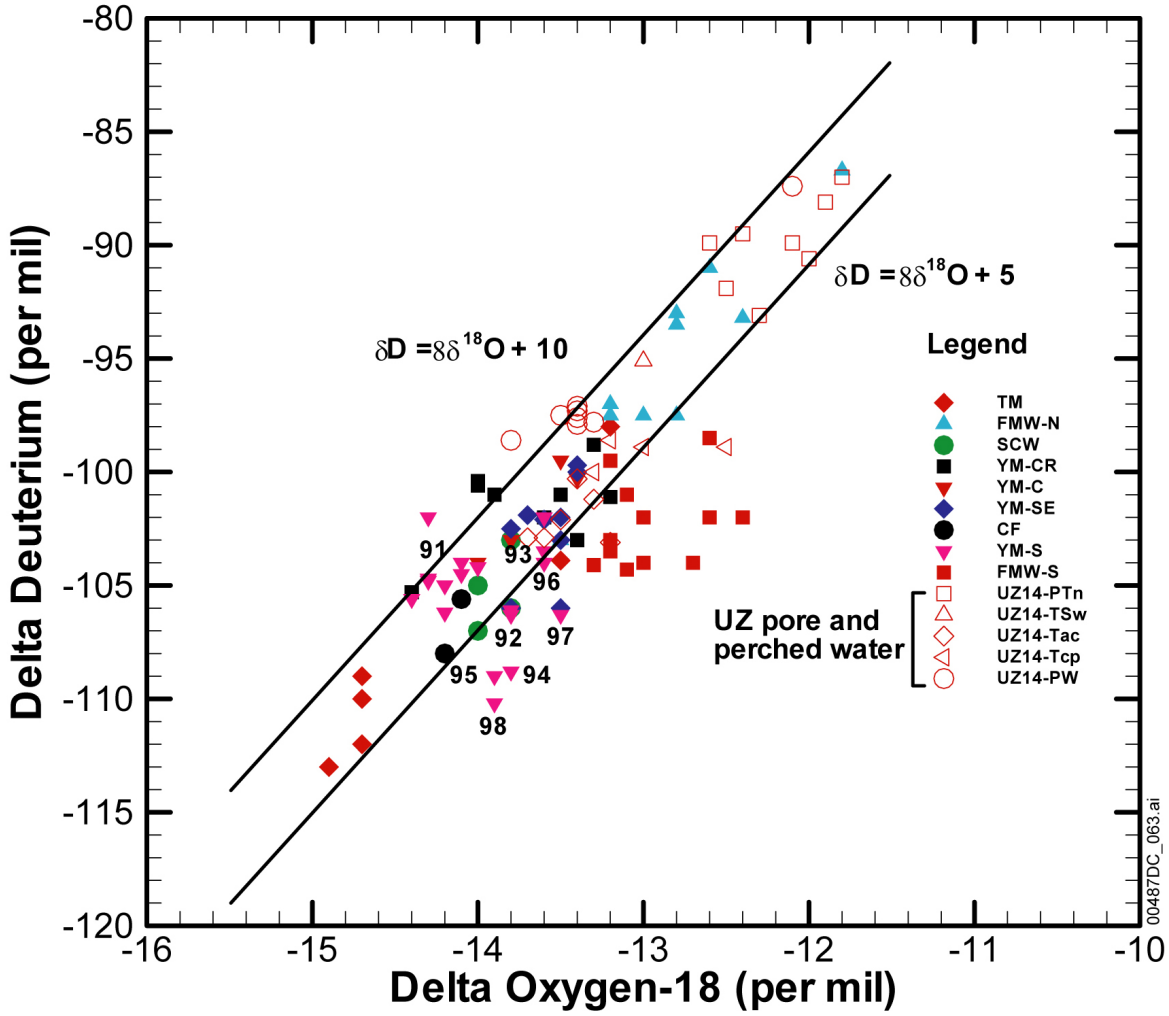

Source: DTN: GS990308312272.002 [DIRS 145692]; Tables A6-2 and A6-5; porewater data for borehole UZ-14 are from Yang et al. 1998 [DIRS 101441] Tables 9–12.

NOTE: This figure has color-coded data points and should not be read in a black and white version. The solid lines are the global meteoric water line (δD = 8 δ^{18}O + 10) (Clark and Fritz 1997 [DIRS 105738], p. 36) and a possible paleometeoric water line for southern Nevada (δD = 8 δ^{18}O + 5) (White and Chuma 1987 [DIRS 108871], pp. 573 to 574).

Figure A6-48. Delta Deuterium and Delta ^{18}O Data for Borehole UZ-14 Unsaturated Zone Pore Water, Perched Water, and Groundwater near Yucca Mountain

In contrast, some of the YM-S area groundwater does not overlap with the deep porewater data from the borehole, raising doubts as to whether it originated predominantly from Yucca Mountain recharge. Many groundwaters from the YM-S group, including Sites 91 (NC-EWDP-2D) and 92 (NC-EWDP-19D composite) near Fortymile Wash are isotopically similar to groundwaters in the Crater Flat (CF) and Solitario Canyon Wash (SCW) groups. Groundwaters from Sites 93 (NC-EWDP-19P) and 96 (NC-EWDP-19D Zone 2) plot nearer to the deep pore water from borehole UZ-14. The remaining groundwater samples from NC-EWDP-19D (Sites 94, 95, 97, and 98) have no clear affinity with groundwater from other areas. In general, it does not appear likely from the δD and δ^{18}O compositions that groundwater

from wells NC-EWDP-2D or NC-EWDP-19D originated from present or paleorecharge along Fortymile Wash, based on the lack of overlap between data from these sites and data from the FMW-N and FMW-S groups. However, for groundwaters from Sites 93 (NC-EWDP-19P) and 96 (NC-EWDP-19D Zone 2), the δD and $\delta^{18}O$ data do not obviously rule out an origin from paleorecharge along Fortymile Wash.

A6.3.6.6.2 Evidence for the Timing of Recharge from Carbon Isotope Data

As is discussed in Section A6.3.1, the ^{14}C ages of groundwater are susceptible to modification through water-rock reactions. Nonetheless, various observations indicate that the ^{14}C ages of the perched-water samples do not require substantial correction for the dissolution of carbonate. First, the ratios of ^{36}Cl to stable chlorine ($^{36}Cl/Cl$) of the perched-water samples are similar to those expected for their uncorrected ^{14}C age, based on reconstructions of $^{36}Cl/Cl$ ratios in precipitation throughout the late Pleistocene and Holocene from packrat midden data (Plummer et al. 1997 [DIRS 107034], Figure 3; DTNs: LAJF831222AQ97.002 [DIRS 145401]; GS950708315131.003 [DIRS 106516]; GS960308315131.001 [DIRS 106517]). Second, Winograd et al. (1992 [DIRS 100094], Figure 2) presented data from calcite deposits that indicated the $\delta^{18}O$ values in precipitation during the Pleistocene were, on average, 1.9 per mil more depleted during pluvial periods compared to interpluvial periods. The $\delta^{18}O$ values of the perched-water samples generally are more depleted than porewater samples from the shallow unsaturated zone at Yucca Mountain by more than 1.0 per mil (Figure A6-48). This consistent difference suggests that, at some boreholes, the perched water may contain a substantial component of water from the Pleistocene.

Values for $\delta^{13}C$ and ^{14}C in perched waters and groundwaters from the Yucca Mountain area are plotted in Figure A6-45. Excluding the perched-water and the Fortymile Wash area (FMW-N) samples, the $\delta^{13}C$ and ^{14}C values reported for the groundwater samples are negatively correlated. In the absence of chemical reactions and/or mixing, waters moving from source areas to Yucca Mountain should experience no change in $\delta^{13}C$, but their ^{14}C activity should decrease with time. If waters infiltrating into the source area had more or less constant $\delta^{13}C$ values, data points for waters infiltrated at different times would form a vertical trend in Figure A6-45. The fact that the data points in the figure do not form a vertical trend suggests either that the $\delta^{13}C$ of waters infiltrated at the source areas are not constant or that chemical reactions or mixing have affected the carbon isotope values. If waters that infiltrate into the source areas have randomly variable $\delta^{13}C$ ratios, then a random relation between $\delta^{13}C$ and ^{14}C values would be expected. Rather the $\delta^{13}C$ and ^{14}C values for Yucca Mountain and Crater Flat groundwaters are well correlated as shown in Figure A6-45.

It has been noted that $\delta^{13}C$ values in infiltrating waters reflect the types of vegetation present at the infiltration point. According to the data of Quade and Cerling (1990 [DIRS 100073], p. 1,550), the $\delta^{13}C$ of modern water infiltrated in cooler climates (for example, at higher elevations) is more negative than for modern water infiltrated in warmer climates (for example, at lower elevations). The change from a relatively wet, cool climate to a relatively warm, dry climate at the end of the Pleistocene would be expected to exert a similar effect on the $\delta^{13}C$ of infiltration as elevation does on modern infiltration. In other words, Pleistocene infiltration would be expected to have lighter $\delta^{13}C$ than modern infiltration at the same elevation. However,

both a climate induced change in $\delta^{13}C$ values, or recharge from a distant, high-elevation source would result in a positive correlation in Figure A6-45 because the older samples (that is, lowest pmc) plotted would tend to have the most negative $\delta^{13}C$ (that is, they infiltrated when the climate was cooler than it is now or in distant, high-elevation areas). Because the observed correlation in the groundwater values is negative instead of positive, the primary cause of the correlation must involve some other process(es). Both calcite dissolution and mixing with groundwater from the carbonate aquifer are possible explanations for this observed trend. Both of these processes would tend to introduce DIC with heavy $\delta^{13}C$ and little ^{14}C. The importance of each process probably varies spatially and can be assessed by determining if increases in other ions and isotopes present at high concentrations in the carbonate aquifer are evident in the groundwater.

A likely cause of the negative correlation evident in Figure A6-45 is the dissolution of carbonate minerals such as calcite. For example, calcite with a $\delta^{13}C$ value of –4 per mil and a ^{14}C activity of zero could readily explain the correlation if it were being dissolved by infiltrating soil waters. This explanation assumes that points on the regression line are of the same age but that the water dissolved different amounts of calcite. In this explanation, the scatter of points about the regression line could represent samples of slightly different ages. For example, δD and $\delta^{18}O$ data suggest that groundwaters from the northern part of Fortymile Wash (FMW-N) and the perched waters have younger ages than most Yucca Mountain groundwaters. This observation is consistent with the data plotted in Figure A6-45.

The data points for groundwater from the FMW-N grouping with high ^{14}C activities (Sites 30 to 32) are of particular interest because they represent recent infiltration based on their high tritium and ^{36}Cl-to-chloride ratios (DTN: LAJF831222AQ98.011 [DIRS 145402]). As shown in Figure A6-45, the ^{14}C activities in these samples vary between 60 and 75 pmc. This result suggests these samples obtained a significant fraction of their bicarbonate concentrations from a source with little or no ^{14}C activity. Interestingly, these samples have lower $\delta^{13}C$ values than most groundwaters from the Yucca Mountain area. This result suggests the bicarbonate source was not calcite typical of the soil zone on Yucca Mountain, as these have $\delta^{13}C$ values between −2 and −8 per mil (Whelan et al. 1998 [DIRS 137305], Figure 5).

In instances where the recharge source for a groundwater can be identified, it is possible to estimate the extent to which the ^{14}C activity of the groundwater has been lowered through water/rock interactions in the saturated zone by comparing the DIC concentrations of the recharge (DIC_{rech}) and the downgradient groundwater (DIC_{gw}) (Clark and Fritz 1997 [DIRS 105738], Chapter 8). The downgradient increase in DIC_{gw} relative to DIC_{rech} represents the extent to which mineral sources of carbon have been added to the groundwater. These mineral sources of carbon may have diluted the initial ^{14}C activity of the recharge by the addition of ^{14}C-free carbon. The extent of this dilution and its effect on the calculated groundwater ^{14}C age can be represented by a correction factor ($q_{DIC} = DIC_{rech}/DIC_{gw}$) which is then applied to the radioactive decay equation to calculate the corrected ^{14}C age, as indicated in footnote (b) to Table A6-9. The basis for the equations given in footnote (b) and their limitations are described in more detail in Section A6.3.9.

As described in Sections A6.3.6.2 to A6.3.6.4, evidence exists that some groundwater samples from Yucca Mountain originated almost exclusively from recharge through Yucca Mountain

itself. Corrections were made to groundwater ^{14}C ages at locations within 18-km of the repository where groundwater had been identified from anomalously high $^{234}U/^{238}U$ ratios as having originated mostly from local recharge (Paces et al. 1998 [DIRS 100072]; see also Table A6-5). Corrections were also made to the ^{14}C ages of groundwater from several locations for which $^{234}U/^{238}U$ activity ratios were not measured, but which may contain substantial fractions of local Yucca Mountain recharge based on proximity to groundwater with high $^{234}U/^{238}U$ activity ratios. For these samples, total DIC concentrations, calcite saturation indices, and logarithms of the partial pressure of carbon dioxide (log P_{CO_2}) were computed with PHREEQC (DTN: MO0309THDPHRQC.000 [DIRS 165529]). In these corrections, the values of DIC_{rech} are allowed to vary between 128.3 and 144 mg/L bicarbonate (HCO_3^-), based on values measured in perched water at Yucca Mountain (Yang et al. 1996 [DIRS 100194], Table A6-5). The correction factor q_{DIC} ranges from 0.74 at borehole WT#12 to 1.0 at several boreholes (Table A6-5). Corrected groundwater ^{14}C ages range from 11,430 years at borehole WT#3 to 16,390 years at borehole WT#12 (Table A6-7). These calculations show that only minor corrections to the groundwater ^{14}C ages are necessary for samples located along the estimated flow path from the repository (see below).

Table A6-7. Chemistry and Ages of Groundwaters from Seven Boreholes at Yucca Mountain

Borehole	$^{234}U/^{238}U$ Activity Ratio	^{14}C Activity (pmc)	*DIC*, as HCO_3^- (mg/L)	log P_{CO_2} (atm)	log (IAP/K_{cal})[a]	Factor q_{DIC}	Corrected ^{14}C Age(yr)[b]	Uncorrected ^{14}C Age (yr)[c]
G-2	7.6	20.5	127.6	–2.352	–0.791	1	13,100	13,100
WT-17	7.6	16.2	150.0	–1.958	–1.175	0.86 to 0.96	13,750 to 14,710	15,040
WT#3	7.2	22.3	144.3	–2.413	–0.515	0.89 to 1.0	11,430 to 12,380	12,400
WT#12	7.2	11.4	173.9	–2.327	–0.313	0.74 to 0.83	15,430 to 16,390	17,950
c#3	8.1	15.7	140.2	–2.458	–0.319	0.92 to 1.0	14,570 to 15,300	15,300
b#1 (Tcb)[d]	—	18.9	152.3	–1.892	–0.757	0.84 to 0.95	12,350 to 13,300	13,770
G-4	—	22.0	142.8	–2.490	–0.305	0.90 to 1.0	11,630 to 12,510	12,500

Source: DTN: LA0202EK831231.002 [DIRS 165507]; Tables A6-1 and A6-2.

[a] log (IAP/K_{cal}) is the calcite saturation index. Negative values indicate undersaturation with calcite.

[b] The corrected age is calculated by multiplying the initial ^{14}C activity ($^{14}A_0$) in Equation A6-3 by q_{DIC}: $t = (-1/\lambda) \ln (^{14}A/(^{14}A_0\, q_{DIC}))$. The factor q_{DIC} is calculated as $q_{DIC} = DIC_{rech}/DIC_{gw}$, where the subscripts *rech* and *gw* indicate the DIC of recharge and downgradient groundwater.

[c] Calculated from Equation A6-3.

[d] The sample from borehole b#1 came from the Bullfrog tuff (Tcb).

A6.3.6.7 Calculations to Determine the Fraction of Young Water in Yucca Mountain Recharge

Given that groundwater samples at Yucca Mountain were often pumped over large depth intervals that mixed shallow and deep water (Table A4-3), it may be difficult to demonstrate conclusively that groundwater does not contain a small fraction of young water. In this section, however, calculations are performed to bound the maximum percentage of young water that could be present in the sampled groundwater.

Recharge at Yucca Mountain has probably been continuous in time, so that the measured groundwater ^{14}C activities result from the mixing of recharge (and possibly groundwater from other areas) having a broad range of ages (Campana and Byer 1996 [DIRS 126814], Figure 5). However, because data on the temporal distribution of recharge, mixing depth, and storage volume required for more detailed analyses are lacking, the fraction of young water in a groundwater sample is calculated in this section by idealizing individual groundwater samples as a binary mixture of younger and older groundwaters. Young water is arbitrarily defined as having a ^{14}C age, or residence time, of less than 1,000 years. In a binary mixture, the total number of ^{14}C atoms in the mixture depends on the ^{14}C activities, volume fractions, and total DIC concentrations of the two components, which in this case, are taken to be young and old waters:

$$(^{14}C_{\text{mix}})(DIC_{\text{mix}}) = (X_{\text{young}})(^{14}C_{\text{young}})(DIC_{\text{young}}) + (X_{\text{old}})(^{14}C_{\text{old}})(DIC_{\text{old}}) \qquad \text{(Eq. A6-8)}$$

where

^{14}C = the ^{14}C activity (in pmc)
DIC_i = dissolved inorganic carbon concentration (mg/L) of component i
X_i = the volume fraction of component i
mix, young, and old = mixed, young, and old components of the groundwater.

The volume fractions sum to one, so that $X_{\text{old}} = 1 - X_{\text{young}}$. Equation A6-8 can be solved for X_{young}:

$$X_{\text{young}} = \frac{(^{14}C_{\text{mix}})\,(DIC_{\text{mix}}) \;-\; (^{14}C_{\text{old}})\,(DIC_{\text{old}})}{(^{14}C_{\text{young}})\,(DIC_{\text{young}}) \;-\; (^{14}C_{\text{old}})\,(DIC_{\text{old}})} \qquad \text{(Eq. A6-9)}$$

The ^{14}C activity of 1,000-yr-old water with an initial ^{14}C activity of 100 pmc is equal to 88.6 pmc. DIC_{young} is expressed in these calculations as equivalent to mg/L HCO^-_3 and is assigned a value of 130 mg/L based on the typical alkalinity of many perched-water samples (Table A6-5). For samples with pH values above 7, which include perched water from the unsaturated zone at Yucca Mountain, alkalinity is approximately equal to the total DIC (Drever 1988 [DIRS 118564], p. 51). The value for $^{14}C_{\text{old}}$ was assigned a value of 10 pmc, which is approximately the lowest value measured in groundwater from the volcanic aquifer at Yucca Mountain (boreholes H-3 (10.5 pmc) and H-4 (11.8 pmc)).

Calculations of the possible fraction of young water in a sample (age less than 1,000 years) considered various *DIC* concentrations for the old component in the mixed water (Table A6-8). In Case 1, the *DIC* concentrations of the water components (mixed, old, and young) are assigned to be essentially equal, so that X_{young} depends only on values of ^{14}C. In Case 2, a moderately high value of 175 mg/L HCO_3^- was assigned for DIC_{old}. In Case 3, a value of 225 mg/L HCO_3^- was assigned for DIC_{old}. For Case 1, the calculated values of X_{young} range from about 0.02 (borehole WT#12) to 0.16 (boreholes WT#3 and G-4). For Case 2, the range of values for X_{young} is similar to, but slightly lower than, those from Case 1. In Case 3, the calculated values for X_{young} were lower than those from Cases 1 and 2, and three values were negative, which indicates that the value of 225 mg/L HCO_3^- for DIC_{old} was too high to be generally applicable.

Table A6-8. Sensitivity of the Permissible Fraction of Young Water Present in Groundwater to Dissolved Inorganic Carbon Concentration Assumed for the Old Component of the Mixed Groundwater

Borehole	Sample ^{14}C (pmc)	Sample *DIC* (mg/L HCO_3^-)	X_{young} (Case 1)	X_{young} (Case 2)	X_{young} (Case 3)
G-2	20.5	127.6	0.134	0.089	0.039
WT#12	11.4	173.9	0.018	0.024	–0.029
WT-17	16.2	150.0	0.079	0.070	–0.019
WT#3	22.3	144.3	0.156	0.150	0.104
c#3	15.7	140.2	0.073	0.046	–0.005
b#1 (Tcb)	18.9	152.3	0.113	0.116	0.068
G-4	22.0	142.8	0.153	0.142	0.096

Sources: DTN: LA0202EK831231.004 [DIRS 180317]; calculated using data from Tables A6-1 and A6-2.

NOTES: Table values were calculated based on data in Tables A6-1 and A6-2, Equation A6-9, and parameter values given in the text. Young groundwater is defined as less than 1,000 years old.
Case 1: $DIC_{old} = DIC_{young} = DIC_{mix}$; Case 2: DIC_{old} = 175 mg/L HCO_3^-; Case 3: DIC_{old} = 225 mg/L HCO_3^-.

Sensitivity studies were conducted to examine the effects of assigning variable values of $^{14}C_{old}$ with DIC_{old} = 175 mg/L HCO_3^-. Results of these studies show that the calculated values of X_{young} are somewhat sensitive to the value of $^{14}C_{old}$ (Table A6-9). Using $^{14}C_{old}$ = 5 pmc (Case 4) more than doubles the calculated value of X_{young} at many boreholes; however, values less than 10 pmc have not been observed at Yucca Mountain, so a value for $^{14}C_{old}$ of 5 pmc is considered unrealistic. A value for $^{14}C_{old}$ of 15 pmc (Case 5) is also generally unrealistic, given the many negative values calculated for X_{young}.

In summary, it is possible that a small fraction of young water (less than 1,000 years old) is present in the saturated zone downgradient from the repository area. Estimates range from a low of about 0.02 at borehole WT#12 to more than 0.15 at boreholes WT#3 and G-4. Smaller fractions of young water would be estimated to be present if water younger than 1,000 years old were assumed in the calculations.

Table A6-9. Sensitivity of the Permissible Fraction of Young Water Present in Groundwater to the Assumed ^{14}C Activity of the Old Component of the Mixed Groundwater

Borehole	Sample ^{14}C (pmc)	Sample *DIC* (mg/L HCO_3^-)	X_{young} (Case 4)	X_{young} (Case 2)	X_{young} (Case 5)
G-2	20.5	127.6	0.164	0.089	–0.001
WT#12	11.4	173.9	0.104	0.024	–0.072
WT-17	16.2	150.0	0.146	0.070	–0.022
WT#3	22.3	144.3	0.220	0.150	0.067
c#3	15.7	140.2	0.125	0.046	–0.048
B#1 (Tcb)	18.9	152.3	0.188	0.116	0.029
G-4	22.0	142.8	0.213	0.142	0.058

Sources: DTN: LA0202EK831231.004 [DIRS 180317]; calculated using data from Tables A6-1 and A6-2.

NOTES: Table values were calculated based on data in Tables A6-3 and A6-4, Equation A6-9, and assumptions given in the text. Young groundwater is defined as less than 1,000 years old. Case 4: $^{14}C_{old}$ = 5 pmc; Case 2: $^{14}C_{old}$ = 10 pmc; Case 5: $^{14}C_{old}$ = 15 pmc.

A6.3.7 Hydrochemical Evidence for Mixing of Groundwater

Groundwater chemical and isotopic compositions in the Yucca Mountain area exhibit both gradual and relatively abrupt spatial variability (Section A6.3.4) that may be related to mixing. Mixing may occur when: (1) groundwater from adjacent flow paths is spread by dispersion and diffusion, (2) the groundwater passes beneath a recharge area, (3) deep groundwater moves upward because of head gradients, faults, or hydraulic barriers, or (4) groundwater from different areas converges toward either natural discharge areas or toward wells. Preliminary mixing relations are investigated in this section through scatterplots involving relatively nonreactive chemical and isotopic species like Cl^-, SO_4^{2-}, δD, and $\delta^{34}S$. Potential mixing relations identified through these scatterplots are further explored through the use of inverse geochemical models in Section A6.3.8 that seek to quantitatively explain groundwater chemical and isotopic evolution in terms of mixing and water-rock interactions.

A6.3.7.1 Mixing Relations South of Yucca Mountain

Groundwater samples from boreholes located south of Yucca Mountain that constitute the YM-S, CF, and CF-SW groupings show a wide range of solute concentrations that generally increase to the northwest. Scatter plots (Figure A6-49) illustrate the distinct hydrochemistry of groundwater affected by carbonate rocks (CF-SW, p#1(c)) when compared to groundwater from the volcanic or tuff-derived alluvial aquifers. In fact, samples from the CF-SW group define a trend with a dilute end member intersecting typical groundwater compositions of the volcanic aquifer at Yucca Mountain. Importantly, some samples from the YM-S group fall along this line. In the YM-S group, groundwaters from borehole NC-EWDP-9SX (Samples 81 to 85) are most similar to samples from the CF-SW group chemically and are also geographically proximal to the CF-SW wells to the north and west. It is interpreted that the hydrochemistry of samples from borehole NC-EWDP-9SX represents a mix of carbonate aquifer-like water from southwest Crater Flat and dilute groundwater from the volcanic aquifer. Samples 89 and 90 also plot along mixing lines between the volcanic aquifer and the carbonate aquifer-like groundwaters. Given the geographic position of these wells, it is unclear as to whether this carbonate aquifer-like water enters the system via upward gradient flow from depth or if it could be due to dispersive

mixing of groundwater from the CF-SW Group. On the Cl^- versus δD plot (Figure A6-49) groundwater from the YM-S group define a trend toward the CF-SW group, not toward the composition of p#1 or deep groundwater from NC-EWDP-1DX Zone 2 (Site 74), indicating dispersive mixing rather than groundwater upwelling as the more likely hypothesis. The Cl^- versus δD plot (Figure A6-49) also helps to eliminate the possibility that the compositional trends defined by these samples are due to water/rock interaction with alluvium that is increasingly dominated by carbonate detritus derived from Bare Mountain because δD is not affected by this process.

A6.3.7.2 Evaluation of Mixing Relationships in the Amargosa Desert Region

The different groundwater groupings in the Amargosa Desert display a great contrast in solute concentration and isotopic data (Section A6.3.4). Indeed, much of the hydrochemical variation displayed in areal plots of chemical and isotopic species is contained in the relatively small area of the Amargosa Desert. This pronounced contrast in hydrochemistry, along with the relatively dense sample distribution allows for detailed evaluation of possible mixing patterns.

Groundwater in the AR grouping is chemically quite distinct with relatively large concentrations of solutes compared to groundwater to the east in Amargosa Desert, and thus, it is readily distinguishable and traceable. East and southeast of the AR grouping the consistent and distinct character of this groundwater is absent. Mixing with the dilute groundwater that constitutes the FMW-W and FMW-S groupings readily explains this observation. On a plot of the conservative solutes Cl^- and SO_4^{2-} (Figure A6-50) the hydrochemically distinct groupings of the AR and FMW-S groupings is evident along with the trend displayed by some samples of the FMW-W group and all of the samples from the AR/FMW grouping. This relationship is taken as sound evidence that intermediate Cl^- and SO_4^{2-} compositions of FMW-W and AR/FMW are a result of mixing of Amargosa Desert groundwater with dilute groundwater of the FMW-W grouping and/or FMW-S grouping (shown as mixing line 1, Mix 1, in Figure A6-50). This hypothesis is also supported by cross plots of other constituents. For example, although the number of samples is limited, Figure A6-51 shows the mixing relationships on a plot of $\delta^{34}S$ versus $1/SO_4^{2-}$. On this plot, the few samples from FMW-W and AR/FMW are near the mixing line drawn between the FMW-S and AR samples (Mix 1). Scatter plots of other constituents show similar relations, although some deviations from the consistent trend displayed in Figure A6-50 suggest that water-rock interaction has modified the hydrochemistry in some samples. Hydrochemical data are interpreted to indicate that samples 121, 122, 125, and 126 (FMW-W) and most samples from the AR/FMW group represent mixtures of AR groundwater with FMW-S and/or dilute groundwater from FMW-W. Samples 139 and 134 from FMW-S also plot along mixing line 1 (Figure A6-50) suggesting that these samples also contain a small fraction of AR groundwater. These samples are among the more westerly in this grouping; thus, the geographic position is consistent with this mixing hypothesis.

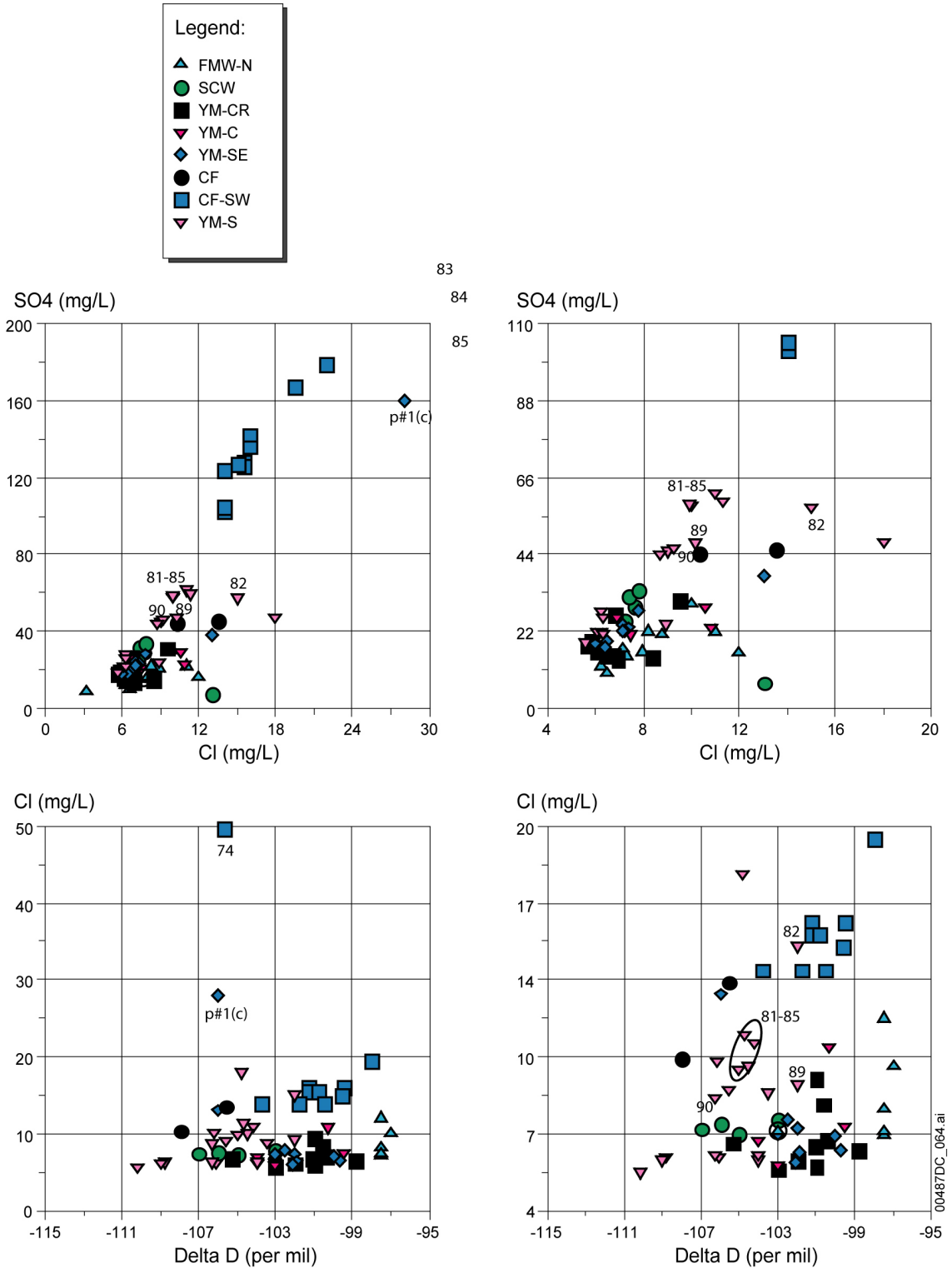

Sources: Tables A6-1 and A6-2.

NOTE: The plots on the right side of this figure have expanded scales compared to similar plots directly to their left to better display details in the tightly clustered data.

Figure A6-49. Scatter Plots Showing Mixing in Southern Yucca Mountain

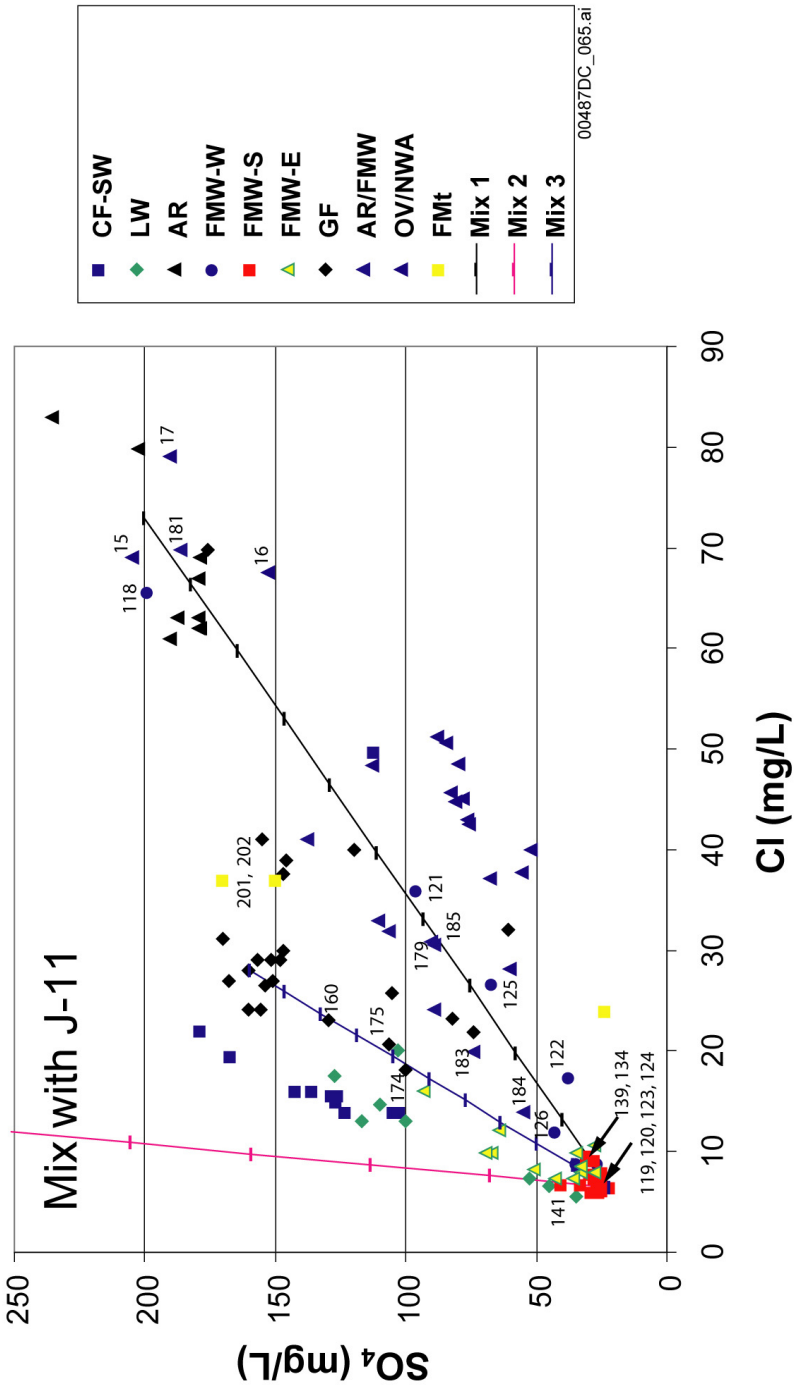

Source: Table A6-1.

NOTES: Mixing lines show 10% increments. End members for the mixing lines are: dilute end member for all mixing lines is 6.5 mg/L Cl^- and 22 mg/L SO_4^{2-}. Mixing line 1 (Mix 1) upper end member is the average of the AR Group of 73 mg/L Cl^- and 200 mg/L SO_4^{2-}. Mixing line 2 (Mix 2) upper end member corresponds to Cl^- and SO_4^{2-} values for J-11 of 17.5 mg/L and 480 mg/L, respectively. Mixing line 3 (Mix 3) upper end member is the visual average of the tight cluster displayed by the GF Group (Cl^- and SO_4^{2-} concentration of 28 mg/L and 160 mg/L, respectively). Mixing lines are drawn by plotting calculated values for Cl^- and SO_4^{2-} obtained by the mixing equation: $[Cl^-]_{mix} = F•[Cl^-]_A + (1 – F)•[Cl^-]_B$, where F is the fraction of component A in the mix. The SO_4^{2-} concentration is determined by substituting values for SO_4^{2-} into the equation.

Figure A6-50. Cross Correlation Plot of Sulfate versus Chloride for Samples in the Amargosa Desert Region

Samples 119, 120, 123, and 124 are the most dilute groundwaters from the FMW-West grouping. Three of four of these are also the most northeasterly wells of the grouping, furthest from the flow pathway of the AR group groundwater. Samples 118, 121, 122, 125, and 126 are located to the south or southwest of the dilute samples and show variable amounts of mixing with Amargosa River groundwater. This pattern is consistent with southeastward groundwater flow from the vicinity of the AR group. The relative amounts of mixed Amargosa River water are not entirely consistent with geographic position, however. Similar to the FMW-W grouping, the mixing percentages for wells of the AR/FMW group do not correlate with geographic position. In fact, the Cl^- and SO_4^{2-} concentrations of samples 118 and 181 are essentially identical to those of the AR group, and these are located adjacent to wells with significantly different anion concentrations. This inconsistency in detailed correlation between hydrochemistry and geographic position may be due to factors that are unknown or poorly understood including well completion, well pumping history, and vertical and horizontal anisotropy in the flow system. The similar hydrochemistry of well 181 compared to that of the AR group suggests a continuous flow pathway between these areas. Doing so, however, isolates sample 179, which clearly plots as a mixed sample with most of this water similar to the dilute water of the FMW-S group, and geographically separates a mixed sample from one of its presumed sources. Again, this inconsistency may be related to vertical heterogeneities or potentially points to another dilute groundwater source in southwestern Amargosa Desert. Although a pristine AR end member groundwater has not been sampled south of well 181, the mixing relationship demonstrated by samples 183 to 185 allows continuation of the flow pathway to the west of these samples.

Groundwater from the Gravity fault group also has a distinct Cl^- and SO_4^{2-} concentrations, although the group does show some variability (Figure A6-50). A mixing line between average Cl^- and SO_4^{2-} concentrations for the tight cluster of the GF and FMW-S group samples is shown on Figure A6-50 (Mix 3). Groundwaters from the LW and FMW-E groups define an array along, though slightly above, this mixing line. These two groups of wells also lie geographically between the two hydrochemical end-member groups. This relationship suggests that the intermediate chemical compositions of the LW and the FMW-E groups may be due to mixing of variable amounts of dilute water from the Fortymile Wash and groundwater from the GF group. Analysis of other constituents, however, suggests that an additional component may be present. As mentioned, samples of the LW and FMW-E groups plot along *but above* the mixing line between the GF samples and the FMW-S samples. In fact, these samples plot intermediate between this mixing line (Mix 3) and a mixing line (Mix 2) between the FMW-S samples and well J-11, which has Cl^- and SO_4^{2-} concentrations of 17.5 mg/L and 480 mg/L, respectively (Figures A6-32 and A6-33, Table A6-1). It is possible, given this relationship and the relative geographic position of these well groupings that some groundwater from the vicinity of well J-11 (Site 67) has mixed with these samples. On the plot of $\delta^{34}S$ and $1/SO_4^{2-}$ (Figure A6-51), the few samples from the LW group and the FMW-E group form a trend between the FMW-S samples and groundwater from well J-11. This trend is strongly suggestive of a mixing relationship between these samples. Mixing calculations using Cl^-, SO_4^{2-}, and $\delta^{34}S$ indicate that a maximum of approximately 20% J-11 well water is present in one of these samples (site 101—the Desert Farms Garlic Plot well). Sample 141 (FMW-S) contains elevated SO_4^{2-} for the measured Cl^- concentration and plots along mixing line 3. The geographic position and hydrochemistry of this sample are consistent with it containing a small percentage of J-11-like water. The data plotted in Figure A6-51 do not support the hypothesis that

groundwater from the LW and FMW-E groups contains a component of GF water, although the data set for $\delta^{34}S$ is incomplete.

Many of the GF samples are also collinear with some samples from FMW-E and LW groups (Figure A6-50). For example, samples 160, 174, and 175 plot intermediate between the tight cluster of GF samples and dilute groundwater of the FMW-S, FMW-E, and LW groups. These samples are also among the more westerly of the GF samples, located geographically between groundwater that defines the tight cluster of GF samples and the FMW-E samples. These samples are also interpreted to be mixtures of GF groundwater and more dilute water of the FMW-E group.

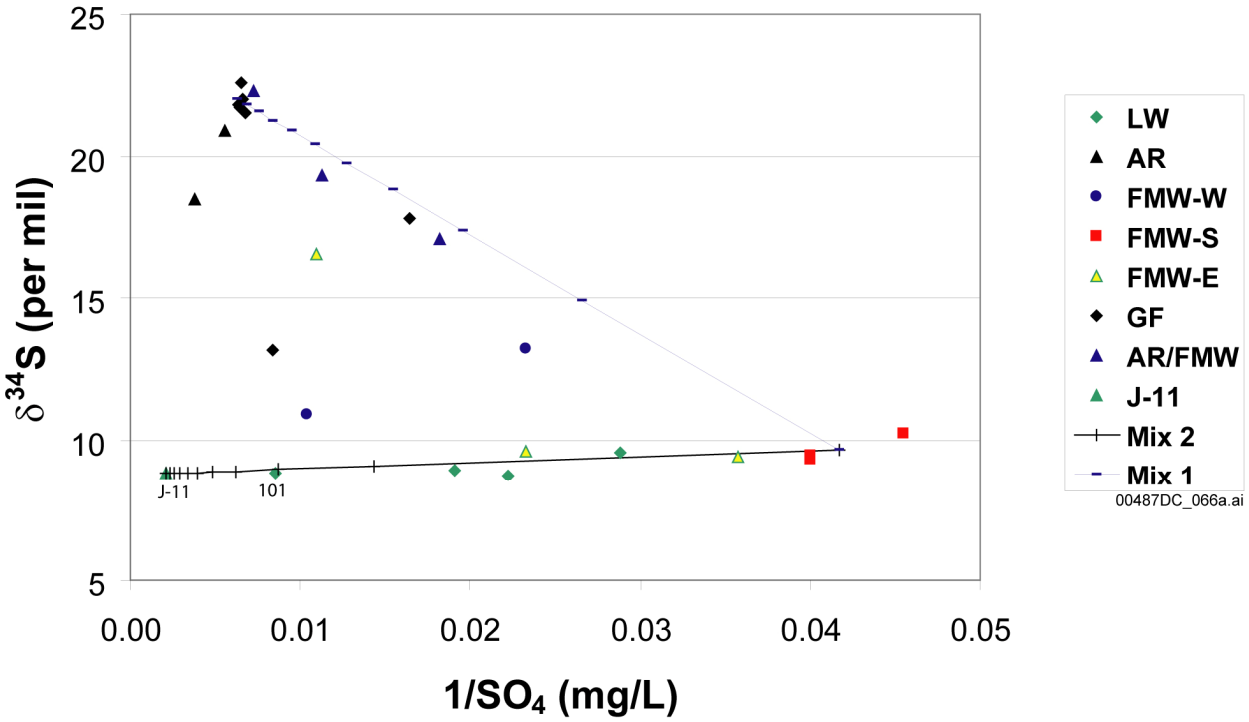

Sources: Tables A6-1 and A6-2.

NOTES: On this diagram, a mixture plots as a straight line. Mixing lines show 10% increments. End members for the mixing lines are: 24 mg/L SO_4^{2-} and 9.65 per mil $\delta^{34}S$ for the dilute end member. Mixing line 1 (Mix 1) upper end member is the visual average of the AR group samples of 160 mg/L SO_4^{2-} and 22 per mil $\delta^{34}S$. Mixing line 2 (Mix 2) upper end members corresponds to SO_4^{2-} and $\delta^{34}S$ values for J-11 of 480 mg/L and 8.8 per mil, respectively. Mixing lines are drawn by plotting calculated values for SO_4^{2-} and $\delta^{34}S$ obtained by the mixing equations: $[SO_4^{2-}]_{mix} = F \bullet [SO_4^{2-}]_A + (1 - F) \bullet [SO_4^{2-}]_B$, where F is the fraction of component A in the mix. Delta sulfur-34 is determined by: $[\delta^{34}S]_{mix} = (F \bullet [SO_4^{2-}]_A \bullet \delta^{34}S_A + (1 - F) \bullet [SO_4^{2-}]_B \bullet \delta^{34}S_B)/[SO_4^{2-}]_{mix}$.

Figure A6-51. Scatter Plot of Delta ^{34}S versus Inverse Sulfate for Samples in the Amargosa Desert Region

A6.3.8 Groundwater Mixing and Reaction Analyses Using PHREEQC

In general, the chemical and isotopic composition of groundwater results from the mixing of groundwater from various upgradient locations as well as water-rock interaction along the individual flow paths. Groundwater mixing can occur naturally as a result of hydrodynamic dispersion and can also be induced during groundwater pumping. In either case, however, groundwater mixing can result in real or apparent changes in the composition of even nonreactive chemical and isotopic species in a downgradient direction.

A number of inverse groundwater mixing and reaction analyses were performed to help identify both the upgradient groundwaters that could be present in a downgradient groundwater and the chemical reactions required to explain the downgradient changes in the composition of reactive species. The groundwaters that are considered as potential components in the downgradient groundwater are identified from relatively nonreactive species such as Cl^-, SO_4^{2-}, δD, $\delta^{18}O$, and $\delta^{34}S$. The composition of these species in the downgradient groundwater is assumed to result only from mixing of upgradient groundwaters. The remainder of the chemical and isotopic species, including other major and minor ions, dissolved SiO_2, and dissolved carbon isotopes, are considered in these models to result both from mixing and from water-rock interaction. After first determining the mixing fractions of the potential components from the nonreactive species, PHREEQC adjusts the amounts of reactive chemical and isotopic species in the mixture by finding some combination of the allowable reactions that satisfy the mass balance constraints for each chemical and isotopic species. The consideration of reactive species limits the number of potential mixing analyses to those for which plausible chemical reactions can also be found.

The potential groundwater components in the mixture were identified from contour maps of hydraulic heads (Figure A6.5-1) and areal plots and scatterplots between the aforementioned nonreactive chemical and isotopic species. For groundwaters in the volcanic or alluvial aquifers, upgradient groundwater could include recharge as well as groundwater in the carbonate aquifer, which at Yucca Mountain has a higher hydraulic head than groundwater in the volcanic aquifer.

The geographic distribution of one or more nonreactive species in a downgradient direction as shown on maps in Section A6.3.4 suggests an initial combination of groundwaters that may lie along a flow path. In some parts of the Yucca Mountain area where only slight differences in solute concentrations exist among wells, scatterplots of both nonreactive and reactive species were used to suggest possible combinations of groundwaters that may be involved in a mixture (Sections A6.3.6.3 and A6.3.7).

The chemical reactions considered in these PHREEQC (DTN: MO0309THDPHRQC.000 [DIRS 165529]) mixing and reaction analyses are restricted to those that are consistent with known ion-exchange reactions and mineral saturation indices. Generally, porewater data from Yucca Mountain (Yang et al. 1996 [DIRS 100194], 1998 [DIRS 101441]) and Rainier Mesa (White et al. 1980 [DIRS 101166]) indicate that Ca^{2+}, Mg^{2+}, and K^+ in solution are exchanged for Na^+ initially on the exchange sites of minerals. The saturation indices calculated in Section A6.3.5 indicate that Ca-clinoptilolite, Na-clinoptilolite, and smectite may precipitate from groundwater in some areas. Conversely, plagioclase, K-feldspar, calcite, fluorite, kaolinite, and amorphous silica are potentially dissolved by groundwater in certain parts of the Yucca Mountain area. Measurements of $CO_2(g)$ in the unsaturated zone at Yucca Mountain indicate a

log P_{CO_2} of about –3.0 (Yang et al. 1996 [DIRS 100194], Figure 18b). Groundwater with calculated log P_{CO_2} greater than –3.0 will therefore potentially degas into the overlying unsaturated zone when the log P_{CO_2} of the groundwater is greater than –3.0 and vice-versa.

A summary of the mineral phases considered in the PHREEQC analyses, their chemical formulas, and any constraints imposed on their precipitation or dissolution is summarized in Table A6-10. Unless otherwise noted in Table A6-12, all mineral phases were considered as potential reactants or products in each PHREEQC analyses discussed in this section.

The inverse analyses identified by PHREEQC are required to simultaneously satisfy mass-balance constraints for pH and for each element contained in the phases listed in Table A6-10. Where the inverse analyses consider groundwater mixing, the proportions of groundwater from various upgradient wells in the mixture are identified from nonreactive elements or isotopes that, by definition, are not contained in the list of reactive phases. These additional nonreactive elements and isotopes include Cl^- and, depending on the model, δD and $\delta^{18}O$. Many of the inverse models were also required to satisfy mass-balance constraints for $\delta^{13}C$, which made it necessary to specify values of ^{14}C and $\delta^{13}C$ for the C-bearing phases in these models (Table A6-10, Note 7).

The groundwater concentrations and isotopic compositions, as well as the isotopic compositions of the gas and mineral phases, are assumed by PHREEQC to be somewhat uncertain because of laboratory analytical error and because of uncertainty associated with the effects of well drilling, completion, and development on groundwater sample compositions. The specified uncertainties varied, depending on the parameter and the model. In general, the specified uncertainties were as follows: pH (0.05 pH units), ions (10% of the measured concentrations), $\delta^{13}C$ (0.1 per mil), $\delta^{18}O$ (0.1 per mil), and δD (1.0 per mil). These uncertainties determined the amount by which the measured chemical or isotopic parameters in each solution could be adjusted by PHREEQC to obtain mass balance for that parameter. In some cases, however, if no convergent analyses were identified because of a mass imbalance for a single chemical or isotopic species, the specified uncertainties for that species were increased from their typical values until a model, or set of models, could be found. For example, in one set of models, the specified uncertainty for $\delta^{13}C$ was increased to 0.5 per mil, and in another set, the uncertainty in $\delta^{18}O$ was increased to 0.4 per mil. In several sets of analyses, it was necessary to increase the uncertainty in F^- to 20% or more of the measured concentrations, effectively eliminating F^- as a chemical constraint for that set of models. For a subset of models, it was necessary to consider dissolution of kaolinite to balance Al^{3+} concentrations; generally, however, Al^{3+} concentrations could be balanced using the other alumino-silicate minerals.

Additional uncertainty associated with these analyses results from the variability in mineral compositions, nonideal chemical compositions for common rock forming minerals like K-feldspar and calcites, and the nonuniqueness of the inverse models themselves. As demonstrated in the following sections, it is often possible to find several combinations of wells and sets of water/rock interactions that can explain the chemical and isotopic composition of groundwater in the downgradient well.

Table A6-10. Mineral Phases and Exchange Reactions Considered in the PHREEQC Inverse Analyses

Phase or Exchange Cation	Formula in PHREEQC Analyses[1]	Constraint	Formula Reference
Carbon dioxide[7]	CO_2	Exsolution only	Parkhurst and Appelo 1999 [DIRS 159511], Table 55
Calcite[7]	$CaCO_3$	Dissolution or precipitation[2]	Parkhurst and Appelo 1999 [DIRS 159511], Table 55
Plagioclase	$Na_{0.8}Ca_{0.2}Al_{1.2}Si_{2.8}O_8$	Dissolution only	Vaniman et al. 1996 [DIRS 105946], Figure 1.22
K-feldspar	$KAlSi_3O_8$	Dissolution only	Parkhurst and Appelo 1999 [DIRS 159511], Table 55
Ca exchange	CaX_2	Sorption only	Parkhurst and Appelo 1999 [DIRS 159511], Table 55
Mg exchange	MgX_2	Sorption only	Parkhurst and Appelo 1999 [DIRS 159511], Table 55
Na exchange	NaX	De-sorption only	Parkhurst and Appelo 1999 [DIRS 159511], Table 55
K exchange	KX	None	Parkhurst and Appelo 1999 [DIRS 159511], Table 55
Amorphous silica	SiO_2	Dissolution only	Parkhurst and Appelo 1999 [DIRS 159511], Table 55
Kaolinite	$Al_2Si_2O_5(OH)_4$	None[3]	Parkhurst and Appelo 1999 [DIRS 159511], Table 55
Smectite	$K_{0.1}Na_{0.02}Ca_{0.14}Al_{4.4}Si_{7.6}O_{20}(OH)_4 \bullet 4H_2O$	Precipitation only	Chipera et al. 1995 [DIRS 100025], Table 1
Ca-Clinoptilolite[4]	$K_{2.5}Na_{1.1}Ca_{1.2}Al_{6.0}Si_{30.0}O_{72.0} \bullet 26.8\ H_2O$	Precipitation only	Chipera and Bish 1997 [DIRS 105079], Tables 1 to 2
Na-Clinoptilolite[4]	$K_{2.8}Na_{1.5}Ca_{0.9}Al_{6.1}Si_{29.9}O_{72.0} \bullet 26.8\ H_2O$	Precipitation only	Chipera and Bish 1997 [DIRS 105079], Tables 1 to 2
Pyrite	FeS_2	Dissolution only	Parkhurst and Appelo 1999 [DIRS 159511], Table 55
Biotite	$KMg_2FeAlSi_3O_{10}(OH)_2$	Dissolution only	Vaniman et al. 1996 [DIRS 105946], Figure 1.22
Gypsum	$CaSO_4 \bullet 2H_2O$	Dissolution only	Parkhurst and Appelo 1999 [DIRS 159511], Table 55
Oxygen	O_2	None[3]	Parkhurst and Appelo 1999 [DIRS 159511], Table 55
Ferrihydrite	$Fe(OH)_3$ (a)	Precipitation	Parkhurst and Appelo 1999 [DIRS 159511], Table 55

Table A6-10. Mineral Phases and Exchange Reactions Considered in the PHREEQC Inverse Analyses (Continued)

Phase or Exchange Cation	Formula in PHREEQC Analyses[1]	Constraint	Formula Reference
Fluorite[5]	CaF_2	Dissolution only	Parkhurst and Appelo 1999 [DIRS 159511], Table 55
Dolomite[6,7]	$CaMg(CO_3)_2$	Dissolution only	Parkhurst and Appelo 1999 [DIRS 159511], Table 55

[1] An X in a formula in this column represents the exchange site.
[2] A dissolution constraint for calcite was imposed for all inverse models except for models involving the Desert Farms Garlic Plot well, for which a precipitation constraint was imposed for calcite.
[3] Although no precipitation (or exsolution) or dissolution constraints were imposed, none of the inverse models required the precipitation of kaolinite or the exsolution of O_2. Kaolinite dissolution was considered only in models for wells NC-EWDP-3D, WT-3, and certain depth intervals of NC-EWDP-19D, for which it was necessary to balance Al^{3+} concentrations in the inverse models. Although groundwaters are assumed to be in equilibrium with kaolinite, kaolinite dissolution can be driven by the precipitation of smectite and clinoptilolite phases from the groundwater.
[4] Either Ca-clinoptilolite or Na-clinoptilolite, but not both, were considered in each inverse model. In the inverse models, the relevant clinoptilolite composition was determined by geography, with models for wells having potential upgradient sources in Crater Flat or Solitario Canyon assigned Na-clinoptilolite as a possible secondary phase and inverse models involving wells in central or eastern Yucca Mountain or near Fortymile Wash assigned Ca-clinoptilolite as a potential secondary phase. These choices were based on trends in clinoptilolite composition noted by Broxton et al. (1987 [DIRS 102004], Figure 8).
[5] Fluorite dissolution was considered only in a subset of inverse models, including those models with wells VH-1, WT-3, NC-EWDP-15P, GEXA Well 4, NC-EWDP-3D, and NC-EWDP-1S as the downgradient wells.
[6] Dolomite dissolution was considered only in a subset of inverse models where the proximity to dolomite outcrops or to alluvium derived from these outcrops had a possible influence on groundwater composition. These inverse models included those models with wells VH-1, GEXA Well 4, NC-EWDP-9S, NC-EWDP-3D, or NC-EWDP-1S as the downgradient well.
[7] The inclusion of $\delta^{13}C$ as a mass-balance constraint requires that the ^{14}C and $\delta^{13}C$ of carbon-bearing phases (CO_2, calcite, and dolomite) be defined. The ^{14}C activity of any CO_2 de-gassing from groundwater was set equal to the ^{14}C of the groundwater at the downgradient well, and the ^{14}C of the calcite and dolomite (if present) were set to 0. The $\delta^{13}C$ of CO_2 de-gassing from the groundwater was assumed to be -18 ± 2 per mil, based on measurements of the $\delta^{13}C$ of CO_2 in the unsaturated zone at Yucca Mountain (Yang et al. 1996 [DIRS 100194], Figure 19). Except for the WT-3 models for which $\delta^{13}C$ was set to -1 ± 3 per mil, the $\delta^{13}C$ of saturated-zone calcite in the volcanic and alluvial aquifers was set to -4 ± 3 per mil, and the $\delta^{13}C$ of dolomite was set to 0 ± 2 per mil, based on data for SZ calcites contained in Whelan et al. (1998 [DIRS 108865], p. 179 and Figure 2).

A6.3.8.1 Desert Farms Garlic Plot

The PHREEQC analyses investigated if groundwater at the Desert Farms Garlic Plot (DFGP) well (Site 101) could be produced by a mixture of groundwater from Fortymile Wash at borehole JF-3 (Site 37) and groundwater from Jackass Flats at well J-11 (Site 67). This PHREEQC analyses was motivated by the similar $\delta^{34}S$ and $\delta^{13}C$ ratios and low HCO_3^- at both J-11 and the DFGP well, and by the mixing relation estimated from $\delta^{34}S$ versus $1/SO_4^{2-}$, which indicated well J-11 and wells from the FMW-S area as potential mixing end members (Figures A6-50 and A6-51). The 6 analyses identified by PHREEQC are of the form:

DFGP well = X_1 JF-3 + X_2 J-11 – calcite + plagioclase + SiO_2(a) + K-feldspar – smectite – Ca-clinoptilolite + biotite + pyrite + O_2 (g) – $Fe(OH)_3$(a) – MgX_2 – KX + NaX

where the fraction of well JF-3 groundwater (X_1) is between 0.76 and 0.77 and the fraction of well J-11 groundwater (X_2) is between 0.23 and 0.24. (Note that in these PHREEQC analyses the "+" indicates the phase was taken in solution along the flow path and "–" indicates the phase left the solution along the flow path. The "X" indicates phases on exchange sites.) Subsets of the phases indicated in the preceding reaction were identified in 6 reaction analyses by PHREEQC for this group of wells. Calcite precipitation was considered as a possible reaction because the groundwater at well J-11 is saturated with calcite (Figure A6.3-34). These mixing analyses did not use $\delta^{34}S$ as a constraint, but these mixing fractions are nonetheless in good agreement with the mixing fractions for Fortymile Wash area groundwaters and well J-11 groundwater estimated using mixing trends based on $\delta^{34}S$ versus $1/SO_4^{2-}$ (Figure A6-51). However, the PHREEQC analyses could not match groundwater F^- or δD data at the DFGP well. The inability to match the δD data could reflect differences in the ages of waters actually mixed to produce the DPGP water. The J-11 water could not be directly mixed with JF-3 because these two wells are kilometers apart. Instead, a water similar to J-11 could have been mixed with a water similar to JF-3 to produce the DFGP water. The actual waters mixed could have been different from J-11 or JF-3 in age. The inability to match the F^- data may reflect analytical errors in the F^- analyses or water/rock interactions not specified in the PHREEQC calculations (e.g., dissolution of fluorite (CaF_2)).

A6.3.8.2 Well 16S/49E-05acc

The PHREEQC analyses investigated whether groundwater at the northernmost well in the FMW-S group (well 16S/49E-05acc) (Site 127) could be produced from groundwater in the southern part of the FMW-N group at well J-12 (Site 37). Groundwater from the JF well J-11 (Site 67) was also included as a potential mixing member. The inclusion of well J-11 as a potential mixing member was motivated by the higher SO_4^{2-} of groundwater in the FMW-S group compared to the FMW-N group and the very high SO_4^{2-} at well J-11 (Figure A6-33). However, no PHREEQC analyses were identified that included well J-11 groundwater at well 16S/49E-05acc. The 3 PHREEQC analyses for well 16S/49E-05acc were of the form:

16S/49E-05acc = J-12 + calcite + plagioclase + K-feldspar + gypsum – Ca-clinoptilolite + biotite + pyrite + O_2 (g) – $Fe(OH)_3$(a)

Subsets of the phases indicated in the preceding reaction were identified in 3 reaction analyses by PHREEQC for this pair of wells. The PHREEQC analyses were able to match the $\delta^{13}C$ at well 16S/49E-05acc but not the $\delta^{18}O$ and δD values. The δD between the FMW-N and FMW-S groups is significantly different (Figure A6-41). The cause of this difference is probably climate change, which has resulted in the upgradient groundwater in the FMW-N group being of more recent origin compared to the downgradient groundwater in the FMW-S group (Figure A6-41). The groundwater in the FMW-S group is older and contains a greater percentage of cooler Pleistocene recharge, which in turn, has lighter δD.

A6.3.8.3 GEXA Well 4

The groundwater at GEXA well 4 (Site 68) was modeled as a mixture of the groundwater in lower Beatty Wash at well ER-OV-03c (Site 23) and local recharge from surface runoff. Recharge from surface runoff is likely because GEXA well 4 is located in a major drainage in

northwest Crater Flat (Figure A6-4). Because the chemical and isotopic characteristics of local recharge from surface runoff have not been measured in this area, the chemical and isotopic characteristics of the local recharge represented by groundwater from 29a#2 (Site 31) in Fortymile Canyon was used. The 9 models identified by PHREEQC were of the form:

GEXA Well 4 $= X_1$ ER-OV-03c + X_2 recharge from runoff + calcite + dolomite + plagioclase + SiO_2(a) + K-feldspar – smectite – Na-clinoptilolite + pyrite + O_2 (g) – $Fe(OH)_3$(a) – CaX_2 – MgX_2 – KX + NaX

where the fraction of well ER-OV-03c groundwater (X_1) ranged from about 0.68 to 0.79 and the fraction of recharge from surface runoff (X_2) ranged from about 0.21 to 0.32. Subsets of the phases indicated in the preceding reaction were identified in 9 reaction analyses by PHREEQC for the group of wells. Dolomite was considered a potentially reactive phase due to the presence of Paleozoic dolomites at Bare Mountain. The PHREEQC analyses successfully matched the $\delta^{18}O$ and δD of groundwater at GEXA well 4 in addition to the ion composition.

A6.3.8.4 Borehole VH-1

The groundwater at borehole VH-1 (site 69) was modeled as a potential mixture of groundwater from GEXA Well 4 (Site 68) and groundwater from Beatty Wash at well ER-OV-03c (Site 23), Coffer Ranch Windmill Well (CRWW) (Site 22), and ER-EC-07 (Site 24). These wells were chosen as potential mixing components because they are all upgradient from borehole VH-1. Furthermore, these upgradient wells spanned a considerable range in Cl^-, SO_4^{2-}, $\delta^{18}O$, and δD (Section A6.3.4), which collectively bounded the values in groundwater at borehole VH-1. The 6 analyses identified by PHREEQC were of the form:

VH-1 = X_1 ER-OV-03c + X_2 CRWW + X_3 ER-OV-07 + X_4 GEXA well 4 + dolomite + plagioclase + SiO_2(a) + K-feldspar – smectite – Na-clinoptilolite + pyrite + O_2(g) – $Fe(OH)_3$(a) – CaX_2 – KX + NaX

where X_1 is the fraction of groundwater from well ER-OV-03c, X_2 is the fraction of groundwater from the CRWW, X_3 is the fraction of groundwater from well ER-OV-07, and X_4 is the fraction of groundwater from GEXA well 4. Subsets of the phases indicated in the preceding reaction were identified in 6 reaction analyses by PHREEQC for this set of wells. Four of the six analyses were two component-mixing models involving roughly equal amounts of ER-OV-03c and CRWW groundwater. Of the two remaining analyses, one model was a three-component mixing model involving roughly equal amounts of ER-OV-03c (X_1 = 0.34), CRWW (X_2 = 0.29), and GEXA well 4 (X_4 = 0.37) groundwater, and one model involved about 10% of groundwater from ER-EC-07 with subequal amounts of ER-OV-03c (X_1 = 0.39) and CRWW (X_2 = 0.53) groundwater. The models collectively indicate that most of the groundwater originates from lower Beatty Wash, with at most, a small component from upper Beatty Wash at well ER-EC-07. In light of the PHREEQC analyses for GEXA well 4 groundwater that indicate a component of local recharge from surface runoff, the groundwater at well VH-1 may also include a small component of local recharge from surface runoff in the northwest corner of Crater Flat. In addition to explaining the ion composition of groundwater at VH-1, the PHREEQC analyses accurately replicate the $\delta^{18}O$ and δD of groundwater at VH-1. However, attempts to

simultaneously model the relatively light $\delta^{13}C$ (–8.5 per mil) of groundwater at borehole VH-1 were unsuccessful.

A6.3.8.5 Well NC-EWDP-1S (Composite)

Groundwater at well NC-EWDP-1S (composite) (Site 77) was evaluated as a potential mixture of groundwater at upgradient wells VH-1 (Site 69) and VH-2 (Site 70). These components were suggested by the hydraulic gradient and fault orientations (Figure A6.5-1) and by the fact that many chemical and isotopic species in groundwater at well NC-EWDP-1S (composite) are very similar in composition to the groundwater at borehole VH-2 (Section A6.3.4). The 9 models identified by PHREEQC were of the form:

NC-EWDP-1S (composite) = X_1 VH-1 + X_2 VH-2 + dolomite – calcite + Plagioclase + SiO_2(a) + K-feldspar – Na-clinoptilolite – smectite – KX + NaX

where the fraction of well VH-1 groundwater (X_1) ranged from about 0.14 to 0.16 and the fraction of groundwater from well VH-2 (X_2) ranged from about 0.84 to 0.86. Subsets of the phases indicated in the preceding reaction were identified in the 9 reaction models by PHREEQC for group of wells. Note that in southwestern Crater Flat, the groundwater is saturated with calcite (Figure A6.3-34), so that calcite precipitation rather than dissolution is likely. In addition to reproducing the ion compositions, the PHREEQC analyses were also able to reproduce the $\delta^{18}O$ and δD compositions of groundwater at NC-EWDP-1S (composite) with a high degree of accuracy. These models indicate that groundwater at NC-EWDP-1S (composite) originates dominantly from groundwater at well VH-2.

A6.3.8.6 Well NC-EWDP-9SX (Composite)

Groundwater at well NC-EWDP-9SX (composite) (Site 81) was evaluated as a potential mixture of groundwater at upgradient wells VH-1 (Site 69) and VH-2 (Site 70). These components were suggested by the hydraulic gradient and fault orientations (Figure A6.5-1) and by the fact that many chemical and isotopic species in groundwater at well NC-EWDP-9SX (composite) are intermediate in composition between the groundwaters at boreholes VH-1 and VH-2 (Section A6.3.7.1). The 3 models identified by PHREEQC were of the form:

NC-EWDP-9SX (composite) = X_1 VH-1 + X_2 VH-2 + plagioclase + SiO_2(a) + K-feldspar – Na-clinoptilolite – smectite – CaX_2 – KX + NaX

where the fraction of well VH-1 groundwater (X_1) ranged from about 0.78 to 0.79 and the fraction of groundwater from well VH-2 (X_2) ranged from about 0.21 and 0.22. Subsets of the phases indicated in the preceding reaction were identified in the 3 reaction models identified by PHREEQC for this group of wells. In addition to reproducing the ion compositions, the PHREEQC analyses were also able to reproduce the $\delta^{18}O$ and δD compositions of groundwater at NC-EWDP-9SX (composite) with a high degree of accuracy. These models are consistent with the interpretation that groundwater at NC-EWDP-9S originates dominantly from groundwater at well VH-1.

A6.3.8.7 Well NC-EWDP-3D (Composite)

Groundwater at well NC-EWDP-3D (composite) (Site 86) was evaluated as a potential mixture of groundwater at upgradient wells VH-1 (Site 69) and WT-10 (Site 42). These components were suggested by the hydraulic gradient and fault orientations (Figure A6.5-1) and by the fact that many chemical and isotopic species in groundwater at well NC-EWDP-3D (composite) are intermediate in composition between the groundwaters at boreholes VH-1 and WT-10 (Section A6.3.4). The 1 model identified by PHREEQC was of the form:

NC-EWDP-3D (composite) = X_1 VH-1 + X_2 WT-10 + calcite + plagioclase + SiO_2(a) + K-feldspar + kaolinite – Na-clinoptilolite – MgX_2 + NaX

with the fraction of well VH-1 groundwater (X_1) equal to 0.80 and the fraction of groundwater from well WT-10 (X_2) equal to 0.20. In addition to reproducing the ion compositions, the PHREEQC models were also able to reproduce the $\delta^{18}O$, δD, and $\delta^{13}C$ compositions of groundwater at NC-EWDP-3D (composite) with a high degree of accuracy. These models indicate that groundwater at NC-EWDP-3D originates dominantly from groundwater at well VH-1.

A6.3.8.8 Well NC-EWDP-15P

The groundwater at well NC-EWDP-15P (Site 90) was modeled as a potential mixture of groundwaters from upgradient wells VH-1 (Site 69) and WT-10 (Site 42). The carbonate-aquifer-like groundwater from borehole VH-2 (Site 70) was also considered as a potential component based on head gradients in southern Crater Flat and Yucca Mountain and on mixing trends that suggested a carbonate-aquifer component in the groundwater in this area (see Section A6.3.7.1). The 2 PHREEQC analyses found for well NC-EWDP-15P took the form:

NC-EWDP-15P = X_1 WT-10 + X_2 VH-2 + X_3 VH-1 + SiO_2(a) + K-feldspar +gypsum – Na-clinoptilolite – smectite

where the fraction of well WT-10 groundwater (X_1) was approximately 0.45 to 0.49, the fraction of carbonate aquifer groundwater from borehole VH-2 (X_2) was 0.05 to 0.06, and the fraction of groundwater from well VH-1 (X_3) was about 0.45 to 0.49. The 2 PHREEQC analyses were able to successfully match the $\delta^{18}O$ and δD at well NC-EWDP-15P with a high degree of accuracy. The $\delta^{13}C$ of groundwater at NC-EWDP-15P was not estimated by the inverse models because no groundwater $\delta^{13}C$ data were available from borehole VH-2. The PHREEQC analyses support the hypothesis that groundwater flows from eastern Crater Flat through wells in southern Yucca Mountain.

A6.3.8.9 Borehole WT-3

The PHREEQC models investigated whether groundwater at borehole WT-3 (Site 65) could have evolved from groundwater in northern Yucca Mountain at borehole WT-24 (Site 44). This possible flow path was suggested by fault orientations and the hydraulic gradient in the northern Yucca Mountain area, the high $^{234}U/^{238}U$ activity ratio at both boreholes, and the fact that groundwater at borehole WT-24 is the only location upgradient from borehole WT-3 with a

higher ^{14}C activity. The reaction models for these wells assumed that calcite dissolved along the flow path had a $\delta^{13}C$ of –1.0 ± 3 per mil because this is a common value measured in saturated zone calcite (Whelan et al. 1998 [DIRS 108865], Figure 3). The reactions identified by PHREEQC for this flow path were of the general form:

WT-3 = WT-24 + calcite + fluorite + SiO_2(a) + K-feldspar + kaolinite – smectite – Ca-clinoptilolite + biotite + O_2(g) – $Fe(OH)_3$(a) – CaX_2 – MgX_2

Subsets of the phases indicated in the preceding reaction were identified in 6 reaction models identified by PHREEQC for this pair of wells. The results of the reaction models confirm this as a plausible flow path.

A6.3.8.10 Well NC-EWDP-19D and -19P

Groundwater at well NC-EWDP-19D (Sites 92 and 94 to 98) was sampled from several different zones in alluvium as well as from longer intervals spanning the depth of the alluvium or the entire well. The chemistry and isotopic compositions of these zones exhibited substantial differences in both chemical and isotopic compositions (see Section A6.3.3). Although cation, bicarbonate, and isotope compositions varied substantially among different zones, the groundwater Cl^- and SO_4^{2-} compositions within almost all zones are uniformly low. The similarity of groundwater Cl^- and SO_4^{2-} compositions in well NC-EWDP-19D and upgradient well WT-3 (Site 65) suggests a flow path between these two wells, in spite of the differences in other chemical and isotopic species. Groundwater at well WT-3 is also the only upgradient groundwater with ^{14}C activity high enough to explain the high ^{14}C activities of some zones in well NC-EWDP-19D. One group of models for well NC-EWDP-19D therefore attempts to explain the compositional difference between wells WT-3 and various zones within well NC-EWDP-19D as the result of water rock interactions along the flow path between the wells. The same set of reactions are applied to varying extents to explain the differences in compositions between various depth intervals in well NC-EWDP-19D:

NC-EWDP-19D (various zones) = WT-3 + calcite + SiO_2(a) + K-feldspar + kaolinite + plagioclase + gypsum – smectite – Ca-clinoptilolite + biotite + pyrite + O_2 (g) – $Fe(OH)_3$(a) – CaX_2 – MgX_2 ± KX + NaX

Scatter plots (Figures A6-42 to A6-46) show that some groundwaters in the SCW group are similar to groundwater at well NC-EWDP-19D. Although slightly higher in Cl^- and SO_4^{2-}, groundwater in the SCW group is similar to groundwater at well NC-EWDP-19D with respect to cation compositions, DIC, and $\delta^{13}C$. However, the groundwater ^{14}C activities in the SCW area are far too low for this groundwater to be the source of groundwater at NC-EWDP-19D unless the SCW groundwater mixes with younger groundwater along its flow path. This younger water is assumed to be local recharge from Yucca Mountain itself, as represented by perched water from borehole SD-7. Some component of local recharge in southern Yucca Mountain is consistent with the hypothesis that much of the groundwater at Yucca Mountain is derived from local recharge (Section A6.3.6). The local recharge represented by perched water from SD-7

also has lower Cl^- and SO_4^{2-} concentrations than the well NC-EWDP-19D, making it a suitable mixing end member. This group of models can be represented as:

NC-EWDP-19D (various zones) = X_1 WT-10 + X_2 local recharge (SD-7 perched water) + calcite + SiO_2(a) + K-feldspar + kaolinite + plagioclase + gypsum – smectite – Ca-clinoptilolite + biotite + pyrite + O_2(g) – $Fe(OH)_3$(a) – CaX_2 – MgX_2 ± KX + NaX

where X_1 is the fraction of groundwater from SCW well WT-10 (Site 42), X_2 is the fraction of local recharge (as represented by perched water from borehole SD-7). Similar chemical processes but different sources are invoked in the two sets of PHREEQC models to explain the composition of groundwater within different zones in well NC-EWDP-19D. Both sets of models are able to explain the chemical compositions and $\delta^{13}C$ values of groundwater in various zones at well NC-EWDP-19D, but neither set of models adequately explains the extremely light $\delta^{18}O$ and δD compositions in some of these zones.

The PHREEQC analyses for groundwater at well NC-EWDP-19P (Site 93) use the same set of reactions as for -19D but consider groundwater flow from well WT-3 and well JF-3 in the FMW-N group as possible sources of groundwater at well NC-EWDP-19P. The PHREEQC analyses results indicate that 80% to 100% of the shallow groundwater in well NC-EWDP-19P originates from the area of well JF-3.

A6.3.9 Evaluation of Groundwater Velocities in the Yucca Mountain Region

In this section, groundwater velocities are estimated along various flow-path segments using the ^{14}C activities of the groundwater along the flow path. The measured ^{14}C activities at the upgradient well defining the segment are adjusted to account for decreases in the ^{14}C activity that result from water-rock interactions the groundwater undergoes between wells, as identified by the PHREEQC mixing and chemical reaction models described in Section A6.3.8. This adjustment to the initial ^{14}C activity at the upgradient well is necessary to distinguish between the decrease in ^{14}C activity caused by water-rock interaction and the decrease in ^{14}C activity due to transit time between the wells. After determining the transit time between wells, linear groundwater velocities are determined by dividing the distance between the wells by the transit time.

The transit time between wells is calculated from the radioactive decay equation for ^{14}C (Section A6.3.1.2.2). A variety of methods have been used to estimate the value of $^{14}A_0$ to use with the radioactive decay law (Clark and Fritz 1997 [DIRS 105738], Chapter 8). One simple method that can be used to correct for the effects of calcite (or dolomite) dissolution in the case where the downgradient groundwater evolves from a single upgradient source is to compare the total DIC in the upgradient well (DIC_u) with the DIC of the downgradient groundwater (DIC_d) (Clark and Fritz 1997 [DIRS 105738], p. 209):

$$q_{DIC} = \frac{DIC_u}{DIC_d} \qquad \text{(Eq. 6-10)}$$

where q_{DIC} represents the fraction of the DIC in the downgradient that originated from the upgradient well, with the remainder acquired from water-rock-gas interactions. Therefore, the

initial value of $^{14}A_0$ is the product of q_{DIC} and the measured ^{14}C activity at the upgradient well ($^{14}A_u$):

$$^{14}A_0 = {}^{14}A_u \bullet q_{DIC} \quad \text{(Eq. 6-11)}$$

Several assumptions are made to simplify this calculation. The method assumes that after infiltration reaches the SZ and becomes recharge, the water is effectively isolated from further interaction with carbon dioxide gas in the unsaturated zone, so that any downgradient increases in the DIC of the groundwater are a result of interactions with carbon-bearing minerals. These minerals are assumed to be depleted in ^{14}C, which is probably the case because most SZ calcite was formed either during a 10-million-year-old hydrothermal event or under unsaturated conditions at a time when the water table was lower than today (Whelan et al. 1998 [DIRS 108865], p. 180). Thus, although the proportions of dissolved carbon-dioxide gas, bicarbonate, and carbonate may change with pH as the groundwater interacts with the rock, the total DIC is fixed unless the groundwater reacts with calcite. This method would not account for any interactions between groundwater and calcite once the groundwater had become saturated with calcite (Table A5-1, Assumption 8), nor would it account for the effects of groundwater mixing. This method was applied to obtain a preliminary estimate for the case that the upgradient groundwater was undersaturated with calcite and mixing was not considered an important process based on the PHREEQC inverse analyses.

Additional simplifying assumptions in evaluating transport times based on ^{14}C ages along flow paths include: groundwater flows along the straight-line distance between wells. This is a necessary, though likely inaccurate, assumption since the quantitative data for a particular nonlinear travel path are lacking. Using the straight-line distance yields the highest flow velocity. Also, the effects of matrix diffusion are not accounted for, though they are likely. Matrix diffusion may add older DIC to the groundwater. Corrections to account for this older component would also increase the calculated flow velocity.

For flow path segments in which PHREEQC inverse analyses indicate the downgradient groundwater evolves from a single upgradient well, the value of $^{14}A_U$ is simply groundwater ^{14}A at the upgradient well and the expression for q_{DIC} is computed as follows:

$$q_{DIC} = (DIC_u)/(DIC_u + DIC_{carbonate}) \quad \text{(Eq. 6-12)}$$

where DIC_u is the DIC at the upgradient well and $DIC_{carbonate}$ is the amount of carbon contributed by water-rock interactions involving carbonate rocks. The denominator in Equation 12 was expressed as $DIC_u + DIC_{carbonate}$ rather than simply as the measured value of DIC_d to allow for the possibility that the measured DIC concentrations were affected by $CO_2(g)$ de-gassing either during flow or during sampling.

For flow path segments for which the PHREEQC inverse analyses identified mixing as an important control on the downgradient groundwater chemistry, the values of $^{14}A_u$ and q_{DIC} were calculated as follows:

$$^{14}Au = (f_1\ {}^{14}A_1\ DIC_1 + f_2\ {}^{14}A_2\ DIC_2 + \ldots + f_i\ {}^{14}A_i\ DIC_i)/(f_1\ DIC_1 + f_2\ DIC_2 + \ldots + f_i\ DIC_i)$$

(Eq. 6-13)

and

$$q_{DIC} = (f_1\, DIC_1 + f_2\, DIC_2 + \ldots + f_i\, DIC_i)/(f_1\, DIC_1 + f_2\, DIC_2 + \ldots + f_i\, DIC_i + DIC_{carbonate})$$

(Eq. 6-14)

where f_i is the fraction of upgradient component i in the mixture. The equations do not consider the effects of CO_2 degassing or dissolution, or calcite precipitation on ^{14}C activity. This omission is an acceptable simplification because the fractionation factor for ^{14}C is small (Clark and Fritz 1997 [DIRS 105738], inside front cover), and the ^{14}C in the CO_2 or calcite exiting the groundwater should leave the ^{14}C in the groundwater relatively unchanged. Gas dissolution by the groundwater should not occur in most instances because the log P_{CO_2} of the groundwater is higher than that of the overlying unsaturated zone (see Section A6.3.8).

It is important to recognize that the hydrogeologic environment at Yucca Mountain represents a departure from the ideal circumstances under which ^{14}C activities can be reliably used to calculate groundwater velocities. Ideally, the ^{14}C method should be used where recharge is added at a known location and moves through a confined aquifer, isolated from the effects of groundwater mixing or downgradient additions of recharge. The degree of confinement of the aquifers at Yucca Mountain is not known, and mixing and downgradient additions of recharge are possible that could cause conditions to depart from the ideal circumstances. The PHREEQC analyses that have identified groundwater mixing as a process affecting groundwater compositions can, in theory, help to calculate the effects of groundwater mixing on ^{14}C activities, as described in Equations 6-13 and 6-14. However, in the Yucca Mountain area, the calculation of groundwater velocities based on ^{14}C activities is made more complicated by the possible presence of multiple, distributed recharge areas. If relatively young recharge were added along a flow path, the ^{14}C activity of the mixed groundwater would be higher, and the calculated transit times shorter, than for the premixed groundwater without the downgradient recharge. Unfortunately, the chemical and isotopic characteristics of the recharge from various areas at Yucca Mountain may not be sufficiently distinct to identify separate sources of local recharge in the groundwater.

Despite these nonideal conditions, groundwater velocities were calculated for several possible flow paths south of the repository in the Yucca Mountain area. The results of the calculations are described in the following subsections. These results should be viewed in light of the reservations noted above.

A6.3.9.1 Flow-Path Segment from Well WT-3 to Well NC-EWDP-19D

The PHREEQC inverse analyses (Section A6.3.8) indicate that groundwater sampled from various zones in well NC-EWDP-19D (Sites 92 and 94 to 98) could have evolved from groundwater at well WT-3 (Site 65). Table A6-11 shows the transit times calculated by using the DIC of groundwater at well WT-3 and PHREEQC estimates of the carbon dissolved by this groundwater as it moves toward various zones at well NC-EWDP-19D (Equation 6-12). The third column of Table A6-11 refers to the transit time estimate made from the measured DIC at well WT-3 and that particular zone in well NC-EWDP-19D. The differences between the transit times based on the PHREEQC analyses results (Table A6-11, Column 2) and the transit times based on the measured differences in DIC concentrations (Table A6-11, Column 3) arise from

the fact that the PHREEQC analyses allow the DIC concentrations at each of the 2 wells to vary within 10% of their measured values, resulting in slightly different estimates of the amount of calcite dissolution along this flow path. These small differences in the estimates of calcite dissolution can cause transit times to vary from positive to negative and vice versa when the differences in ^{14}C activity between the upgradient and downgradient wells are small, as in the models involving zones 1 and 2 of NC-EWDP-19D (sites 95 and 96).

As Table A6-11 indicates, groundwater in the composite well and alluvial groundwaters require approximately 1,000 years to travel the approximately 15-km distance between wells WT-3 and NC-EWDP-19D. This transport time equates to linear groundwater velocities of approximately 15-m/yr. The groundwater in the deeper alluvial zones (Zones 3 and 4) requires approximately 1,500 to 3,000 years and, thus, travels at a linear groundwater velocity of 5 to 10-m/yr. In contrast, the transit times calculated for groundwater from shallow Zones 1 and 2 have transit times that range from 0 to about 350 years. Many of the calculated groundwater transit times were negative, indicating that the differences between ^{14}C activities in groundwater at well WT-3 and these zones in well NC-EWDP-19D were too small, and the uncertainty in DIC reactions estimated by PHREEQC too large, to adequately resolve the transit times. Using the upper transit time of 188 years, groundwater flow from well WT-3 to Zone 2 in well NC-EWDP-19D is about 80-m/yr. Likewise, using the upper transit time of 535 years, groundwater flow from WT-3 to zone 1 of NC-EWDP-19D is about 28 m/yr. These relatively high velocities may indicate that some of the shallow groundwater at well WT-3 moves along major faults like the Paintbrush Canyon fault, the effects of regionally convergent groundwater flow indicated by the hydraulic gradient (Figure A6.5-1), or they may simply reflect uncertainty in some assumptions implicit in this method, as discussed above in Section A6.3.9.

Table A6-11. Calculated Groundwater Transit Times (in years) Between Well WT-3 and Various Depth Zones in Well NC-EWDP-19D

Zone in NC-EWDP-19D	Mean transit time based on PHREEQC analyses (years)[a]	Transit time based on $q_{DIC} = DIC_U/DIC_D$ (years)
1	535 ± 1	-926[b]
2	–115 ± 112[b]	188
3	3110[c]	1601
4	1684 ± 2	1681
alluvial zone	1065 ± 2	1063
Composite (combined alluvial and volcanic zones)	870 ± 2	866

Sources: DTNs: LA0310EK831232.001 [DIRS 165995] (inverse analyses); LA0310EK831231.001 [DIRS 171889] (calculated travel times); Table A6-2 (^{14}C data); Table A6-3 (DIC concentrations).

[a] Uncertainties are 1 standard deviation of the times estimated using the model results.
[b] Negative transit times were calculated because of small differences in the ^{14}C activities of the upgradient and downgradient wells and uncertainty in the DIC concentrations and PHREEQC reaction analyses.
[c] No standard deviation was calculated because only 1 model for this zone was identified.

A6.3.9.2 Flow Path Segment from Well WT-24 to Well WT-3

The transit times calculated by using the DIC of groundwater at well WT-24 (Site 44) and PHREEQC estimates of the carbon dissolved by this groundwater as it moves toward well WT-3 (site 65) averaged -499 ± 147 years. The transit time estimate based on the measured differences in DIC of groundwater at wells WT-24 and WT-3 is 216 years. The differences in the estimates arise from the fact that the PHREEQC analyses allow an uncertainty of 10% in the DIC concentrations at each of the wells, which allows a slightly larger amount of calcite to be dissolved in the models (33 to 39 mg/L in the PHREEQC analyses versus 23 mg/L based on the measured DIC values). Using the estimate of transit time based on the measured DIC values and a linear distance between wells WT-24 and WT-3 of 10-km results in a linear groundwater velocity of 46-m/yr.

A6.3.10 Groundwater Flow Patterns Simulated with the Saturated Zone Flow Model

The saturated zone site-scale flow model (DTN: LA0304TM831231.002 [DIRS 163788]), or simply, the SZ flow model, was used to simulate the movement of a conservative tracer through various features in the model. The location of these hydrogeologic features and their numerical designations in the model are described and shown in *Saturated Zone Site-Scale Flow Model* (BSC 2004 [DIRS 170037], Figure 6-5 and Table 6-17), *Hydrogeologic Framework Model for the Saturated Zone Site Scale Flow and Transport Model* (BSC 2004 [DIRS 170008], Figure 6-3), and the journal article by Zyvoloski et al. (2003 [DIRS 163341], Figure 2b). The goal of these simulations was to provide an understanding of where groundwater at any location in the flow system may have originated and to what extent groundwaters originating from various locations may mix. These simulation results are then qualitatively evaluated in the context of the understanding gained from the analysis of the hydrochemical and isotopic data discussed in the previous sections.

The simulations performed with FEHM used the advection-dispersion (trac) macro embedded in that code to simulate the steady-state distribution of a tracer originating from most boundary segments and from Yucca Mountain and Fortymile Wash recharge. In each simulation, an assigned longitudinal dispersivity of 10 m and a transverse dispersivity of 1 m were used. Small dispersivities were assumed to better observe the effects of heterogeneities on groundwater mixing and dilution. Nonetheless, as in most simulations that use the advection-dispersion equation, some numerical dispersion due to the mesh discretization may also have affected the tracer simulation results. For this reason, the simulation results are not analyzed quantitatively, and comparisons to the geochemical data are qualitative in nature.

The flow-system behavior illustrated by these simulations is partly the result of the distributions of aquifers and confining units in the model (Figure A6-52). Where an aquifer exists along the boundary of the model, relatively large amounts of water enter the model along that boundary segment and the tracer originating from that segment dominates the character of the downgradient groundwater for a considerable distance. Conversely, where confining units are present along the boundary, groundwater inflow is small, and the tracer originating from that segment is readily diluted by the relatively larger amounts of untraced groundwater entering the model along the neighboring boundary segments.

Two simulations were done for each boundary segment considered. The first simulation for each segment examined the steady-state distribution of inflow along the pre-Tertiary rocks contained within that boundary segment. These pre-Tertiary rocks include the granitic rocks, the Lower Clastic Confining Unit, the Lower Carbonate Aquifer, the Upper Clastic Confining unit, the Lower Carbonate Aquifer Thrust, and the Upper Carbonate Aquifer Thrust. The Tertiary rocks (and sediment) include the remainder of the model units shown on Figure A6-52. The Prow Pass tuff, the Bullfrog tuff, and the Tram tuff, although not explicitly identified as aquifers in Figure A6-52, comprise the Lower Volcanic Aquifer of Luckey et al. (1996 [DIRS 100465], Figure 7).

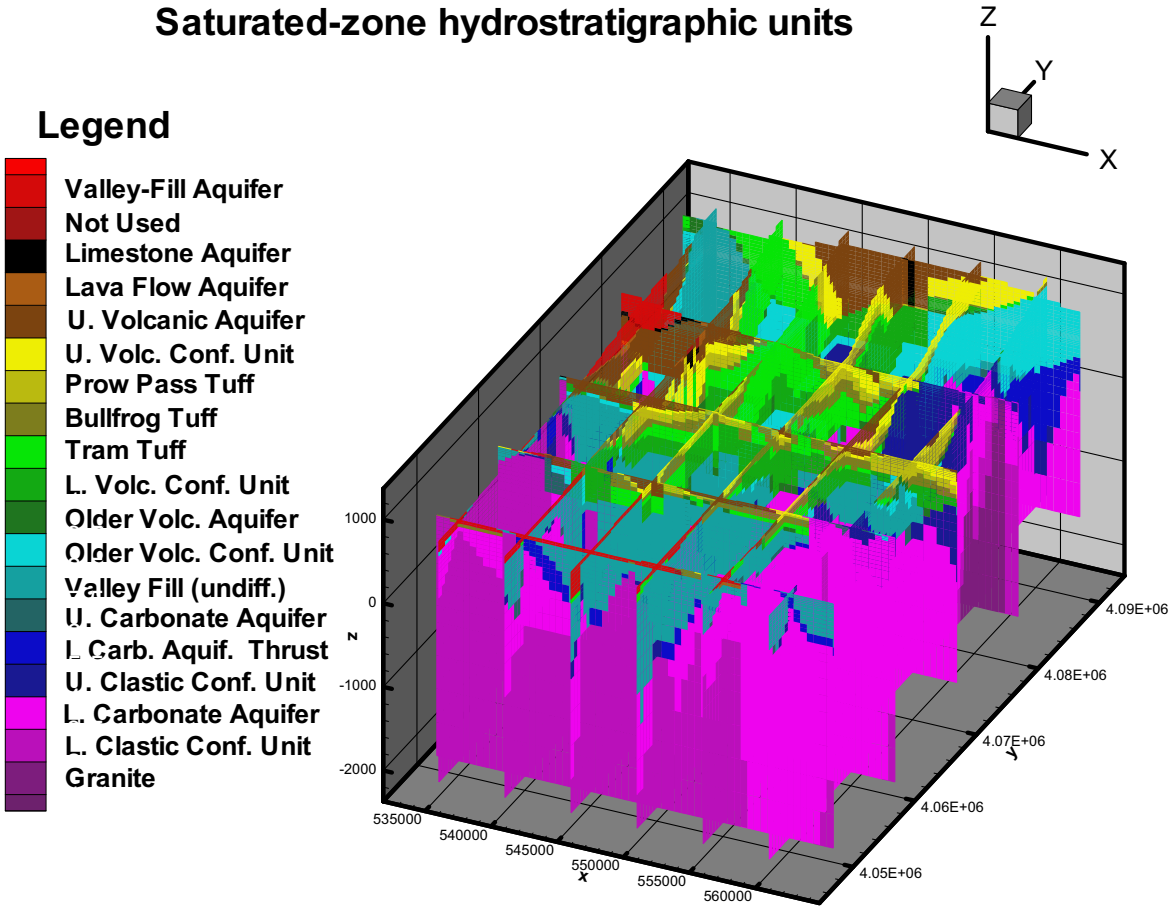

Sources: DTNs: LA0304TM831231.002 [DIRS 163788]; LA0309EK831231.001 [DIRS 171887].

NOTES: The X and Y coordinates are Universal Trans-Mercator Projection (UTM) coordinates in meters. The Z coordinate is elevation relative to sea level in meters. X = UTM-Easting and Y = UTM-Northing.

Figure A6-52. Geologic Units Defined in the Saturated Zone Flow Model

The first simulation result presented here shows the steady-state distribution of Yucca Mountain recharge in the model (Figure A6-53). Also shown in the figure are the locations of the boreholes that provided head data used in the calibration of the SZ flow model. Some key boreholes that figured prominently in the earlier discussions of the hydrochemistry are labeled in this and subsequent figures. The boreholes extend from ground surface (not shown) through the water table, which in this case, coincides with the top of the model. The plotted length of each borehole in these figures, from ground surface to the top of the model (the water table), thus approximates the thickness of the unsaturated zone at that location.

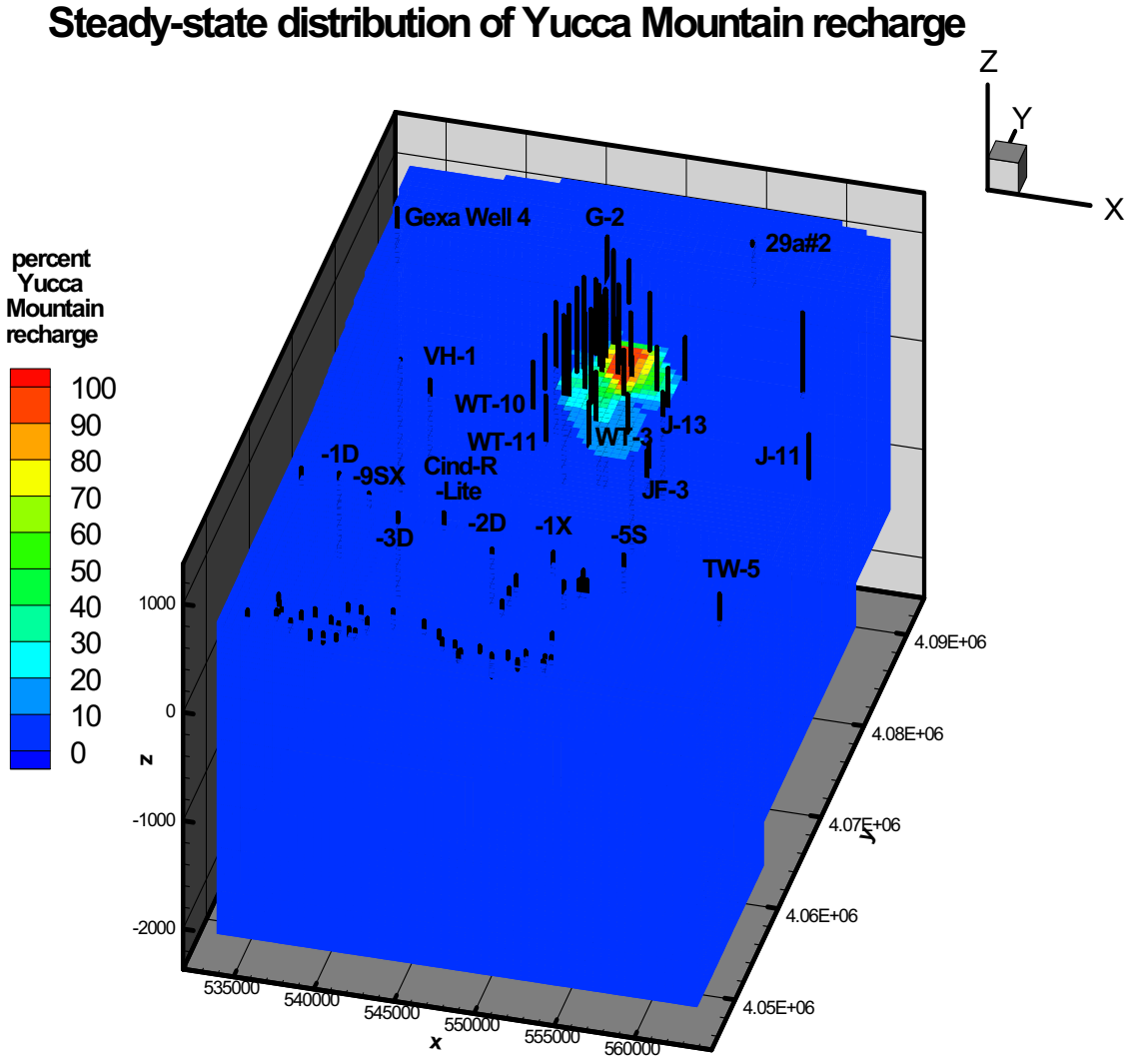

Sources: DTNs: LA0304TM831231.002 [DIRS 163788]; LA0309EK831231.001 [DIRS 171887].

NOTES: The X and Y coordinates are Universal Trans-Mercator Projection (UTM) coordinates in meters. The Z coordinate is elevation relative to sea level in meters. X = UTM-Easting and Y = UTM-Northing.

Figure A6-53. Steady-State Distribution of the Percentage of Yucca Mountain Recharge in Downgradient Groundwater Calculated Using the Saturated Zone Flow Model

The longest boreholes are located along Yucca Crest where the unsaturated zone thickness can reach 750 m.

The Yucca Mountain recharge entering the model was tagged with a concentration of 100 units, whereas all other water entering the model was given a tracer concentration of 0 units. The percentage of Yucca Mountain recharge at any location in the model is therefore equivalent to the tracer concentration at that location. The simulation results indicate that Yucca Mountain recharge is substantially diluted by groundwater flowing from adjacent parts of the flow system by the time it passes the Dune Wash area near well WT-3 (Site 65). The percentage of Yucca Mountain recharge in the groundwater is less than 10% near well NC-EWDP-2D (Site 91) along U.S. Highway 95. The downgradient decrease in tracer concentrations associated with Yucca Mountain recharge cannot be explained by spreading of the plume due to numerical dispersion because, in this case, the plume tends to become narrower and more focused in the downgradient direction. A more likely explanation is that as Yucca Mountain recharge moves downgradient, it is mixed and diluted by groundwater moving from more active parts of the flow system. These results are consistent with observed hydrochemical patterns and help to explain the difficulty in identifying Yucca Mountain recharge in groundwater near and south of U.S. Highway 95.

The flow entering along the northern boundary of the model (zone 61) in northwest Crater Flat is shown in Figures A6-54 to A6-56. The flow through the pre-Tertiary rocks is predicted to emerge into the shallow part of the flow system in several points of the model, including the central part of Crater Flat near borehole VH-1 (Site 69) and the southern part of Crater Flat near well NC-EWDP-3D (Site 86) and the NC-EWDP-15P well (Site 90). The groundwater at borehole VH-2 (Site 70) in central Crater Flat does appear to have many of the characteristics of groundwater from the carbonate aquifer, and groundwater at well NC-EWDP-3D (Site 86) and the NC-EWDP-15P well (Site 90) were analyzed with the PHREEQC code to be partially derived from the carbonate aquifer, in agreement with these results. The deep groundwater flowing through Crater Flat is apparently forced both upward and to the east by a buried ridge formed by the low-permeability Lower Clastic Confining unit (compare Figures A6-52 and A6-55). The groundwater entering Crater Flat through the undifferentiated Valley Fill in zone 61 dominates the shallow flow system in most of Crater Flat, except for the westernmost part of Crater Flat where the groundwater enters from the western boundary along Bare Mountain. Although most of the groundwater entering the undifferentiated Valley Fill in northwest Crater Flat flows southward from borehole VH-1 (Site 69) to wells NC-EWDP-9SX (Sites 81–85) and NC-EWDP-3D (Site 86), as analyzed with the PHREEQC calculations (Sections A6.3.8.6 and A6.3.8.7), a part of this groundwater flows southeastward past well WT-10 (Site 42) and into southern Yucca Mountain to become a component of the groundwater near the NC-EWDP-15P well (Site 90) and NC-EWDP-2D (Site 91). PHREEQC calculations for these well NC-EWDP-15P and for nearby well NC-EWDP-19D indicated that groundwater from well WT-10 (Site 42) could constitute a significant fraction of the groundwater at these wells (Sections A6.3.8.8 and A6.3.8.10).

Because of the very low permeability of the pre-Tertiary rocks near Zone 62 at Timber Mountain, very little groundwater enters the model from this area and tracer concentrations indicate that inflow from this area exerts little influence on the downgradient water chemistry (figure not shown). The Tertiary rocks from Zone 62 include the relatively permeable upper volcanic aquifer, which permits a considerably greater amount of groundwater to enter the model

than the pre-Tertiary rocks in this zone. The steady-state distribution of tracer concentrations (Figure A6-57) indicates that groundwater entering through the Tertiary rocks of Zone 62 flows southward through Yucca Mountain and forms a component of the groundwater throughout the Yucca Mountain area, including southeastern Crater Flat at wells WT-10 (Site 42), NC-EWDP-3D (Site 86), the Cind-R-Lite well (Site 89), and wells NC-EWDP-2D (Site 91) and NC-EWDP-19D (Sites 92 and 94 to 98) in southern Yucca Mountain near Fortymile Wash. The $\delta^{13}C$ of shallow groundwater in the northernmost part of Yucca Mountain is too light for that groundwater to have originated from groundwater directly to the north at well ER-EC-07 (Site 24) in Beatty Wash. However, the increase in groundwater $\delta^{13}C$ southward at Yucca Mountain is consistent with an increasing component of groundwater from the area of well ER-EC-07 (Site 24) present in the Yucca Mountain groundwater.

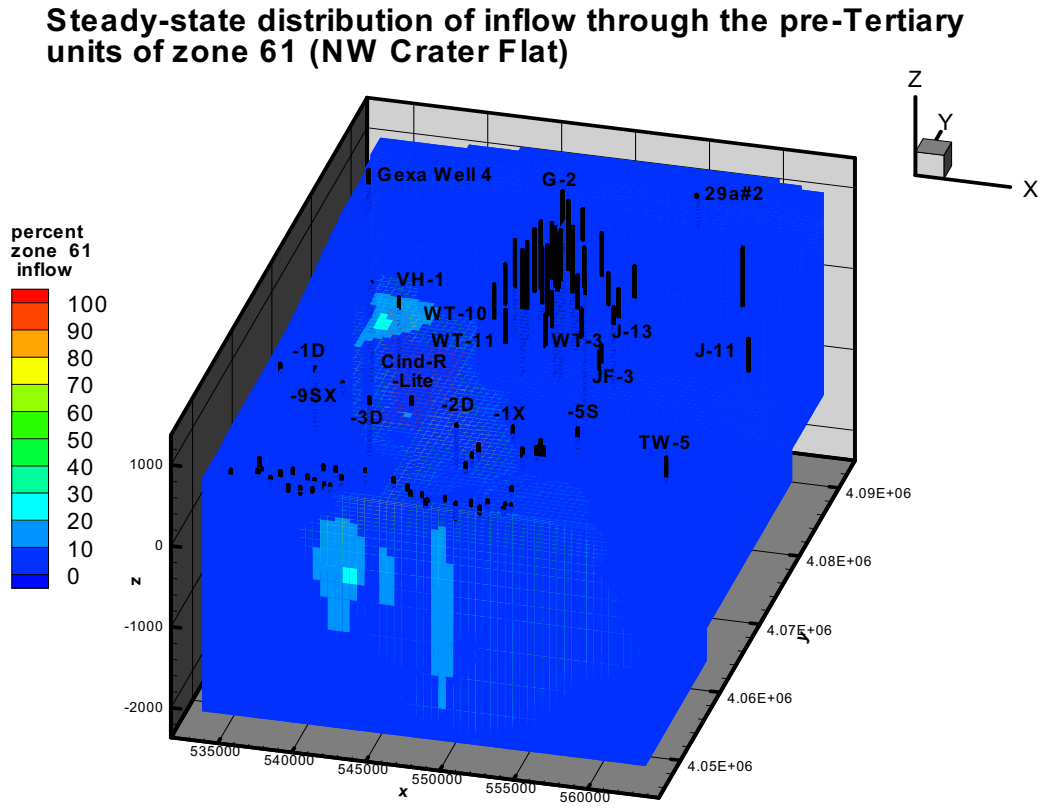

Sources: DTNs: LA0304TM831231.002 [DIRS 163788]; LA0309EK831231.001 [DIRS 171887].

NOTES: The X and Y coordinates are Universal Trans-Mercator Projection (UTM) coordinates in meters. The Z coordinate is elevation relative to sea level in meters. X = UTM-Easting and Y = UTM-Northing.

Figure A6-54. Map View of Steady-State Distribution of the Percentage of Inflow through the Pre-Tertiary Units of Northwest Crater Flat Groundwater Calculated Using the Saturated Zone Flow Model

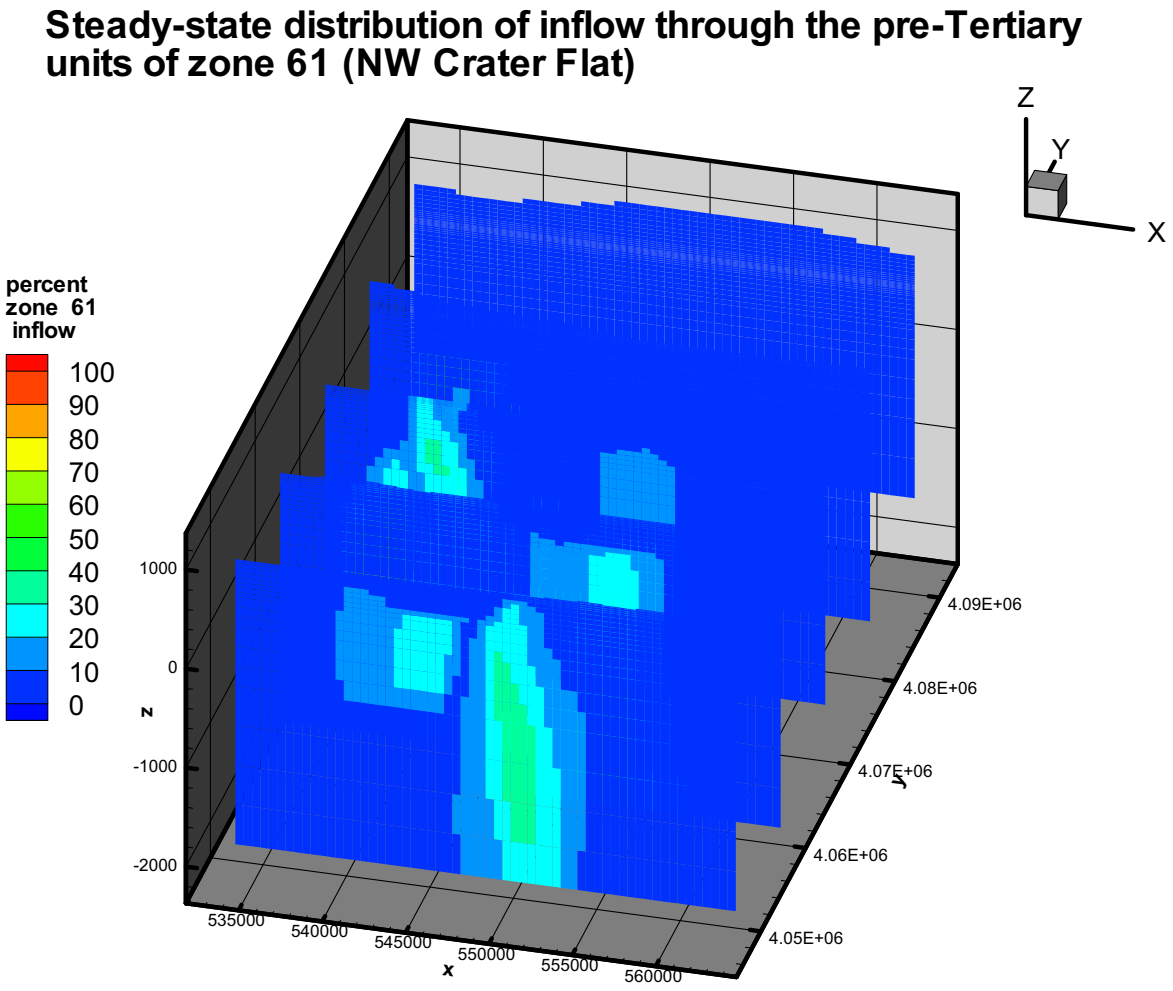

Sources: DTNs: LA0304TM831231.002 [DIRS 163788]; LA0309EK831231.001 [DIRS 171887].

NOTES: The X and Y coordinates are Universal Trans-Mercator Projection (UTM) coordinates in meters. The Z coordinate is elevation relative to sea level in meters. X = UTM-Easting and Y = UTM-Northing.

Figure A6-55. Cross Sectional View of Steady-State Distribution of the Percentage of Inflow through the Pre-Tertiary Units of Northwest Crater Flat Groundwater Calculated Using the Saturated Zone Flow Model

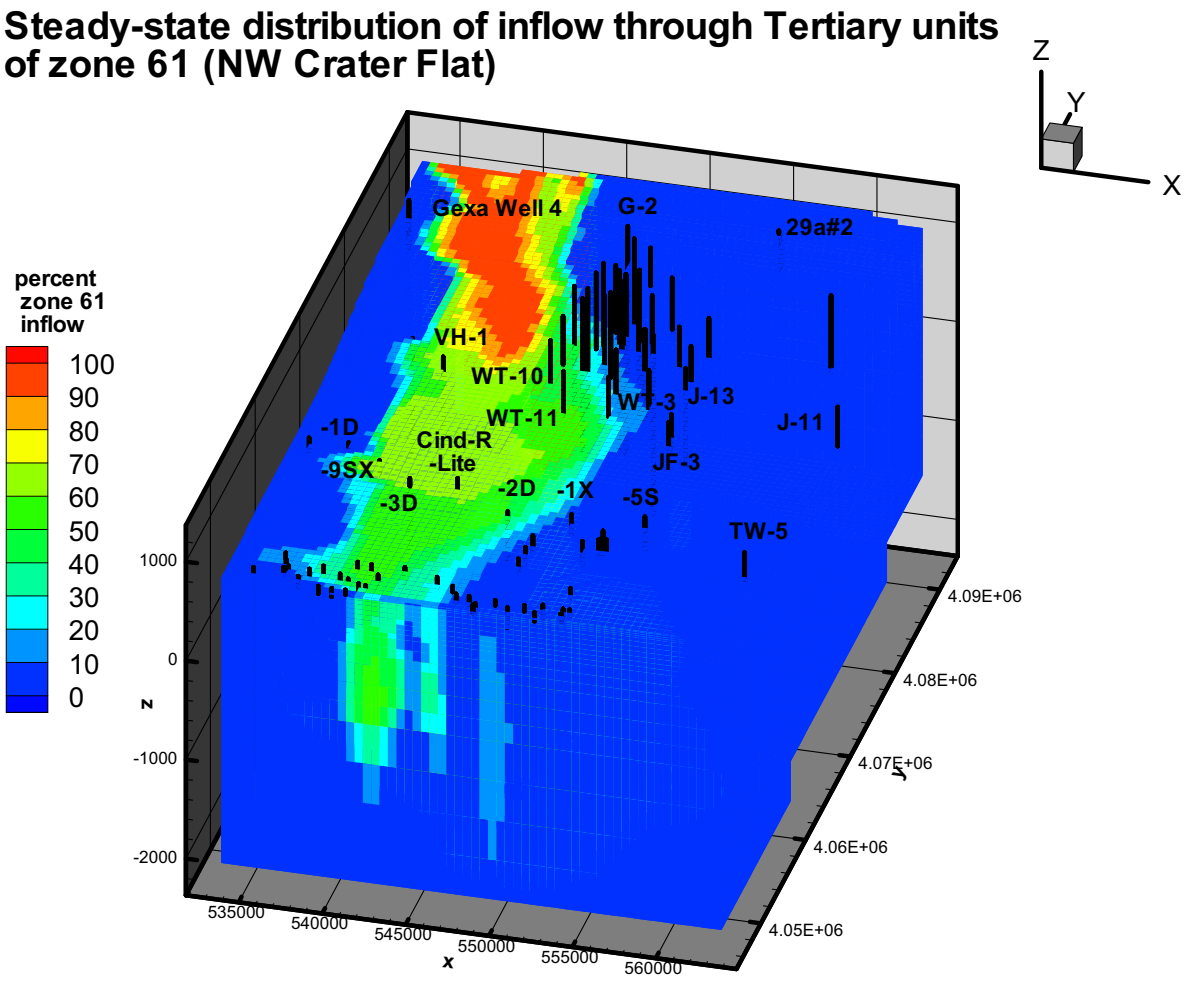

Sources: DTNs: LA0304TM831231.002 [DIRS 163788]; LA0309EK831231.001 [DIRS 171887].

NOTES: The X and Y coordinates are Universal Trans-Mercator Projection (UTM) coordinates in meters. The Z coordinate is elevation relative to sea level in meters. X = UTM-Easting and Y = UTM-Northing.

Figure A6-56. Steady-State Distribution of the Percentage of Inflow through the Tertiary Units of Northwest Crater Flat Groundwater Calculated Using the Saturated Zone Flow Model

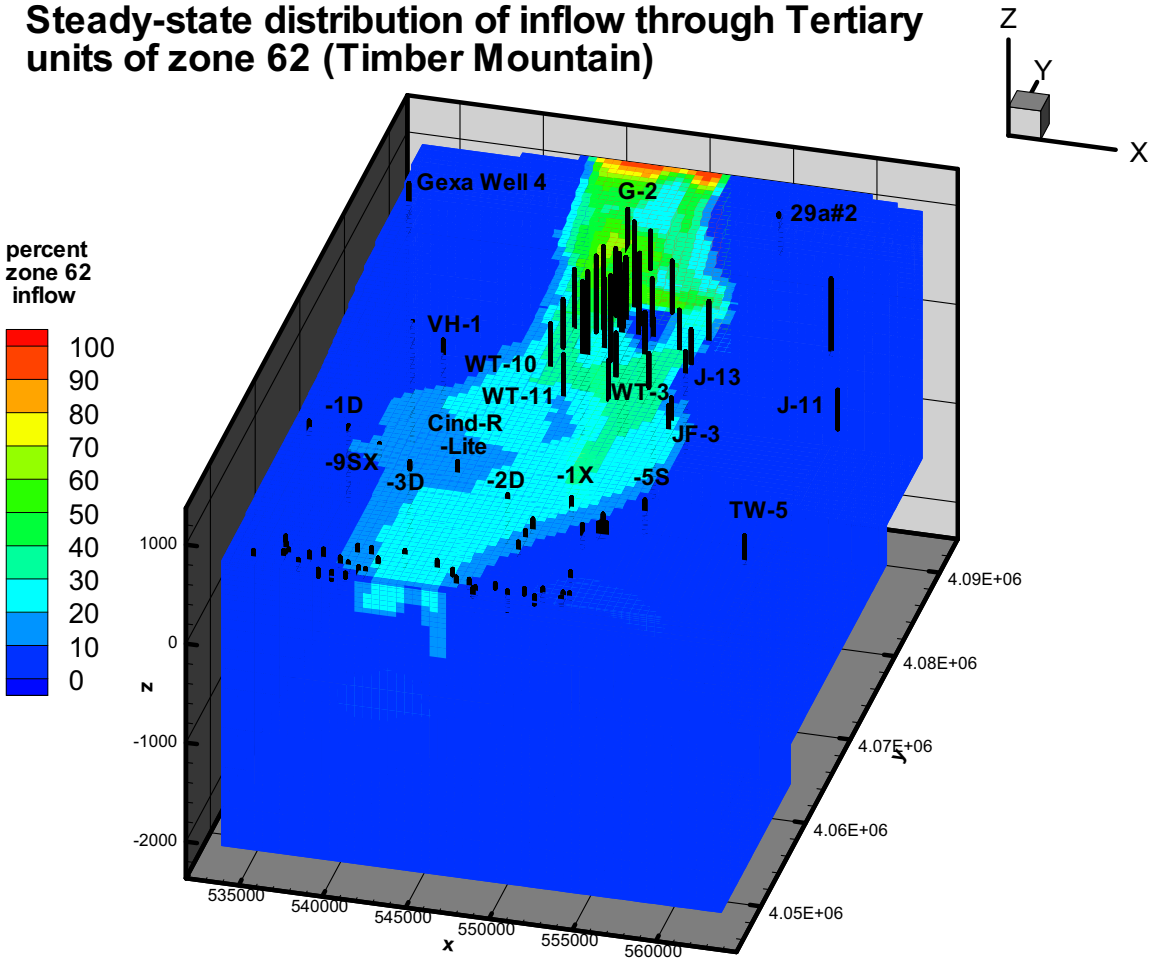

Sources: DTNs: LA0304TM831231.002 [DIRS 163788]; LA0309EK831231.001 [DIRS 171887].

NOTES: The X and Y coordinates are Universal Trans-Mercator Projection (UTM) coordinates in meters. The Z coordinate is elevation relative to sea level in meters. X = UTM-Easting and Y = UTM-Northing.

Figure A6-57. Steady-State Distribution of the Percentage of Shallow Timber Mountain Area Groundwater through the Tertiary Units Calculated Using the Saturated Zone Flow Model

Groundwater entering the model domain from the pre-Tertiary rocks of Zone 63 near Fortymile Canyon follows a sinuous pathway through the Fortymile Wash area and western Jackass Flats as it moves southward through the model (Figures A6-58 and A6-59). The sinuous movement of this tracer plume in the model may be related to the deflection of groundwater eastward around the buried ridge of the Lower Clastic Confining unit in the southwestern part of the model (Figure A6-52) and, later, by the large amount of inflow from Zone 81 in the southeast part of the model (see below). Groundwater from the pre-Tertiary rocks of Zone 63 is predicted by the SZ flow model to be a small component of the shallow groundwater at borehole JF-3 (Site 37) and other Fortymile Wash area boreholes in the northern Amargosa Desert and in the Amargosa Valley area. The groundwater from the pre-Tertiary rocks of Zone 63 could be the component of groundwater from western Jackass Flats predicted from an analysis of sulfur isotopes to be present in minor amounts in some LW and FMW-E groundwaters (Figure A6-51).

The steady-state distribution of groundwater entering the Fortymile Canyon area of the model through the Tertiary rocks of Zone 63 indicates that this groundwater is diluted by groundwater from other areas, including Yucca Mountain (Figure A6-60) by the time it has reached well J-13 (Site 35) in Fortymile Wash. The shallow groundwater entering Zone 63 again becomes a small component of the groundwater southward along Fortymile Wash near JF-3 (Site 37) and in southern Yucca Mountain near well NC-EWDP-2D (Site 91), but does not persist as an identifiable part of the groundwater in the FMW-S area wells. Dilution of the shallow inflow from Zone 63 by downgradient recharge along Fortymile Wash is not a plausible explanation for the dilution of the Zone 63 in flow, given the small amount of Fortymile Wash recharge present in the model. The geochemical and isotopic data from the FMW-N and FMW-S wells indicate a much more significant component of inflow from Zone 63, and perhaps of recharge along the wash, than is indicated by the SZ flow model.

Like groundwater from the pre-Tertiary units of Zone 63, the groundwater entering the northern boundary through the pre-Tertiary rocks of Zone 64 beneath Shoshone Mountain follows a sinuous trajectory through western Jackass Flats and emerges into the shallow flow system in the vicinity of well NC-EWDP-5S (Site 154) of the Amargosa Valley area (figure not shown). Some of the groundwater entering the model through Zone 64 leaves the model along its eastern boundary. The model results suggest that the deep groundwater from Zone 64 could also be the component of groundwater from western Jackass Flats identified from $\delta^{34}S$ analysis to be present in some of the LW and FMW-E area wells. The Tertiary rocks of Zone 64 are comprised of confining units (Figure A6-52) and virtually no groundwater enters the model through these rocks.

The groundwater in the southeast corner of the model near the Skeleton Hills area is dominated by inflow from pre-Tertiary rocks of Zone 81 (Figure A6-61). The model results are consistent with the geochemical and isotopic data from this area, which suggest that the groundwaters near the Gravity fault, and as far west as NC-EWDP-5S (Site 154) and some LW- and FMW-E area wells, contain a component of groundwater from the carbonate aquifer leaking into the alluvium across the Gravity fault.

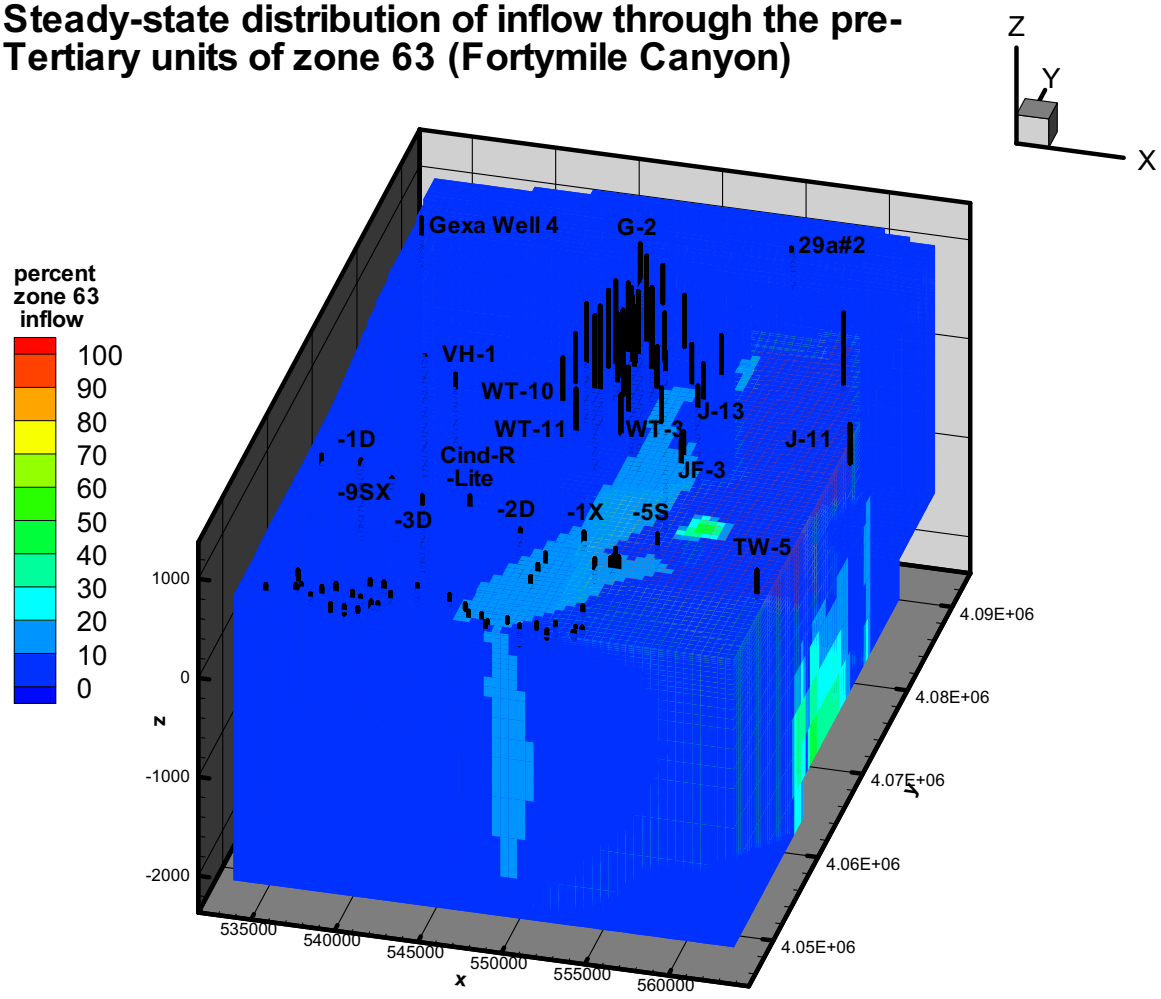

Sources: DTNs: LA0304TM831231.002 [DIRS 163788]; LA0309EK831231.001 [DIRS 171887].

NOTES: The X and Y coordinates are Universal Trans-Mercator Projection (UTM) coordinates in meters. The Z coordinate is elevation relative to sea level in meters.

Figure A6-58. Map View of Steady-State Distribution of the Percentage of Shallow Upper Fortymile Wash Area Groundwater through the Pre-Tertiary Units Calculated Using the Saturated Zone Flow Model

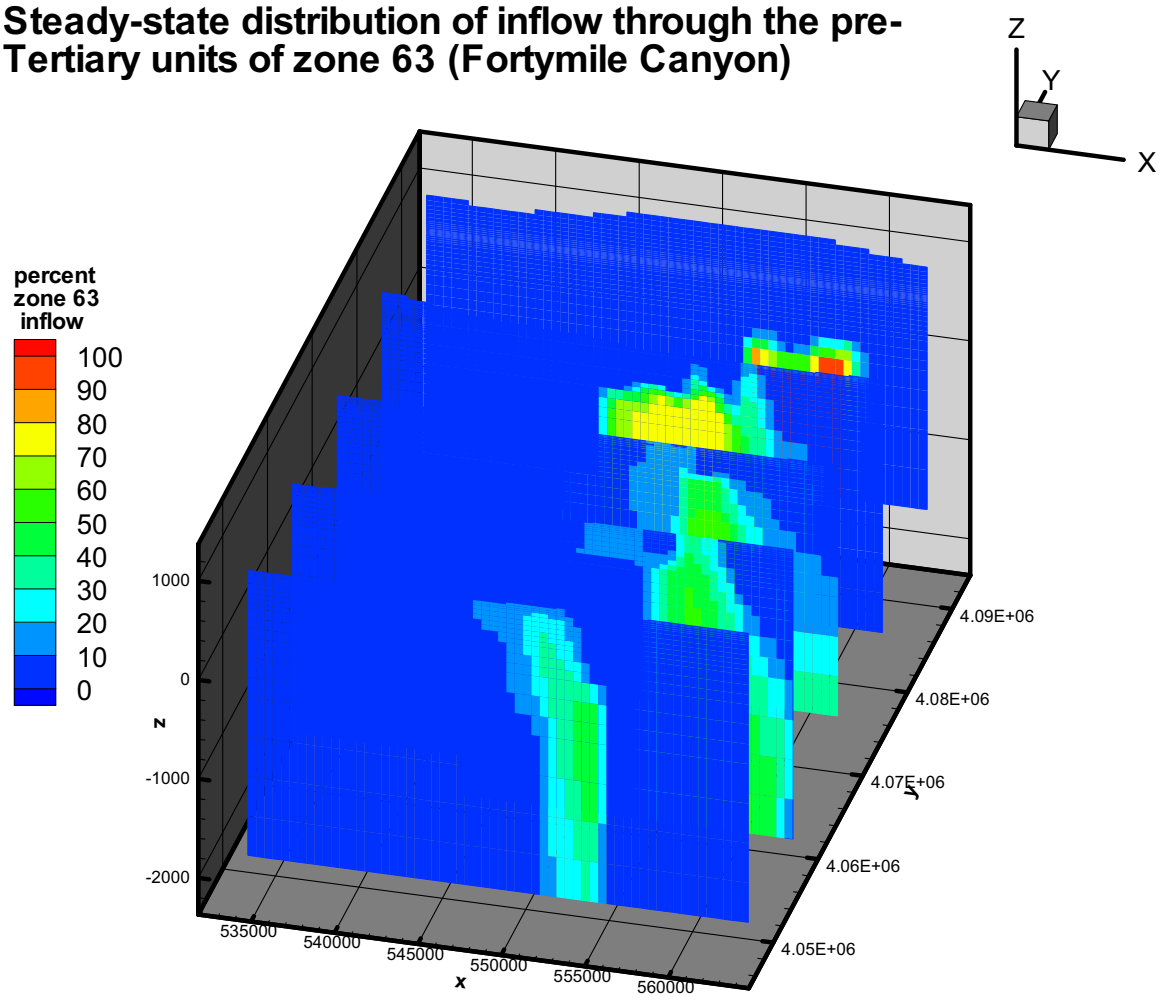

Sources: DTNs: LA0304TM831231.002 [DIRS 163788]; LA0309EK831231.001 [DIRS 171887].

NOTES: The X and Y coordinates are Universal Trans-Mercator Projection (UTM) coordinates in meters. The Z coordinate is elevation relative to sea level in meters.

Figure A6-59. Cross Sectional View of Steady-State Distribution of the Percentage of Shallow Upper Fortymile Wash Area Groundwater through the Pre-Tertiary Units Calculated Using the Saturated Zone Flow Model

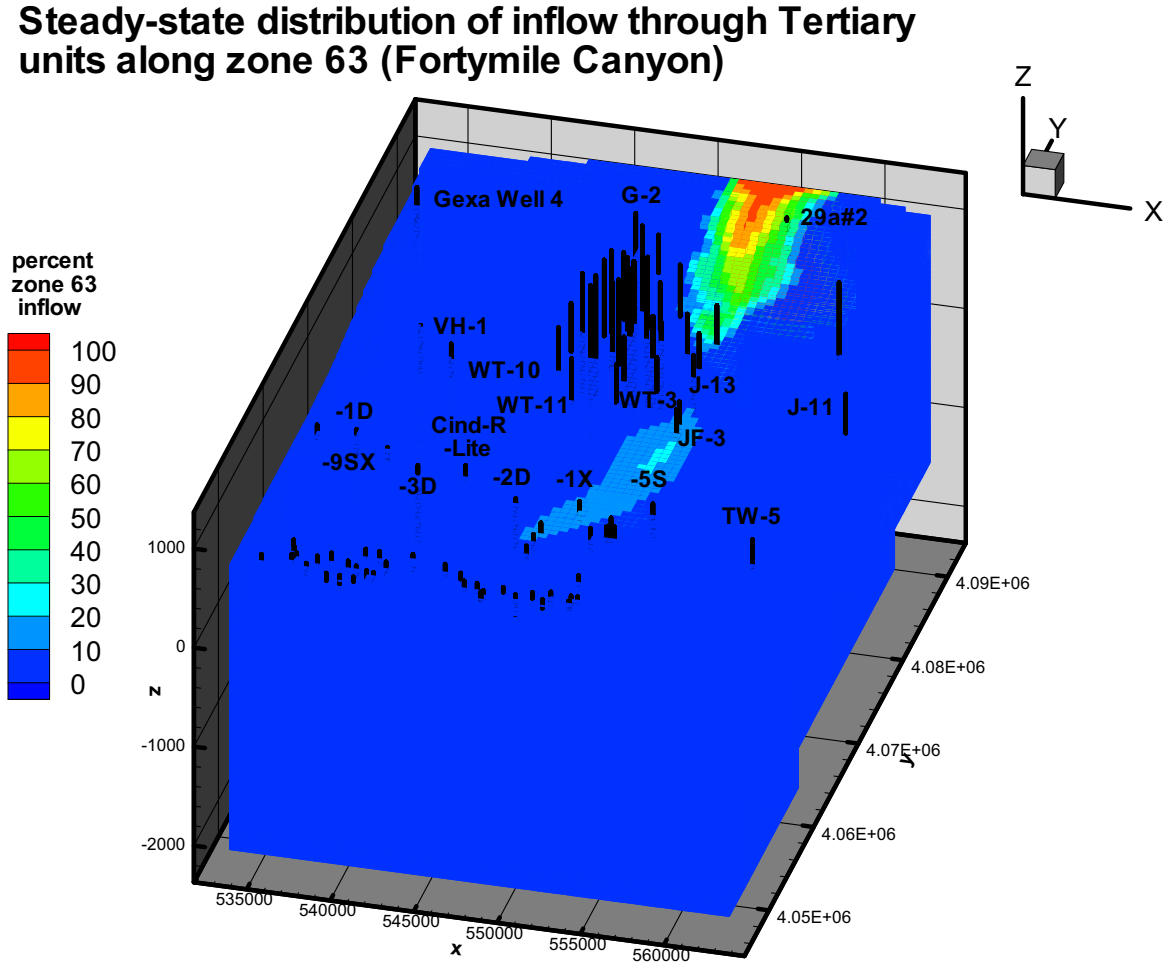

Sources: DTNs: LA0304TM831231.002 [DIRS 163788]; LA0309EK831231.001 [DIRS 171887].

NOTES: The X and Y coordinates are Universal Trans-Mercator Projection (UTM) coordinates in meters. The Z coordinate is elevation relative to sea level in meters.

Figure A6-60. Steady-State Distribution of the Percentage of Shallow Upper Fortymile Wash Area Groundwater through the Tertiary Units Calculated Using the Saturated Zone Flow Model

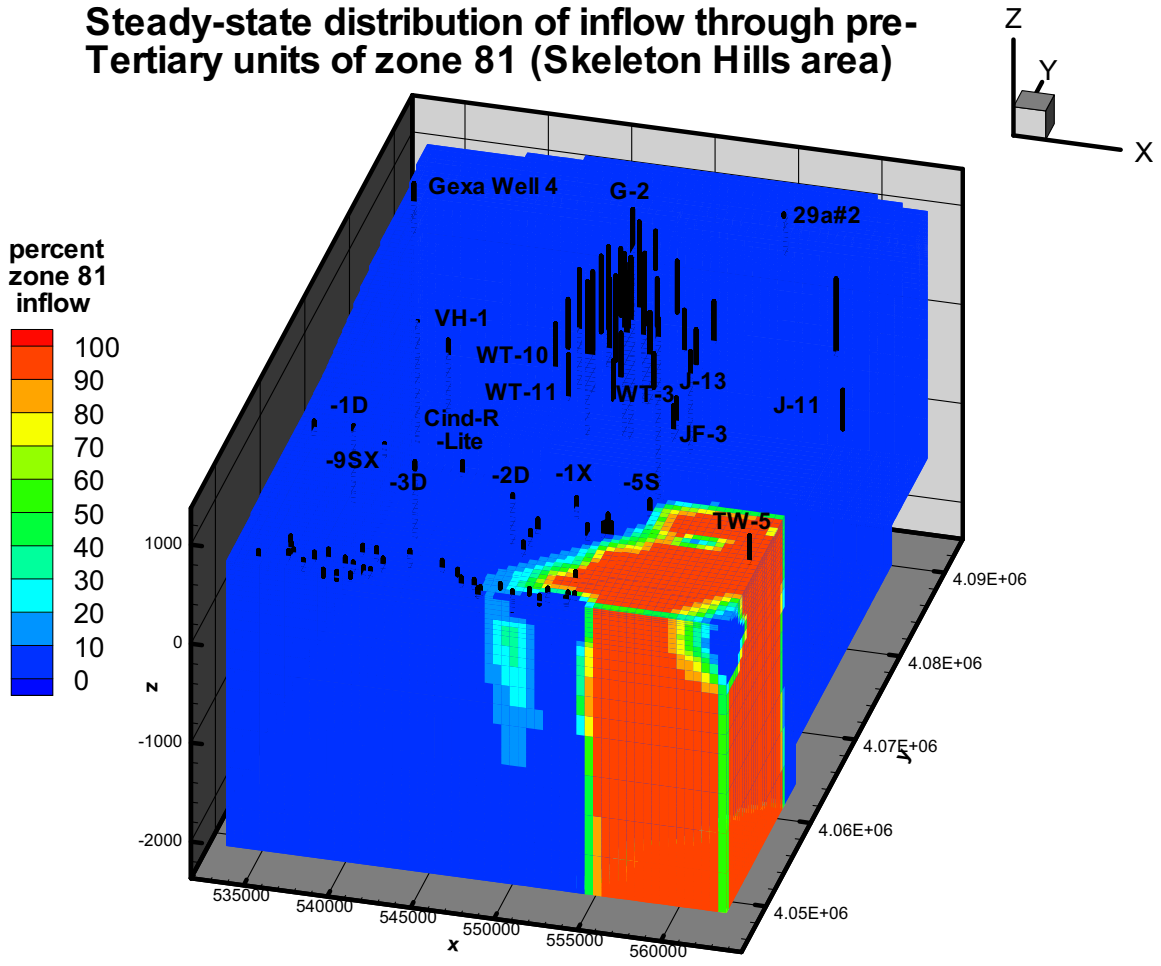

Sources: DTNs: LA0304TM831231.002 [DIRS 163788]; LA0309EK831231.001 [DIRS 171887].

NOTES: The X and Y coordinates are Universal Trans-Mercator Projection (UTM) coordinates in meters. The Z coordinate is elevation relative to sea level in meters.

Figure A6-61. Steady-State Distribution of the Percentage of Pre-Tertiary Rocks of the Skeleton Hills Area Groundwater Calculated Using the Saturated Zone Flow Model

In summary, the flow patterns and mixing relations identified with the SZ flow model are similar in many ways to the flow patterns and mixing relations inferred from the hydrochemical and isotopic data for the area. Of particular importance are the simulations of movement of recharge from the Yucca Mountain area. These simulations indicate that groundwater from Yucca Mountain may not be easily identifiable in groundwaters south of Yucca Mountain because of dilution by groundwater from other, more active parts of the flow system. The SZ flow model appears to underestimate the quantity of inflow from the Fortymile Canyon area through the Tertiary units. This conclusion is based on the observation that groundwater along Fortymile Wash through Jackass Flats and the Amargosa Desert is chemically and isotopically unique

compared to the surrounding groundwaters, but the tracer simulations indicate that groundwater inflow from Fortymile Canyon or from downgradient recharge along the wash is present only in dilute amounts along Fortymile Wash. Some of the discrepancy between the simulations and the data for the Fortymile Wash area may be due to recharge of some or most of this chemically distinct groundwater during wetter climate periods.

A6.3.11 Regional Flow Paths Inferred from Hydrochemical Data

Groundwater flow paths and mixing zones are identified on the basis of the preceding discussions of measured and calculated geochemical and isotopic parameters. The hydraulic gradient shown on the potentiometric surface map (Figure A6-3) is used to constrain flow directions only insofar as groundwater cannot flow from areas of lower hydraulic head to areas of higher hydraulic head. Chemical and isotopic composition of groundwater were then used to locate flow pathways in the context of the hydraulic gradient and considering the possibility that flow paths can be oblique to the potentiometric gradient because of anisotropy in permeability.

The analysis of flow paths that follows assumes that Cl^- and SO_4^{2-} values are conservative and that changes to these are due to mixing along flow paths. This same assumption holds for isotopes of hydrogen and oxygen; however, because recharge waters have almost certainly changed over time, it is to be expected that isotopic variability in these constituents will occur in groundwaters of different ages (Benson and Klieforth 1989 [DIRS 104370], Figure 11; Winograd et al. 1992 [DIRS 100094], Figure 2). In spite of the potential reactive nature of Na and Ca, the contrast in concentrations between some areas is great enough that meaningful inferences about flow directions can be made.

Flow paths can be traced using conservative constituents only where compositional differences exist that allow some directions to be eliminated as possible flow directions. Some chemical and isotopic species in some areas have relatively uniform compositions and, thus, provide no information about flow paths. In other areas, they show more distinct compositional differences and, thus, can be used to infer flow directions. Because no single chemical or isotopic species varies sufficiently to determine flow paths everywhere in the study area, multiple lines of evidence were used to construct the flow paths inferred in this section. This evidence includes the areal distribution of chemical and isotopic species, sources of recharge, groundwater ages and evaluation of mixing/groundwater evolution through scatterplots, and inverse mixing and reaction models as presented in the previous sections.

Flow path 1 (Figure A6-62) traces the movement of groundwater southeastward from Oasis Valley (OV/NWA group) through the Amargosa Desert along the axis of the Amargosa River (AR and AR/FMW groups) to its confluence with Fortymile Wash (FMW-S group). This flow path is identified from areal plots of chloride (Figure A6-15) and scatterplots of SO_4^{2-} versus Cl^- (Figure A6-50) that support this flow path. It is inferred from Figure A6-50 that the more dilute groundwater from the Oasis Valley area (OV/NWA group) became concentrated by evapotranspiration as it moves from the Oasis Valley area into the northwestern Amargosa Desert toward sites 15 to 17. This inference is based on the common trend of the OV/NWA and AR groups in Figure A6-50, which indicates that the composition of the AR group can be derived by concentrating groundwater from the OV/NWA group through evapotranspiration downgradient from the Oasis Valley sample locations. Data contained in White (1979

[DIRS 101165], Table 2, sample sites 28 and 29) corroborate this interpretation. These data show that groundwater exiting Oasis Valley through Beatty Narrows into the NW Amargosa Desert has a Cl^- concentration of between 76.9 and 100.0 mg/L and SO_4^{2-} concentrations of between 183.5 and 249.8 mg/L. The more dilute solute concentration of these two samples is nearly identical to that from Sites 15 to 17. The data in Figure A6-50 also indicate that groundwater in the CF-SW group has a much lower Cl^- concentration than groundwater in the AR group, making it unlikely that groundwater from the CF-SW wells is a major component of groundwater in the AR and FMW-W wells. Groundwater along flow path 1 becomes more dilute in the AR/FMW wells as it becomes increasingly mixed with FMS-S group groundwater near Fortymile Wash (see below). Northwest of this mixing zone, high groundwater ^{14}C activities (Figure A6-28) and variable δD (Figure A6-24) and $\delta^{18}O$ (Figure A6-25) compositions at the AR wells indicate the presence of relatively young recharge in the groundwater due to runoff or irrigation in the area.

Flow path 2 (Figure A6-62) traces the movement of groundwater from the Fortymile Canyon area southward along the axis of Fortymile Wash into the Amargosa Desert. This flow pathway is drawn on the basis of similar anion and cation concentrations along the flow line and dissimilarities compared to regions to the east and west (see, for example, Figures A6-15, A6-16, and A6-22). Groundwater along the northern part of this flow path (FMW-N groups samples) is distinguished from groundwater at Yucca Mountain by δD and $\delta^{18}O$ compositions that are heavier and/or more offset from the global meteoric water line ($\delta D = 8\ \delta^{18}O + 10$) than the groundwater found under Yucca Mountain (Figure A6-48). It is inferred that the groundwater found along the FMW-S wells in the Amargosa Desert is derived, in part, from groundwater flow from the FMW-N wells, based on the similarly dilute SO_4^{2-} (Figure A6-16) and Cl^- (Figure A6-15) compositions of these groundwaters. Differences in the δD compositions of the FMW-N and FMW-S groundwaters (Figure A6-24) are attributed to the effects of changing climatic conditions on the δD composition of recharge (see Section A6.3.6.6.1). Groundwater flow from the FMW-N area wells southward into the Amargosa Desert along the axis of the wash is also compatible with expected and observed chemical evolution trends between the two areas, such as downgradient increases in pH (Figure A6-14), calcite saturation indices (Figure A6-37), and HCO_3^- (Figure A6-17) and SiO_2 (Figure A6-1) concentrations. Some part of the groundwater along Fortymile Wash may also be derived by recharge from overland flow, based on the observation that ^{14}C activities do not decrease systematically southward in either the northern or southern segments of the wash (Figure A6-28). Groundwater flow from the eastern and western parts of the Amargosa Desert toward Fortymile Wash is relatively minor, however, based on the much higher solute contents (Figures A6-15 to A6-17, and A6-34) and distinct isotopic compositions (Figures A6-26 and A6-27) of groundwaters adjacent to the FMW-S area wells.

Flow path 3 (Figure A6-62) traces the movement of groundwater from Jackass Flats in the vicinity of well J-11 (Site 67) as it moves along the western edge of the Amargosa Valley (LW) area wells and arcs southward through the FMW-E area wells. The identification of groundwater from Jackass Flats in this mixture of groundwaters is possible because the high SO_4^{2-} and low $\delta^{34}S$ characteristics of groundwater from well J-11 distinguish it from the high SO_4^{2-} and high $\delta^{34}S$ groundwater characteristic of the Gravity fault (GF group) and the low SO_4^{2-} and low $\delta^{34}S$ groundwater of the Fortymile Wash area (FMW-S group) on scatterplots of $\delta^{34}S$ versus $1/SO_4^{2-}$

concentration (Figure A6-51). A source for this high SO_4^{2-} groundwater from Jackass Flats rather than the Gravity fault area is also indicated by the similarly light $\delta^{13}C$ of groundwater along this flow path (Figure A6-27).

Flow path 4 (Figure A6-62) traces the movement of groundwater from the lower Beatty Wash area (southern TM group samples) into northwestern Crater Flat. This groundwater flows predominantly southward in Crater Flat through Sites 69 (borehole VH-1) and Site 86 (NC-EWDP-3D). The chemistry and isotopic composition of this groundwater appears to be a mixture of subequal amounts of groundwater from Sites 22 and 23 in lower Beatty Wash, with much smaller amounts of recharge from local runoff in Crater Flat or groundwater flow from Site 24 (Section A6.3.8.4). Dashed lines are used to illustrate these relationships on Figure A6-62. Groundwater from Site 68 (GEXA Well 4), which may be groundwater from Site 23 modified by recharge from surface runoff (Section A6.3.8.3), also contributes groundwater to this flow path. Scatterplots and PHREEQC inverse models (Sections A6.3.8.3 and A6.3.8.4) show that a mixture of groundwater from Sites 22 and 23 is required to account for both the relatively low Cl^- and the light $\delta^{18}O$ and δD activity ratios characteristic of this flow path, whereas small amounts of recharge from local runoff or flow from Site 24 are needed to decrease the $\delta^{13}C$ of the lower Beatty Wash groundwater.

Most groundwater at Timber Mountain north of Yucca Mountain (TM group) is characterized by $\delta^{13}C$ values that are too heavy (–6 to 0 per mil) and ^{14}C values that are too low for it to be a major source of groundwater at Yucca Mountain (Figure A6-45). The absence of significant amounts of Timber Mountain groundwater beneath Yucca Mountain is also indicated by the extremely low $\delta^{87}Sr$ and high Sr^{2+} concentration of the Timber Mountain groundwater compared to Yucca Mountain (Figure A6-32 and A6-31). The extremely light $\delta^{13}C$ (Figures A6-27 and A6-45) and high $\delta^{87}Sr$ (Figure A6-32) of groundwater in northern Yucca Mountain (YM-CR group) compared to Timber Mountain (TM group) groundwater indicates that groundwater from the Timber Mountain/Beatty Wash area does not flow south through northern Yucca Mountain. One well in upper Beatty Wash (Site 24 - ER-EC-07) has a high ^{14}C activity (Figure A-28), and $\delta^{13}C$ (Figure A6-27) and $\delta^{87}Sr$ values (Figure A6-32) similar to those of groundwaters in the Solitario Canyon Wash area (SCW group) and to groundwater south of Drill Hole Wash at Yucca Mountain. Based on Figure A6-45, some groundwater from the area of well ER-EC-07 in upper Beatty Wash could be present in Yucca Mountain groundwater south of Drill Hole Wash (YM-C, YM-SE, and YM-S groups) and along Solitario Canyon Wash (SCW group) if sorption on rock removed most of the Sr^{2+} from the Beatty Wash area along its flow path.

Flow path 5 (Figure A6-62) traces groundwater with a distinct chemical composition that comprises the SW Crater Flat (CF-SW) Group. Groundwater from site 70 (borehole VH-2) is chemically and isotopically distinct from groundwater that characterizes flow path 4, with higher concentrations of many major ions (Figures A6-15 to A6-17) (but lower concentrations of F (Figure A6-18) and SiO_2 (Figure A6-19)) and relatively high $\delta^{18}O$ (Figure A6-25) and δD (Figures A6-24 and A6-49) values. The $\delta^{18}O$ and δD of groundwater from borehole VH-2 is similar to groundwater from Species Spring (Rose et al. 1997 [DIRS 144725]), a perched spring at Bare Mountain, suggesting that groundwater at borehole VH-2 and other CF-SW group wells are derived principally from local recharge and runoff from Bare Mountain. Dashed east and southeast-oriented lines schematically illustrate this

flow (Figure A6-62). Groundwater in Oasis valley has some of the lightest groundwater δD and $\delta^{18}O$ values in the Yucca Mountain area (Figures A6-24 and A6-25), eliminating flow from Oasis Valley under Bare Mountain as a possible source of groundwater in southwest Crater Flat. The similar chemical and isotopic characteristics between groundwater from borehole VH-2 and other southwest Crater Flat boreholes (Section A6.3.4) and PHREEQC models of Sites 77 and 81 (Sections A6.3.8.5 and A6.3.8.6) indicate a dominantly north-south flow along this flow path as far south as these sites. Importantly, the chemically distinct groundwater along this flow pathway is not observed in boreholes to the south in the Amargosa Desert (AR and FMW-S groups) (for example, see Figure A6-50). Mixing relationships discussed in connection with Figure A6-49, and PHREEQC models of Sites 86 and 90 (Sections A6.3.8.7 and A6.3.8.8), suggest that this groundwater likely flows to the east and southeast and mixes with wells from the YM-S group (Figure A6-49).

Flow path 6 (Figure A6-62) traces the movement of groundwater from Site 42 (well WT-10) southward toward Sites 89 (Cind-R-Lite well) and 90 (well NC-EWDP-15P). This flow path is identified from PHREEQC models that indicate that groundwater from well NC-EWDP-15P is formed from subequal amounts of groundwater from Sites 69 (well VH-1) and 42 (well WT-10), with a minor component (5%) of groundwater like that from Site 70 (well VH-2) (see Section A6.3.8.8). Mixing trends indicated by plots of Cl versus δD (Figure A6-49) also suggest leakage from Crater Flat toward the YM-S group in southern Yucca Mountain. Although the predominant direction of flow from the Solitario Canyon (SCW group) area is southward along the Solitario Canyon fault, evidence for the leakage of small amounts of groundwater eastward across the fault is also provided by similarities in the ion concentrations and isotopic values of groundwaters in the SCW and YM-CR area wells (Section A6.3.6.3, Figures A6-42 to A6-46). This chemical and isotopic similarity indicates that groundwater as far east as borehole NC-EWDP-19D may have some component of groundwater from the Solitario Canyon Wash area. The short southeast-oriented dashed lines from Solitario Canyon group wells schematically illustrate this leakage.

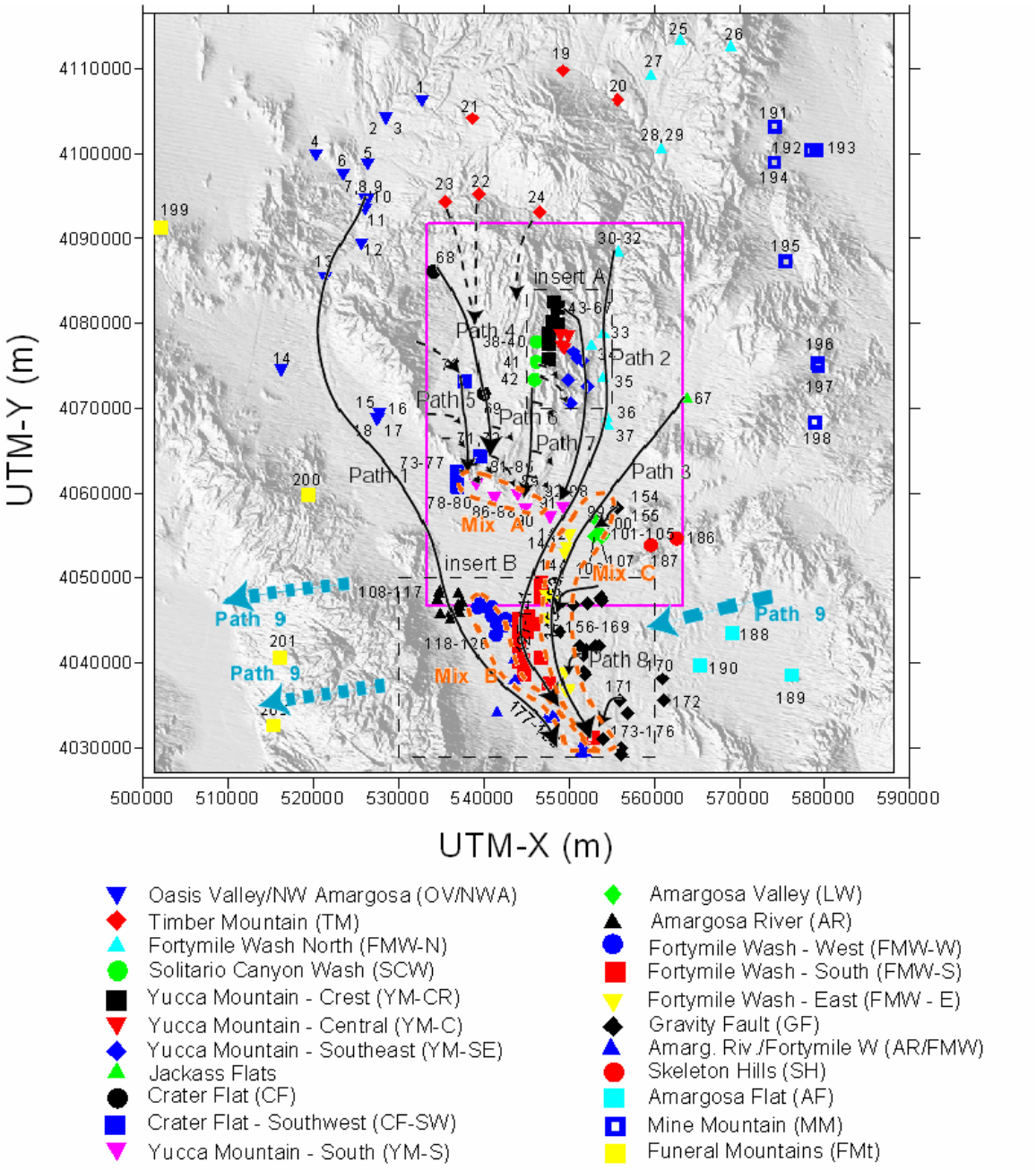

Source: DTN: LA0308RR831233.001 [DIRS 171890].

NOTES: This figure has color-coded data points and should not be read in a black and white version. Solid lines indicate a relatively high degree of confidence in the interpretations; dashed flow paths indicate relatively less confidence. Base map shows borehole designators and inserts; for reference see Figure A6-5 and Table A4-3.

UTM-X = UTM-Easting, UTM-Y = UTM-Northing; UTM = Universal Transverse Mercator.

Figure A6-62. Regional Flow Paths Inferred from Hydrochemical and Isotopic Data

Flow path 7 (Figure A6-62) traces the movement of groundwater from northern Yucca Mountain southeastward toward YM-SE wells in the Dune Wash area and then southwestward along the western edge of Fortymile Wash. The upper segment of this flow path is motivated by the high groundwater $^{234}U/^{238}U$ activity ratios found in the northern Yucca Mountain and Dune Wash areas (Figure A6-47). High $^{234}U/^{238}U$ activity ratios (greater than 7) typify both perched water and groundwater along and north of Drill Hole Wash but not groundwater along Yucca Crest at borehole SD-6 (Site 50) or perched water at borehole SD-7. Based on the conceptual model for the evolution of $^{234}U/^{238}U$ activity ratios described in Section A6.3.6.2, dissolution of thick vitric tuffs that underlie the Topopah Spring welded tuff along Yucca Crest south of Drill Hole Wash would be expected to decrease the $^{234}U/^{238}U$ activity ratios of deep unsaturated zone percolation south of the Wash. High $^{234}U/^{238}U$ activity ratios are expected only where these vitric tuffs are absent, as in northern Yucca Mountain. Results of a PHREEQC analysis of the evolution of groundwater between site 44 (well WT-24) in northern Yucca Mountain and Site 65 (well WT-3) in the Dune Wash area are consistent with this segment of flow path 7 (Section A6.3.8.9). The southern segment of flow path 7 is based on PHREEQC analyses of groundwater evolution between well WT-3 and various depth intervals of well NC-EWDP-19D (Sites 92 and 94 to 98) (Section A6.3.8.10). Groundwater at well NC-EWDP-19D has low Cl^- (Figure A6-15) and SO_4^{2-} (Figure A6-16) concentrations that are characteristic of groundwater at well WT–3. The light $\delta^{18}O$ and δD values eliminate Fortymile Wash as a possible source of the dilute groundwater at well NC-EWDP-19D (Figures A6-24, A6-25, A6-44 and A6-48). An alternative set of PHREEQC analyses was developed that interprets the groundwater at NC-EWDP-19D to be a result of the mixing of groundwater from well WT-10 and local southern Yucca Mountain recharge, as represented by perched water from borehole SD-7 (Section A6.3.8.10). Both sets of models explain the major-ion chemistry and $\delta^{13}C$ values of groundwater at NC-EWDP-19D. The arrows leading from flow path 6 toward NC-EWDP-19D (Figure A6-62) reflect this alternative groundwater path. It should also be noted that the $\delta^{18}O$ and δD values of groundwater at well NC-EWDP-19D are substantially lighter than for groundwater at either wells WT-3 or WT-10, requiring that climate change be invoked as a possible explanation for their differences.

Flow Path 8 (Figure A6-62) schematically illustrates leakage of groundwater from the carbonate aquifer (GF and AF Groups) across the Gravity fault. Hydrogeologists and geochemists have recognized this leakage across the fault for many years (Winograd and Thordarson 1975 [DIRS 101167]; Claassen 1985 [DIRS 101125]). These hypotheses are also compatible with the hydraulic gradient and our understanding of the regional groundwater flow patterns (Lacziak et al. 1996 [DIRS 103012]). The carbonate aquifer component in this groundwater is recognized by many of the same chemical and isotopic characteristics that typify groundwater discharging from the carbonate aquifer at Ash Meadows. These characteristics include high concentrations of Ca^{2+} (Figure A6-20) and Mg^{2+} (Figure A6-21), low SiO_2 (Figure A6-19), heavy $\delta^{13}C$ values (Figure A6-27), low ^{14}C activity (Figure 6-28), and comparable $\delta^{18}O$ and δD values as the Ash Meadows groundwater. Westward seepage of this groundwater mixes with the southward flow of groundwater along path 3 to produce groundwater with compositions intermediate between the two (Section A6.3.7.2). Evidence for these flow paths is best defined in groundwater compositions of some of the more westerly samples of the GF group such as samples 160, 175, and 175 (Figure 6-50).

Flow path 9 (Figure A6-62) is drawn to schematically illustrate deep underflow of groundwater from the carbonate aquifer, east of and including the GF and AF groups, beneath the Amargosa Desert and Funeral Mountains to the discharge points in Death Valley. The similarity in the chemical and isotopic characteristics of groundwater found in the Gravity fault area and groundwater that discharges from springs at sites 201 (Nevares Spring) and 202 (Travertine Spring) support this interpretation. The dissimilarity in Cl^- (Figure A6-15), Mg^{2+} (Figure A6-21), and SiO_2 (Figure A6-19) concentrations in these springs compared to the groundwater from the alluvial aquifer along the Amargosa River suggests that this alluvial groundwater is not the predominant source of the spring discharge in Death Valley.

A6.3.11.1 Mixing Zones

Figure A6-62 also highlights three zones (Mix A, B, and C) within which there is good evidence for mixing as demonstrated by trends of multiple solutes and isotope ratios on cross-correlation plots. Details of the mixing relations were given in Section A6.3.7.

Mixing zone A is defined by YM-S and CF-SW samples along U.S. Highway 95. The mixing zone is indicated by groundwater compositions of samples 78 to 85, 89, and 90 that are intermediate between the compositionally distinct groundwater of the CF-SW group and dilute groundwater of the YM-S group that is interpreted to have originated in the Yucca Mountain area (see Figure A6-49 and the discussion of flow paths 6 and 7 in Section A6.3.11). The location of the southernmost CF-SW samples coincides with a steep hydraulic gradient (Figure A6-3), which remains steep to the west but decreases to the east. Evidence for the distinct groundwater of the CF-SW group in boreholes to the south in the Amargosa Desert is lacking (for example, Figure A6-50). Thus, hydrochemical data and the hydraulic gradient suggest that southward flow indicated by flow path 5 is effectively blocked to the south. This flow is at least partly diverted to the east where it mixes with more dilute groundwater of the YM-S group to the east.

Mixing zone B consists of samples from the FMW-W and AR/FMW groups and a few samples from the FMW-S groups. The zone highlights groundwater with compositions that are intermediate between the distinct and consistent groundwater compositions of the AR group and the dilute groundwater of the FMW-S group (Figure A6-50). Flow path 1 is drawn to skirt the edge of mixing zone B and to connect the groundwater from the Amargosa River group to sample 181, which has a similar groundwater composition and is interpreted to represent undiluted groundwater from the AR group.

Mixing zone C consists of all samples from the LW and FMW-E groups, a few of the more westerly samples form the GF group, and at least one sample (141) from the FMW-S group. The mixing zone is characterized by small percentages of the distinctively high SO_4^{2-} groundwater from borehole J-11 (Figure A6-51) in groundwater near flow path 3. This distinct hydrochemical signature persists in variable percentages as far south as borehole 150. Groundwater with this distinctive signature is mixed to variable degrees with dilute water from the FMW-S group to the west or groundwater from the carbonate aquifer (GF Group) to the east.

An important conclusion derived from identification of these mixing zones is that they qualitatively illustrate the extent of transverse dispersivity along certain flow pathways. The mixing zones also illustrate that, although some flow pathways may remain intact for great distances (e.g., paths 1 and 2), even these most-persistent flow paths eventually loose their distinct character, largely through mixing. This effect is best illustrated in southern Amargosa desert where flow paths 1, 2, and 3, with contributions from 8, converge and mix. The distinct end member groundwater of the AR and FMW-S groups, representing flow paths 1 and 2, appears to be absent at the southern boundary of the study area. Whereas it is possible that these end member groundwaters have not yet been sampled, the proximity of mixed groundwater samples in the southern part of the study area (samples 141, 174, 175, 183, 184, and 185) leaves little room for unmixed (end member) groundwater to move through the area. The hydrochemical data are interpreted to indicate that groundwaters from distinct sources that merge in the Amargosa Desert eventually lose their hydrochemically distinct character and flow southward as partially mixed groundwater.

A7. SUMMARY, DATA TRACKING NUMBERS, AND UNCERTAINTIES

A7.1 SUMMARY

Hydrochemical data from the saturated zone in the Yucca Mountain region were compiled, documented, and analyzed in this appendix. The hydrochemical data are used together with physical hydraulic data to evaluate the local and regional flow system at Yucca Mountain. This report provides an independent assessment of the flow patterns (Section A6.3.11) and recharge rates (Section A6.3.6) near Yucca Mountain that can be compared with flow paths and recharge rates associated with the SZ site-scale flow model documented in *Water-Level Data Analysis for the Saturated Zone Site-Scale Flow and Transport Model* (BSC 2004 [DIRS 170008]), and for which the model input/output files are in DTN: LA0304TM831231.002 [DIRS 163788]. This report also provides an independent basis for calculating groundwater residence times (Section A6.3.9) that can be compared with particle breakthrough curves calculated using the site-scale SZ transport model. Additionally, this appendix contributes to the resolution of technical issues associated with groundwater residence times and flow path lengths in alluvium and tuff, as discussed below. The methods used in this appendix are widely accepted, the data are sufficient and the analysis appropriate for the intended use if this document.

A7.1.1 Summary of Overview Sections (Sections A6.3.1 to A6.3.5)

Areal distributions of chemical and isotopic data as well as calculated parameters show many consistent patterns throughout the study area. Groundwater that has low concentration of most solutes characterizes groundwater beneath Yucca Mountain and in Fortymile Wash. Dilute groundwaters characterize the northern part of Fortymile Wash as well as the southern part in the Amargosa Desert. Increases in most solute concentrations occur to the west of Yucca Mountain and along the southern margin of Yucca Mountain near U.S. Highway 95. Dilute groundwaters are flanked by less dilute groundwaters to the east and west in the Amargosa Desert. Hydrochemical data presented in these sections provide first-order constraints on flow pathways. Groundwater beneath Yucca Mountain and in Fortymile Wash is characterized by low concentrations of most solutes.

Section A6.3.3 reveals that some wells display significant hydrochemical variability with depth. An important example is illustrated in the data from wells NC-EWDP-19D and -19P, which show that groundwater in all zones is similar to groundwater from the volcanic aquifer at Yucca Mountain, whereas groundwater in -19P is more chemically similar to groundwater in Fortymile Wash. These data illustrate potentially important information regarding flow pathways that may be obscured when only groundwater samples from open boreholes are available, as is the case for most data in this report. In the absence of additional discrete vertical sampling data, the two-dimensional analysis will form the basis of the flow-path analysis described herein.

A7.1.2 Summary of Sources and Evolution of Recharge at Yucca Mountain (Section A6.3.6)

Particular attention is given to this topic to set the stage for evaluation of flow from Yucca Mountain. Hydrochemistry of perched water is considered a reliable surrogate for potential recharge water. The hydrochemistry of perched groundwater is quite similar to that of groundwater beneath Yucca Mountain. Some perched water and groundwater beneath Yucca Mountain has similarly elevated $^{234}U/^{238}U$ activity ratios and relatively small uranium concentrations. Depth-dependent trends in uranium activity ratios of unsaturated-zone pore water and perched water are also consistent with a model for local recharge. Local recharge of groundwater beneath Yucca Mountain is also supported by hydrochemical evaluation of potential upgradient sources of groundwater. Significant hydrochemical differences between most of these waters argue against the possibility that significant percentages of upgradient groundwater are present at Yucca Mountain. It is therefore concluded that much of the water present beneath Yucca Mountain was derived from local recharge.

Estimates of the magnitude of recharge at Yucca Mountain were obtained using the chloride mass balance method. For groundwaters within the immediate vicinity of Yucca Mountain, chloride concentrations range from 5.7 to 10.8 mg/L (excluding p#1-v), indicating local recharge rates between 4.7 and 17.9 mm/yr using an average, present-day precipitation rate of 170 mm/yr and an estimated range of Cl^- concentrations in precipitation of 0.3 to 0.6 mg/L.

The timing of recharge at Yucca Mountain was evaluated using hydrogen and oxygen isotopes as well as ^{14}C ages. Although the hydrogen and oxygen isotope data do not place an absolute age on the groundwater, they do indicate that the groundwater was recharged under paleoclimatic conditions that existed until the late Pleistocene. Corrected groundwater ^{14}C ages range from 11,430 years at borehole UE-25 WT#3 to 16,390 years at borehole UE-25 WT#12. These calculations are based on the averaged, that is, mixed age, of the groundwater sample. Calculations are also presented to bound the fraction of young water present in Yucca Mountain recharge. Estimates using an age of 1,000 years for the young component range from a low of about 0.02 at borehole UE-25 WT#12 to more than 0.15 at boreholes UE-25 WT#3 and USW G-4. Smaller fractions of young water would be present if water younger than 1,000-year-old were assumed in the calculations.

A7.1.3 Summary of Groundwater Flow and Evolution Away From Yucca Mountain (Sections A6.3.7 to A6.3.10)

Areal distribution plots reveal regions where steep gradients in solute concentrations and isotopic signatures exist. Based on evaluating elemental and isotopic correlation and PHREEQC analyses, it is concluded that mixing does readily explain compositional gradients in some areas. For example, mixing explains the compositional gradient displayed by the Nye County wells along U.S. Highway 95 where dilute groundwater to the southeast mixes with groundwater with high solute concentrations present to the northwest. Mixing also readily accounts for many of the groundwater compositions found in the Amargosa Desert. Here, dilute groundwater present along the Fortymile Wash drainage in the central part of the Amargosa Desert mixes with groundwater to the east and west to produce intermediate compositions. It is also concluded that sulfate-rich groundwater similar to that found in well J-11 is present in the Amargosa Desert. PHREEQC analyses help to confirm mixing relationships and define other components that must be added or removed through water-rock interaction to achieve observed groundwater compositions.

In Section A6.3.9, groundwater velocities are estimated along a selected flow path south of the repository in the Yucca Mountain area. Velocities are estimated by evaluating the ^{14}C activities of the groundwater along the flow path in context with PHREEQC analyses of groundwater evolution. Estimated groundwater velocities along a linear flow path from WT-24 to WT-3 are 46 m/yr or higher. Groundwater velocities were also estimated along a flow path from WT-3 to the various zones sampled at NC-EWDP-19D. These velocities range from approximately 80 m/yr to 5 m/yr. The faster velocities are suggested to indicate that some of the shallow groundwater at well WT-3 moves along major faults such as the Paintbrush Canyon fault.

The site-scale saturated zone flow model (or, simply, SZ flow model) was used to simulate the movement of a conservative tracer from various segments along the boundaries in the model (Section A6.3.10). Flow patterns and mixing relations identified with the SZ flow model were generally consistent with flow patterns and mixing relations inferred from the hydrochemical and isotopic data for the area. Of particular importance are simulations of the movement of recharge from the Yucca Mountain area. These simulations indicate that groundwater from Yucca Mountain may not be easily identifiable in groundwaters south of Yucca Mountain because of dilution by groundwater from other, more active parts of the flow system. This groundwater mixture includes contributions from northwest Crater Flat, Timber Mountain, and Fortymile Canyon. In some other respects, the SZ flow model differs from what is inferred from the geochemical data. For instance, the SZ flow model appears to underestimate the quantity of inflow from the Fortymile Canyon area through the Tertiary units. This conclusion is based on the observation that groundwater along Fortymile Wash through Jackass Flats and the Amargosa Desert is chemically and isotopically unique compared to the surrounding groundwaters, but the tracer simulations indicate that groundwater inflow from Fortymile Canyon or from downgradient recharge along the wash is present only in dilute amounts along Fortymile Wash. Some of the discrepancy between the simulations and the data for the Fortymile Wash area may be due to recharge of some or most of this chemically distinct groundwater during wetter climate periods.

A7.1.4 Summary of Flow Pathways (Section A6.3.11)

Flow paths can be traced using areal plots and scatterplots of geochemical and isotopic data, inverse mixing and water/rock interaction analyses involving PHREEQC, and simulations done with the SZ flow model. Because no single chemical or isotopic species varies sufficiently to determine flow paths everywhere in the study area, multiple chemical and isotopic species were considered.

Flow Path 1 (Figure A6-62) shows groundwater moving roughly parallel to the Amargosa River from an area west of Bare Mountain toward the southwest corner of the site model area. Flow Path 2 indicates that groundwater flows parallel to Fortymile Wash to connect upgradient areas in Fortymile Canyon with downgradient areas in the Amargosa Desert. Groundwater following Flow Path 3 flows from central Jackass Flats near well J-11 through the eastern part of the Amargosa Desert. Flow Paths 4 and 5 shows groundwater moving predominantly south-southeast through Crater Flat. Mixing relations and modeling suggest that these groundwaters leak across a region with a steep hydraulic gradient to mix with more dilute groundwaters to the southeast. Flow Paths 6 and 7 show groundwater flow from the Solitario Canyon area to the south. Again, leakage to the southeast across a steep hydraulic gradient coincident with the Solitario Canyon fault is suggested by hydrochemical trends. Groundwater from northern Yucca Mountain is interpreted to flow southeast toward lower Dune Wash and then southwestward toward wells located west of Fortymile Wash near U.S. Highway 95 (Flow Path 7). The location of Flow Path 7 implies that groundwater from the repository area will flow further to the west of this path. Flow Path 8 illustrates leakage to the east across the hydrologic boundary between the carbonate aquifer to the east and the alluvial aquifer in Amargosa Desert. Flow Path 9 schematically illustrates deep underflow of groundwater from the carbonate aquifer, east of and including the GF and AF groups, beneath the Amargosa Desert and Funeral Mountains to the discharge points in Death Valley.

Regions where mixing relations are strongly suggested by hydrochemical data are also shown in Figure A6-62. An important conclusion derived from drawing these mixing zones is that they document and qualitatively illustrate the extent of transverse dispersivity along certain flow pathways. The mixing zones also illustrate that although some flow pathways may remain intact for great distances (e.g., Paths 1 and 2), even these most persistent flow paths eventually lose their distinct character largely through mixing as is demonstrated in southern Amargosa Desert along the southern border of the map area.

A7.2 DATA TRACKING NUMBERS

Several data tracking numbers (DTNs), generated in this appendix are cited elsewhere in this report where they are used as indirect input. These intermediary output DTNs are listed below in an order that coincides with the structure of the appendix. These results are not qualified and cannot be used as direct input without qualification:

- Regional groundwater hydrochemical data: DTNs: LA0309RR831233.001 [DIRS 166546] and LA0309RR831233.002 [DIRS 166548]

- Calculated hydrochemical parameters: DTN: LA0310EK831232.001 [DIRS 165995]

- Calculation of corrected and uncorrected groundwater ^{14}C ages: DTN: LA0202EK831231.002 [DIRS 165507]

- Calculations of fractions of young water in selected Yucca Mountain groundwaters: DTN: LA0202EK831231.004 [DIRS 180317]

- Groundwater travel-time calculations for selected wells: DTN: LA0310EK831231.001 [DIRS 171889]

- FEHM groundwater models of nonreactive tracer transport in the Yucca Mountain area: DTN: LA0309EK831231.001 [DIRS 171887]

- A map of groundwater flow paths in the Yucca Mountain area: DTN: LA0308RR831233.001 [DIRS 171890].

A7.3 UNCERTAINTIES AND RESTRICTIONS

The evaluations and conclusions presented in this appendix are interpretive in nature. The overall uncertainty of these interpretations is a function of the analytical uncertainty of the data on which the interpretations were based, the distribution of data both areally and with depth, the representativeness of these data for various parts of the groundwater system, and the uncertainty in the conceptual models that formed the framework for the interpretations.

Results presented in this appendix are affected to different degrees by each of these uncertainties. The following sections list the key uncertainties associated with each of the DTNs cited in Section A7.2.

A7.3.1 Compilation of Hydrochemical Data

The uncertainty associated with the DTNs results primarily from the analytical uncertainty associated with the measurements and the representativeness of the data for those parts of the aquifer from which the groundwater samples were taken. Ideally, groundwater samples are taken after the well has been pumped for some time after drilling so that the effects of foreign drilling fluids and borehole cuttings on in situ groundwater compositions have been mitigated. Although this is true of the vast majority of the samples used in this report, a small number of samples used in this report originated from wells in which the samples were bailed prior to a "clean-out" period. This approach may have caused the chemical characteristics of these samples to change somewhat relative to in situ groundwater. In general, bailed samples were used in this report only if later pumped samples were not available from a particular well. The representativeness of sampled groundwater of in situ groundwater compositions is also related to the depth interval over which the sample was taken. Most hydrochemical data reported here are from single-interval boreholes, the hydrochemistry of which will represent an average of the sampled depth intervals. Hydrochemical data for discrete depth intervals are presented in Section 6.7.3.

The representativeness of sampled groundwater of in situ conditions may also be affected by the sampling method. For example, choice of container or prolonged exposure to atmosphere may

affect groundwater chemistry. Most sample data presented herein were collected by the United States Geological Survey (or by their contractors), who have a long and proven record of groundwater sampling using proven techniques. Furthermore, Yucca Mountain Project Quality Assurance Programs also govern many of these sampling procedures. This program is designed to assure that methods utilized are appropriate for the desired purpose. Thus, the data are accepted to be representative of in situ conditions. All analytical data presented herein have uncertainty associated with the individual values. These uncertainties reflect limits of precision of the analytical technique combined with accuracy of the measurement, which is typically determined by replicate analysis of samples (standards) with known values. The data presented herein were determined using a variety of analytical techniques by a number of laboratories, collected over a span of more than 20 years, during which time analytical techniques and associated uncertainties have changed. In some cases, uncertainties for individual analytes or groups of analytes are presented in the original data sources, however, in other data sets analytical uncertainties are neither given nor discussed. Some examples of stated uncertainties are presented below.

The National Water Quality Laboratory produced many of the data presented herein for the Yucca Mountain Program at the United States Geological Survey and uncertainties are stated in some of the DTNs. For example, accuracy for major anions, cations and strontium concentration is estimated to be better than 10% except for fluoride, which is estimated at 15% (DTN: GS000308312322.003 [DIRS 149155]). Uncertainty in concentration of major anions and cations as well as strontium concentration is quoted at less than 10% in DTN: GS011108312322.006 [DIRS 162911]. This DTN also presents uncertainties for isotopic measurements as follows (all given in per mil): deuterium 3.0, ^{18}O 0.2, ^{13}C 0.2, and ^{34}S 0.2. In some cases, strontium was determined by isotope dilution, mass spectrometry methods, for which data are more precise (e.g. 0.5%, DTN: GS970708315215.008 [DIRS 164674]). Uncertainties for ^{14}C are 0.1 pmc for data presented in DTN: GS011108312322.006 [DIRS 162911]. Uncertainties for uranium concentration are given as better than 1% (Paces et al. 2002 [DIRS 158817]). Uncertainties in uranium isotope ratios ($^{234}U/^{238}U$) are typically given with each individual analysis in the original data source. For example, uncertainties presented in Paces et al. (2002 [DIRS 158817], Table 2) range from 0.09% to 4.5% with a mean of 0.73% (with the exception of a single analysis of a rainfall sample with small U concentration for which uncertainty in the $^{234}U/^{238}U$ ratio is 9.8%). Uncertainties for strontium isotope ratios ($^{87}Sr/^{86}Sr$) are typically quoted at 0.00001 for absolute values (e.g., DTN: GS011108312322.006 [DIRS 162911] and for Nye County wells), which translates to an uncertainty of approximately 0.01 in $\delta^{87}Sr$ units.

For the purpose of this report, uncertainties assigned to analytical data are based on one or more of the following: (1) stated uncertainties in the original data set; (2) consideration that data produced by the same facility, for which no uncertainties are stated, are likely to have similar uncertainties to data with stated uncertainties; (3) typical uncertainties given in the literature; or (4) the authors' personal experience with typical uncertainties associated for various analytical techniques and analytes. Where uncertainties are not stated, the following uncertainties are assigned to the analytical data: Major anions and anions and strontium concentration: 10 %; fluoride concentration: 15%; stable isotopes of hydrogen, oxygen, sulfur, and carbon (expressed as δH, δO, δS, and δC in per mil): 0.2; and ^{14}C: 0.2 pmc. Uncertainties in uranium concentration and uranium and strontium isotope ratios are given in the original data sets.

In addition to analytical errors, many of the samples in the portion of the data set that had no prior DTNs may have an additional uncertainty in that they were obtained from a database (geochem02.mdb) that does not represent the primary source of the data. Hence, the possibility of transcription errors is compounded. Where original published sources could be found and checked against that database, some transcription errors in the database were evident. This uncertainty affects only groundwater samples at locations to the west, north, and east of the site model area, outside of the site model area.

It is prudent to point out that most of the evaluations presented herein are based on hydrochemical groupings and general data trends displayed within and among these groupings as opposed to any one analysis or data set from any one sample. Generally, the range of analytical values displayed within a single hydrochemical grouping is greater than the analytical uncertainty for any individual analysis. Hydrochemical groupings and data trends remain valid and essentially unaffected by considerations of analytical uncertainty.

A7.3.2 Calculated Hydrochemical Parameters

The uncertainty in the calculated hydrochemical parameters reflects the analytical uncertainty of the measurements, the representativeness of these measurements of in situ groundwater conditions, and uncertainty in the solubility constants of the minerals for which saturation indices were calculated. Uncertainty in the applicability of the solubility constants arises from (1) inaccurate, incomplete or inconsistent thermodynamic data, (2) nonstoichiometric or variable mineral compositions, (3) differences in the particle sizes of minerals that produced the thermodynamic data and particle sizes of minerals to which the data were applied, (4) model assumptions and limitations, such as which aqueous complexes are considered in the model, and (5) kinetic effects arising from slow reaction rates relative to groundwater residence times (Langmuir 1997 [DIRS 100051], p. 221). In addition, because solubility constants are a function of temperature, uncertainty in groundwater temperatures affects the calculated saturation indices. Measured groundwater temperatures were used to calculate saturation indices for most wells considered in this report. For a relatively small number of wells in the Yucca Mountain area, groundwater temperatures were estimated from published maps of water table temperatures. Groundwaters in the Amargosa Desert with no temperature data were assumed to be at 25°C based on the measured groundwater temperatures of nearby wells. A sensitivity analysis to examine the effect of temperature changes on log P_{CO2} and mineral saturation indices for groundwater from well J-13 indicated the following uncertainties as assumed temperatures were varied by ±5°C around 25°C: log P_{CO2} (±0.06), $SI_{calcite}$ (±0.04), $SI_{smectite}$ (±1.72), $SI_{Ca\text{-}clinoptilolite}$ (±4.77), $SI_{SiO2(a)}$ (±0.04), $SI_{fluorite}$ (±0.06), SI_{albite} (±0.28), $SI_{K\text{-}feldspar}$ (±0.34), and $SI_{dolomite}$ (±0.14). Saturation indices for calcite and dolomite and log P_{CO2} increase with temperature, but the remaining saturation indices decrease with temperature. The saturation indices of smectite and Ca-clinoptilolite are particularly sensitive to temperature because of the large enthalpies estimated for these minerals (Table A6-4); however, groundwaters in the Amargosa Desert are typically very supersaturated with these minerals (Figures A6-38 and A6-39), so that a temperature uncertainty of ±5°C does not change the fundamental conclusion that groundwaters in the Amargosa Desert are supersaturated with these minerals. For other minerals, uncertainty in groundwater temperatures of 25 ±5°C introduces less absolute uncertainty into the calculated saturation indices.

Another source of uncertainty in the calculated saturation indices of alumino-silicate minerals concerns the assumption that total dissolved Al^{3+} concentrations are in equilibrium with kaolinite. This assumption was based on an empirical fit to dissolved Al^{3+} concentrations from a subset of the Yucca Mountain area wells for which dissolved Al^{3+} data exist (see Section A6.3.5). Estimates of Al^{3+} concentrations that rely on assumed equilibrium with kaolinite underestimate measured Al^{3+} concentrations by –3.0 ±2.9 ppb. If the actual Al^{3+} concentrations were approximately 3 ppb higher than was estimated for the Yucca Mountain area, the saturation indices of all Al-bearing minerals would increase. Assuming Al^{3+} equilibrium with kaolinite, most groundwaters in the Yucca Mountain area are estimated to be saturated with smectite and Ca-clinoptilolite (Figures A6-38 and A6-39). With higher Al^{3+} concentrations, these groundwaters would be even more supersaturated with these minerals. Groundwaters in the Yucca Mountain area are presently estimated to be both undersaturated and supersaturated with K-feldspar (Figure A6-37). With higher Al^{3+} concentrations, some groundwaters that are estimated to be undersaturated with K-feldspar might be calculated to be saturated or supersaturated with K-feldspar.

A7.3.3 Calculated ^{14}C Ages

The calculations of ^{14}C ages used the downgradient increase in the DIC concentrations of selected Yucca Mountain area groundwaters, relative to the DIC concentrations of Yucca Mountain perched waters to estimate the extent of ^{14}C dilution by calcite dissolution in the saturated zone (Section A6.3.6.6.2). The selected groundwater samples were chosen because they, like the perched water samples, had high $^{234}U/^{238}U$ activity ratios relative to many Yucca Mountain area groundwaters, thus indicating the likelihood of a common origin. The estimated increases in the DIC concentrations of the groundwaters were then used to reduce the initial ^{14}C activities to below their original atmospheric values to calculate a "corrected" ^{14}C age for the groundwater. The critical assumptions in this analysis are that (1) the perched water itself required no age corrections and (2) that the measured increases in groundwater DIC relative to perched water limit the amount of ^{14}C dilution by calcite. Assumption (1) appears to be valid based on the historic variations of $^{36}Cl/Cl$ and ^{14}C activities measured on organic carbon in pack-rat middens and similar relations between $^{36}Cl/Cl$ and ^{14}C activities measured for inorganic carbon in perched water. Assumption (2) requires that no reductions in groundwater DIC concentrations take place through exsolution of CO_2 during groundwater flow or during sampling. Although CO_2 losses from groundwater to the unsaturated zone are estimated to be small because of the low diffusion of CO_2 in groundwater, exsolution of CO_2 during groundwater sampling may be a more significant effect. However, groundwater at the wells where ^{14}C age corrections were made typically had relatively low (< 7.8) pH values, indicating that the effects of degassing on DIC concentrations during sample collection were minimal.

A7.3.4 Calculations of the Fractions of "Young" Water in Yucca Mountain Groundwaters

These calculations interpret the measured ^{14}C activities of groundwater beneath Yucca Mountain to result from the mixing of groundwater that has been recharged at different times from the unsaturated zone at Yucca Mountain. Although recharge may have been added continuously over time at varying rates to Yucca Mountain groundwater, the calculations simplify the actual distribution by assuming that the measured ^{14}C activities result from the mixing of an "old"

component and a "young" component that are widely separated in time. This approach effectively replaces the actual (but unknown) distribution of groundwater ages by a bimodal distribution of ages with the same mean age. This idealized distribution of ages places more emphasis on the very young and very old groundwaters than the actual age distribution would indicate. This method provides upper bounds to the fraction of young groundwater in the mixture, which is the quantity of interest in these calculations.

A7.3.5 PHREEQC Inverse Models of Groundwater Mixing and Water-Rock Interaction

The PHREEQC inverse models of groundwater mixing and water-rock interaction described in Section A6.3.8 are affected by uncertainties in the accuracy and representativeness of groundwater compositions (see Section A7.3.1), uncertainties in mineral-phase compositions, and uncertainties in the conceptual model. The uncertainties in the accuracy and representativeness of groundwater compositions are accounted for in the PHREEQC models through user-specified uncertainty criteria. Generally, uncertainties specified in the PHREEQC models were 10% or less of the measured concentrations for major and minor ions, 0.1 per mil for $\delta^{18}O$, 1.0 per mil for δD, 0.1 per mil for $\delta^{13}C$, and 0.05 pH units for pH. These uncertainties were intended to reflect not only analytical uncertainty in the measurements (See Section A7.3.1) but also the representativeness of the groundwater samples in light of the chemical and isotopic heterogeneity that exists in groundwaters from closely spaced wells. It was necessary to specify some uncertainty in these models in order to simultaneously satisfy the multiple mass-balance constraints involved in any particular model. There is also some variability in mineral phase compositions from Yucca Mountain and, hence, some uncertainty in specifying a single representative phase composition for the entire area. This variability is particularly true of clinoptilolites, which are known to have east-to-west chemical variations across the Yucca Mountain area (Broxton et al. 1987 [DIRS 102004]). Generally, clinoptilolite compositions used in any particular model were chosen to be representative of the area near the wells considered by that model. For reactions involving the dissolution or precipitation of calcite (or dolomite), it was necessary to specify the $\delta^{13}C$ composition of the calcite. The $\delta^{13}C$ compositions are variable in SZ calcites and, therefore, some uncertainty exists in choosing a single representative value. Calcite in the volcanic aquifers was assumed to have $\delta^{13}C$ values of between -4 ± 3 and -1 ± 3 per mil, whereas calcite in the alluvial aquifers near Fortymile Wash was assumed to be -4 ± 3 per mil. Although the values of $\delta^{13}C$ used for the volcanic aquifer are in agreement with measured values (Whelan et al. 1998 [DIRS 137305]), the isotopic characteristics of calcite in alluvium have not been measured at Yucca Mountain. The calcite in alluvium was assumed to have isotopic characteristics ($\delta^{13}C = -4$ per mil) similar to pedogenic calcite at the surface of Yucca Mountain (Table A5-1 in Assumption 9).

The specified uncertainty in solution compositions and in the isotopic composition of the minerals is propagated through the PHREEQC inverse models so that, for each model, upper and lower bounds are also estimated for the mixing ratios and amounts of each mineral phase dissolved. However, although quantitative measures of uncertainty are provided for each model discussed in this report (DTN: LA0310EK831232.001 [DIRS 165995]), these uncertainty estimates do not consider the other combinations of mineral reactions and mixing end members present in alternative models identified by PHREEQC. Additionally, these uncertainty estimates do not consider the conceptual model uncertainty.

Conceptual-model uncertainty includes the choice of mineral phases to be considered in a particular model, any constraints on the precipitation/dissolution or exchange reactions imposed on these phases, and the choice of groundwaters considered in these models as potential mixing components. The rationale behind selection of these various parameters is discussed in Section A6.3.8. It is acknowledged; however, that all possible combinations of these parameters were not exhaustively evaluated. Other combinations of end-member mixing components and reaction history could possibly be modeled to yield a particular downgradient water chemistry. Given all the potential combinations of mixing end members and reaction models, it is impossible to quantify uncertainty related to uncertainties in the conceptual model.

A7.3.6 Groundwater Velocities

The groundwater velocities calculated in Section A6.3.9 were based on the measured groundwater ^{14}C activities at wells defining a flow path segment, the linear distance between the wells, and the water-rock interactions identified by the PHREEQC models for that flow-path segment. The calculated velocities are, therefore, affected by the accuracy and representativeness of the groundwater ^{14}C measurements (see Section A7.3.1), the assumption that groundwater flows along a straight path between the wells defining the flow-path segment, and the uncertainties associated with the PHREEQC models, as described in Section A7.3.5. An indication of the quantitative uncertainty associated with transit times is provided by the standard deviations associated with transport times based on the PHREEQC models and differences between the means of these estimates and estimates made based on downgradient increases in DIC concentrations (Table A6-11). An additional uncertainty that may impact these calculations concerns the implicit assumption that no additional ^{14}C is added to the groundwater from downgradient recharge as the groundwater moves from the upgradient to downgradient wells defining a flow-path segment. Recharge at Yucca Mountain may not vary enough spatially to guarantee that upgradient and downgradient recharge could be recognized in a mixture.

A7.3.7 FEHM Groundwater Models of Nonreactive Tracer Transport in the Yucca Mountain Area

The FEHM simulations of nonreactive tracer transport described in Section A6.3.10 used the Yucca Mountain site-scale saturated zone flow model documented in *Water-Level Data Analysis for the Saturated Zone Site-Scale Flow and Transport Model* (BSC 2004 [DIRS 170008]), using the model input/output files in DTN: LA0304TM831231.002 [DIRS 163788]. Uncertainty in flow modeling arises from a number of sources including, but not limited to, the conceptual model of the processes affecting groundwater flow, water–level measurements and simplifications of the model geometry, boundary conditions, hydrogeologic unit extent and depth, and the values of permeability assigned to hydrogeologic units. Such uncertainties associated with this flow model are identified and quantified in *Saturated Zone Site-Scale Flow Model* (BSC 2004 [DIRS 170037], Section 6.8). An additional uncertainty that pertains to the tracer simulations but not the flow model itself concerns numerical dispersion associated with the advection/dispersion equation. Numerical dispersion would tend to cause greater apparent mixing and dilution than would be present solely because of hydraulic conductivity variations in the model. These effects are likely to have influenced the tracer concentration distributions shown in Section A6.3.10 and, in particular, the relatively dilute concentrations near the edges of these tracer plumes may be an artifact of this numerical dispersion.

A7.3.8 A Map of Groundwater Flow Paths for the Yucca Mountain Area

The map of groundwater flow paths in the Yucca Mountain area (Figure A6-62) was developed on the basis of areal variations of chemical and isotopic species (Section A6.3.4), scatterplots that indicated mixing between groundwaters from different areas (Section A6.3.7), and PHREEQC models of groundwater mixing and chemical evolution (Section A6.3.8). The flow-path map is affected, therefore, by the uncertainties already described for these associated technical data products in Sections A7.3.1, A7.3.2, and A7.3.5.

Possibly, the most important uncertainty in the flow path map relates to the source of the groundwater at well NC-EWDP-19D (Sites 92 and 94 to 98). Two equally plausible sets of groundwater mixing and reaction models were developed with PHREEQC for groundwater at well NC-EWDP-19D, each of which implies a different direction for groundwater flow from the repository area in southern Yucca Mountain. The first set of models indicates that groundwater from various depths at NC-EWDP-19D originates from groundwater in the Dune Wash area (represented by groundwater from well WT-3) and a set of water-rock-gas reactions. These results are represented on the flow-path map as the southern part of Flow Path 7. Groundwater from the repository area would be constrained by the southern part of Flow Path 7 to move predominantly southward or southwestward through southern Yucca Mountain, thereby avoiding most of the alluvium north of U.S. Highway 95. The second group of PHREEQC models for groundwater from various zones in well NC-EWDP-19D indicated that these groundwaters are a mixture of groundwaters from the Solitario Canyon Wash area (represented by groundwater from well WT-10) and local Yucca Mountain recharge (represented by perched water from borehole SD-7), plus a set of water-rock reactions. This origin for the groundwater at well NC-EWDP-19D indicates that groundwater from the repository area will follow a more southeasterly trajectory and would probably encounter more of the alluvium west of Fortymile Wash than is indicated by Flow Path 7. The leakage of groundwater from the Solitario Canyon area across the Solitario Canyon fault beneath Yucca Mountain is indicated by the southeast-trending arrows originating from Flow Path A6.

INTENTIONALLY LEFT BLANK